Title
ENERGETIC AND STRUCTURAL RELATIONSHOPS INVOLVED IN THEINTERCALATION OF GRAPHITE BY FLUOROSPECIES

Author
Kourtakis, K.

Publication Date
1987-02-01

Lawrence Berkeley Laboratory
UNIVERSITY OF CALIFORNIA

Materials & Chemical Sciences Division

ENERGETIC AND STRUCTURAL RELATIONSHIPS INVOLVED IN THE INTERCALATION OF GRAPHITE BY FLUOROSPECIES

K. Kourtakis
(Ph.D. Thesis)

February 1987

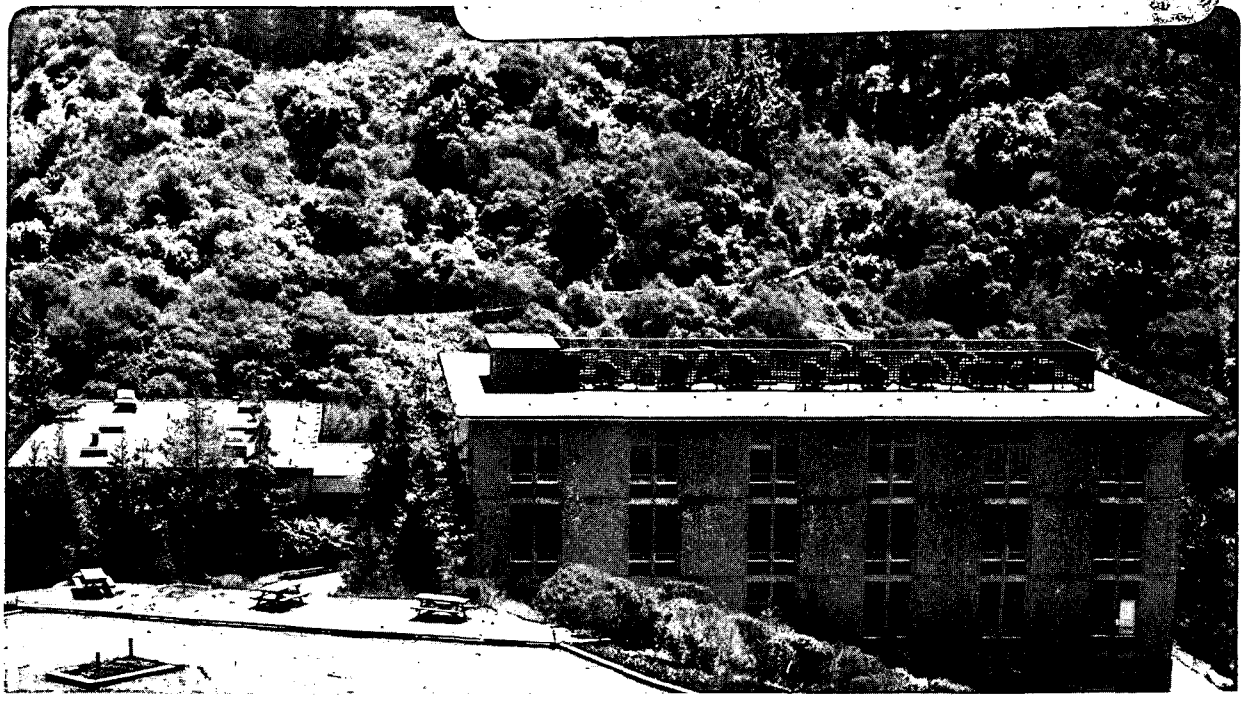

Prepared for the U.S. Department of Energy under Contract DE-AC03-76SF00098

DISCLAIMER

LBL-23329

ENERGETIC AND STRUCTURAL RELATIONSHIPS INVOLVED IN THE INTERCALATION OF GRAPHITE BY FLUOROSPECIES

Kostantinos Kourtakis

Ph.D. Thesis

Department of Chemistry
and
Lawrence Berkeley Laboratory
University of California
Berkeley, California 94720

February, 1987

This work was supported by the Director, Office of Energy Research, Office of Basic Energy Sciences, Chemical Sciences Division of the U.S. Department of Energy under Contract Number DE-AC03-76SF00098.

ENERGETIC AND STRUCTURAL RELATIONSHIPS INVOLVED IN THE INTERCALATION OF GRAPHITE BY FLUOROSPECIES

Table of Contents

List of Tables

List of Figures

ENERGETIC AND STRUCTURAL RELATIONSHIPS INVOLVED IN THE INTERCALATION OF GRAPHITE BY FLUOROSPECIES

Kostantinos Kourtakis

Department of Chemistry
University of California
Berkeley, California 94720

ABSTRACT

Raman spectra of the products of the low temperature reaction:

$$ONCl_{(g)} + ClF_2^+AsF_6^-(s) \rightarrow NO^+AsF_6^-(s) + "Cl_2F_2"$$

show that a novel chlorine fluoride is formed. This "Cl_2F_2" species is unstable above -30 °C, and will decompose into chlorine monofluoride: "$Cl_2F_2 \rightarrow 2ClF$". Raman spectra below -30 °C show strong bands at 794(1), 752(1) and 673(1) cm^{-1}. A comparison of this spectrum with low temperature spectra of $ClF_{3(\ell)}$ and $ClF_{(\ell)}$ suggests "Cl_2F_2" is not a "T"-shaped derivative of ClF_3, but is instead a loosely bound complex of two interacting ClF molecules.

The following fluoride ion donor enthalpies, ($AF_{x(g)} \rightarrow AF_{x-1(g)} + F^-_{(g)}$) have been determined from experimental evidence: $\Delta H°(IF_{7(g)} \rightarrow IF_6^+{}_{(g)} + F^-_{(g)}) = 209$; $\Delta H°(SF_{4(g)} \rightarrow SF_3^+{}_{(g)} + F^-_{(g)}) = 215$; $\Delta H°(ClF_{3(g)} \rightarrow ClF_2^+{}_{(g)} + F^-_{(g)}) > 220$ kcal mol^{-1}. In addition, $-(\Delta H°(WF_{6(g)} + e^- \rightarrow WF_6^-{}_{(g)})$ has shown to be less than 97 kcal mol^{-1}.

These results have been used to further clarify the thermochemistry of graphite intercalation. Additional support is presented for a thermodynamic barrier to the oxidation of graphite by fluoro-guest species. Evidence is presented which corroborates the proposal of a kinetic barrier which prevents the full reduction of C_xPF_6 (x= 29-33) by PF_3 to graphite ($PF_6^- + 1/2\ PF_3 \rightarrow 3/2\ PF_5 + e^-$). This barrier is present even when the graphite fluorophosphate (C_xPF_6) has not been fluorinated. The rapid removal of volatiles after reduction by PF_3 demonstrates that the neutral reduction products are

not slowly percolating through charged species. The remaining PF_6^- must be in "closed pockets". Since graphite is not intercalated by PF_5 even under high pressure of the gas, the reduction of C_xPF_6 to graphite by PF_3 would be complete except for this kinetic barrier.

When PF_5 is in excess of F_2 in a reaction mixture used to prepare second stage C_xPF_6 (x= 23-33), conductivity data indicate that fluorination of the carbon host is minimized. Conductivity measurements were performed on polycrystalline pellets rather than samples prepared from HOPG (highly oriented pyrolitic graphite). The large particle size of the latter makes the accurate determination of stoichiometry difficult because of the slow removal of neutral molecules close to the centers of the particles.

The displacement of PF_5 from C_xPF_6 salts (of second stage or higher) by BF_3 has been shown to be quantitative. This unexpected finding has been accounted for by the discovery that neutral BF_3 molecules are incorporated into the BF_4^- salt product. The net reaction stoichiometry (for the vacuum stable product) is:

$$C_xPF_6 + 4/3\ BF_3 \rightarrow C_xBF_4 \cdot 1/3(BF_3),\ x= 23\text{-}33$$

The BF_3 acts as an effective dielectric to screen the BF_4^- from one another. X-ray diffraction data have been employed to show that the guest species (both BF_4^- and BF_3) in $C_xBF_4 \cdot 1/3(BF_3)$ are close-packed, such that the F ligands constitute a hexagonal close-packed double layer, with the B atoms inserted in either tetrahedral (for BF_4^-) or trigonal (for BF_3) holes. Fluorination of $C_xBF_4 \cdot 1/3(BF_3)$:

$$C_xBF_4 \cdot 1/3(BF_3) + \sim 2/3F_2 \rightarrow C_x(BF_4)_{\sim 4/3}$$

destroys this close packing and as a consequence, fourth or third stage $C_xBF_4 \cdot 1/3(BF_3)$ salts are converted to second stage materials. This is a consequence of the removal of the screening influence of the neutral BF_3 molecules.

Chapter 1

1.1 Introduction

This thesis is divided into three sections. The first section (Chapter 2) deals with some thermodynamic considerations of the strengths of fluoroacids and bases. The second (Chapter 3) consists mainly of studies on the new interhalogen fluorospecies Cl_2F_2. Finally, fluoroborate and fluorophosphate intercalation salts of graphite will be discussed in Chapters 4-6 and a general overview of their chemistry presented. In these last chapters I have tried to establish a link between graphite intercalation and the thermochemistry of the intercalating fluorospecies.

1.2 General Experimental

1.21 Vacuum Line Techniques: All reactions were performed in a stainless steel 3/8" o.d. vacuum line fitted with new, lower pressure Autoclave Engineers valves (HT-A11437, 7500 psi at room temperature) and "T" and cross connectors (HT847661T, 7500 psi). The vacuum line was connected to two good vacuum pumps, one on either side of the line. Pressure could be monitored by a Helicoid gauge (0-1500 mm Hg) and a Varian 0531 thermocouple gauge (5-500 μ). Fluorine was disposed of through a soda lime tower attached to the second pump. The vacuum line was routinely passivated with ClF_3 prior to use. Pyrex liquid nitrogen traps protected each vacuum pump.

Under these conditions, pressures of 10-30 μ could be routinely attained, with 40 μ used as a ceiling for all manipulations. Virtually no maintenance was required of the vacuum line, excluding the vacuum pumps themselves. Connections were made using metal ferrules and the autoclave valves proved to be very rugged and resistant to corrosion.

1.22 Infrared spectra were routinely recorded in the gas phase in large (100 ml) monel infrared cells of 10 cm path length fitted with AgCl windows (5 mm thick). The inner walls of the cell were coated with silver metal, and a Whitey low pressure valve was attached. A Perkin-Elmer 591 spectrophotometer, and later a Nicolet 5DX Fourier Transform spectrophotometer were used to acquire the infrared spectra (resolu-

tion ≈ 2 cm^{-1}). The infrared cell was well passivated with ClF_3 prior to use. It was found that $Ag^+PF_6^-$ and $Ag^+BF_4^-$ will form on the AgCl windows after passivation with ClF_3 and exposure to PF_5 or BF_3. PF_3, BF_3 and AsF_5 will displace PF_5 from the $Ag^+PF_6^-$ on the cell walls; the products were visible in the infrared spectra of the volatiles. The infrared cell was seasoned with each volatile before an infrared spectrum was recorded.

1.23 Raman spectra were recorded on a Jobin-Yvon HG2S spectrophotometer controlled by a Nicolet 1180E computer. Details of the low temperature experimental conditions are given in Chapter 3.

1.24 X-ray data were obtained using the Debye-Scherrer method. Quartz capillaries (0.5 and 0.7 mm, Charles Supper Co., Natick, Mass.) were used for all samples. Typical air-sensitive samples were loaded in a moisture-free argon atmosphere Drilab (Vacuum Atmospheres, Inc.) and capped with silicon grease prior to sealing with a microtorch. X-ray diffraction experiments of the high pressure in situ capillary reactions normally employed a Whitey valve and a swagelock 1/4" to 1/8" adapter fitted, using teflon ferrules, to a 0.7 mm quartz capillary. Pressure was monitored with a high pressure Acco gauge (0 to 500 psi).

Chapter 2

Thermodynamic Studies

2.1 Introduction

The stabilization of unusually high oxidation state species, an ongoing concern in this research group, requires the use of potent oxidizers. An earlier noteworthy example[1] of this is the stabilization of the cation O_2^+ in the salt $O_2^+PtF_6^-{}_{(c)}$. The ionization energy of $O_{2(g)}$ is 281 kcal mol^{-1}, indicating that PtF_6 is one of the strongest oxidizers known; Bartlett[2] was subsequently able to show that even Xe^+ could be stabilized by this hexafluoride through the synthesis of $XePtF_6$, the first noble gas compound.

The determination of the relative oxidizing strengths of the third transition series hexafluorides was desirable to provide a basis for an understanding of their extraordinarily high electron affinities. (In Chapter 6 the oxidizing ability of the third transition series and its link to graphite intercalation chemistry is summarized.) Electron affinity evaluations were initially based upon thermochemical estimates and observations[3] of the reactivity of the metal hexafluorides with $NO_{(g)}$ and $ONF_{(g)}$; some of this chemistry is summarized in Table **6.4.** From such studies it appeared that the electron affinity of the third transition series increases smoothly by about 1 eV with each increase in atomic number[4]. These early evaluations were very rough, however, and more recent work has assessed them more accurately.

In order to determine the oxidizing strength of the hexafluorides and other fluorospecies, an accurate determination of the lattice enthalpy of the ionic salts involved in the Born-Haber cycle is required. If, in addition, the reaction entropy ($\Delta S°$) is known or can be evaluated, a range limit for the enthalpy of reaction ($\Delta H°$) can be arrived at on the basis of the observed chemistry. The cycle below illustrates the interplay of these parameters.

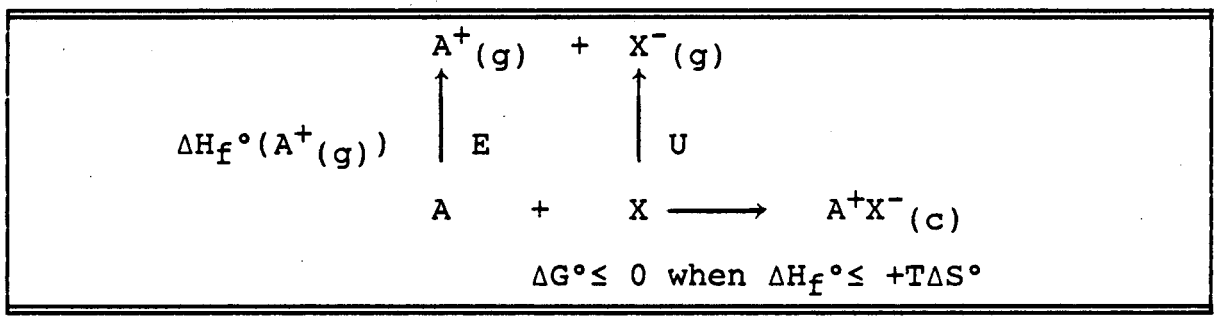

Since the enthalpy of formation of gaseous ion A^+ is often known from experiment, the electron affinity (E) can be obtained if $\Delta H_{reaction}$ (A + X) and U are also known. The evaluation of $\Delta H_{reaction}$ can be made calorimetrically but if $\Delta G \approx 0$ it must be numerically equal to $+T\Delta S$. In this instance, then, where A, X and $AX_{(c)}$ are in equilibrium the $\Delta H_{reaction}$ can be estimated from the entropy change.

While the entropies of gaseous neutrals are generally available, the entropies of many ionic solids are not. Recently some accurate and useful trends for the entropies of highly ionic solids were compiled by Bartlett and Mallouk[5]. It was found that these entropies varied in a linear fashion with the formula unit volumes according to the equation:

$$S°(\text{cal mol}^{-1}\ \text{deg}^{-1}) = 0.44\ V\ (\text{Å}^3) \qquad (1)$$

Likewise, an inverse linear relation between the lattice enthalpy and the cube root of formula unit volumes was observed to hold well for complex fluorides of general formula A^+X^-:

$$U_{\text{lattice}}\ (\text{kcal mol}^{-1}) = 556.3\ V^{-1/3}(\text{Å}^{-1}) + 26.3 \qquad (2)$$

The second relationship is valid because the lattice enthalpies of ionic salts have Madelung components which comprise 90% of the total lattice enthalpy and which vary as the inverse of the sum of the "ionic" radii. The first relationship is somewhat more surprising; however, the correlation of the relationship is excellent (accurate to within 5-10 cal $\text{mol}^{-1}\ \text{deg}^{-1}$) and, at least for the fluorides investigated in this study, appears to be a good empirical rule. With reliable lattice energy and entropy evaluations at hand it is then usually possible to determine the electron affinity necessary to stabilize the salt $A^+X^-_{(c)}$. This however deals only with the issue of the stabilization of $A^+X^-_{(c)}$ with respect to charge transfer (A and X neutral). Another important concern has to be with transfer of an anionic fragment of X^- from X^- to A^+. This is a common mode of decomposition in fluoroanion salts of high oxidation state species, when F^- is transferred from anion to cation.

An instance of this fluoride ion capture by the cation is the reversible dissociation of $IF_6^+BF_4^-{}_{(c)}$, which was investigated in this work:

$$IF_6^+BF_4^-(c) \rightarrow IF_{7(g)} + BF_{3(g)}$$

Here the fluoride ion donor strength of IF_7, the fluoroacid strength of BF_3, the lattice enthalpy and the entropy change make for a system in equilibrium at room temperatures.

Fluoride ion transfers as well as electron transfers occur in graphite intercalation compounds, and account for the complexity of that chemistry; this will be discussed in Chapter 4.

In this work, experimental evidence is presented from which the fluoride ion donor enthalpy of $IF_{7(g)}$ ($\Delta H°(IF_{7(g)} \rightarrow IF_6^+{}_{(g)} + F^-{}_{(g)})$) is derived. A comparison is drawn between IF_7, its electronic relative XeF_6, and its transition element relative ReF_7 as well as several other fluoride ion donor molecules. The evaluation of the lattice enthalpies used to determine the electron affinities of some transition metal hexafluorides are also described.

2.2 Results and Discussion

2.21 The Fluoride Ion Donor Enthalpy of $IF_{7(g)}$, $SF_{4(g)}$ and $ClF_{3(g)}$

The salt $IF_6^+BF_4^-$ was first reported by Seel and Detmer[6] but an evaluation of its thermodynamic stability has so far been lacking. In this work Raman spectra of the product of the interaction of IF_7 and BF_3 indicate that the $IF_6^+BF_4^-$ salt exists at -60°C, but dissociates to the separate molecules IF_7 and BF_3 at higher temperatures. Evidently, $WG°_{213}(IF_{7(g)} + BF_{3(g)} \rightarrow IF_6^+BF_4^-{}_{(c)}) \approx 0$, and it follows that evaluation of the $T\Delta S$ term will then provide the fluoride ion donor enthalpy $\Delta H°(IF_{7(g)} \rightarrow IF_6^+{}_{(g)} + F^-{}_{(g)})$.

The standard entropy of $IF_6^+BF_4^-{}_{(c)}$ at 213 K obtained from the correlation with ionic volume given in equation (1), in combination with $S°(IF_{7(g)})$[7] = 82.8 cal mol^{-1} deg^{-1} and $S°(BF_{3(g)})$[7] = 60.7 cal mol^{-1} deg^{-1} yields $-T\Delta S°$= 16(3) kcal mol^{-1}. Thus $\Delta H°(IF_{7(g)} + BF_{3(g)} \rightarrow IF_6^+BF_4^-{}_{(c)}) \approx$ -16(3) kcal mol^{-1}. The fluoride-ion affinity of $BF_{3(g)}$ has been recently evaluated[5]: $\Delta H°(BF_{3(g)} + F^-{}_{(g)} \rightarrow BF_4^-{}_{(g)})$= -92(3) kcal mol^{-1}. From the linear correlation of the lattice enthalpy with the inverse of the cube root of the ionic volume (equation (2)), $\Delta H°_{lattice}(IF_6^+{}_{(g)} + BF_4^-{}_{(g)} \rightarrow IF_6^+BF_4^-{}_{(c)})$ = -132(4) kcal mol^{-1}. Hence, $\Delta H°(IF_{7(g)} \rightarrow IF_6^+{}_{(g)} + F^-{}_{(g)})$ = 208(6) kcal mol^{-1}.

In addition, present studies show that the following reaction is near equilibrium (see Figure 2.1):

$\Delta G°_{243}(IF_6^+AsF_6^-(c) + SF_{4(g)} \rightarrow IF_{7(g)} + SF_3^+AsF_6^-(c)) \approx 0$

This allows us to draw a comparison between the fluoride donor ability of $SF_{4(g)}$ and $IF_{7(g)}$. The lattice enthalpy of $IF_6^+AsF_6^-$ has been evaluated using the method of Bertaut[8] as modified by Templeton[9] and is believed to be highly reliable. From that approach[10] $\Delta H_{lattice}(IF_6^+AsF_6^-) = -126$ kcal mol^{-1}; this is a point on the line described by equation (2). An evaluation of the lattice enthalpy for $SF_3^+AsF_6^-$ using equation (2) gives $\Delta H_{lattice}(SF_3AsF_6) = -133$ kcal mol^{-1}. Since the reaction involves the same number of moles of gas in reactants and products, and in each salt one F^- is transferred to make the two gaseous molecules, $T\Delta S°_{243} \approx 0$. Thus, $[\Delta H°(SF_{4(g)} \rightarrow SF_3^+(g) + F^-(g)] - [\Delta H(IF_{7(g)} \rightarrow IF_6^+(g) + F^-(g))]$ = 7 kcal mol^{-1}. Hence, the fluoride ion separation energy of $SF_{4(g)}$ is 215(6) kcal mol^{-1}. An independent determination[5] gives 211(5) kcal mol^{-1}, which is in agreement within the experimental error.

Although the reverse reaction could not be achieved, $ClF_{3(g)}$ was observed to react with $SF_3^+AsF_6^-(c)$:

$$ClF_{3(g)} + SF_3^+AsF_6^-(c) \rightarrow ClF_2^+AsF_6^-(c) + SF_{4(g)}$$

This permits a lower limit determination of the fluoride ion donor strength of $ClF_{3(g)}$. From the lattice enthalpy correlation of equation (2), $\Delta H_{lattice}(SF_3^+AsF_6^-(c)) = 134$ kcal mol^{-1} and $\Delta H_{lattice}(ClF_2^+AsF_6^-(c)) = 139$ kcal mol^{-1}. For the same reasons given in the preceding case, $T\Delta S° \approx 0$. Thus, $[\Delta H°(ClF_{3(g)} \rightarrow ClF_2^+(g) + F^-(g))] - [\Delta H°(SF_{4(g)} \rightarrow SF_3^+(g) +$

$F^-_{(g)})]$ > 5 kcal mol^{-1}. Using a value for the $SF_{4(g)}$ fluoride ion donor energy of 215(6) kcal mol^{-1}, we obtain $\Delta H°(ClF_{3(g)} \rightarrow ClF_2^+{}_{(g)} + F^-_{(g)})$ > 220 kcal mol^{-1}. Mallouk[5] had estimated, by an independent route, this value to be 223 kcal mol^{-1}.

2.22 Lattice enthalpy calculation of $KOsF_6$

A detailed calculation of the lattice enthalpy of $KOsF_6$, for which the structure is accurately known[11], was performed using the methods outlined in Table 2.1 and described in detail in reference (5). $\Delta H°(WF_{6(g)} + e^- \rightarrow WF_6^-{}_{(g)})$ was re-evaluated from thermochemical data of Burgess et al.[12]. They had measured the heats of alkaline hypochlorite hydrolysis of $M^+WF_6^-$ and $M^+MoF_6^-$ salts (M = K, Rb, Cs), and used Kapustinskii's equation[13] to calculate the lattice enthalpies. The newly calculated value for the lattice energy of $K^+OsF_6^-$ was found to be 2 kcal mol^{-1} less exothermic than the value obtained from equation (2), described earlier. This 2 kcal mol^{-1} change in intercept for equation (2) was used in the evaluation of the lattice enthalpies of structurally similar[14] $A^+MF_6^-$ salts listed in Table 2.2. These new lattice enthalpy values were then used, in place of those evaluated by Kapustinskii's equation, to calculate a corrected electron affinity.

2.23 The electron affinity of WF_6

Present studies show that $NO_{(g)}$ and $WF_{6(g)}$ will not react even at -30°C and in solvents such as SO_2ClF. (Although NO and WF_6 are each soluble in this molecular solvent, it is known that $NO^+MF_6^-$ has very low solubility in it). This evidence for the absence of charge transfer interaction between the NO and WF_6 provide for a determination of the lower limit for the electron affinity of $WF_{6(g)}$.

The entropy and lattice enthalpy of $NOWF_6$ can be determined by using equations (2) and (1), respectively: $\Delta H°_{lattice}(NO^+WF_6^-{}_{(c)}) = -134$ kcal mol^{-1}; $S°(NO^+WF_6^-{}_{(c)}) = 56$ cal mol^{-1} deg^{-1}. Therefore, $T\Delta S° = -18$ kcal mol^{-1} at -30°C for the reaction:

$$NO_{(g)} + WF_{6(g)} \rightarrow NO^+WF_6^-{}_{(c)}$$

and the enthalpy change, $-\Delta H°$, must be less than 18 kcal mol^{-1}; otherwise, the reaction would occur spontaneously. Since[15] $\Delta H°(NO_{(g)} \rightarrow NO^+_{(g)} + e^-) = 213(1)$ kcal mol^{-1}, then $-[\Delta H°(WF_{6(g)} + e^- \rightarrow WF_6^-{}_{(g)})] < 97$ kcal mol^{-1}. This differs from the value cited by Compton *et al.* [16], who found a lower limit of 113 kcal mol^{-1} by observing the collisional energy threshold for production of WF_6^- in crossed beams of WF_6 and alkali atoms. This also disagrees with the corrected electron affinity (110 kcal mol^{-1}) described earlier and in Table 2.2. In contrast, Beauchamp *et al.*[17] observed, in cyclotron resonance studies involving $WF_{6(g)}$ and $F^-_{(g)}$ or $Cl^-_{(g)}$, that electron transfer occurred in the former interaction and not

in the latter. Accordingly, they concluded that the electron affinity of $WF_{6(g)}$ had a value of 81(3) kcal mol^{-1}. This is the value which the present studies support.

If we also accept the experimental value of Nikitin *et al.* for $E(PtF_6)$[18] =184(7) kcal mol^{-1} and accept the smooth increase in $E(MF_6)$ which the chemical evidence supports[4] the $E(MF_6)$ values are those listed in Table **4.5**. These values represent an increase of ∿26 kcal mol^{-1} per unit increase in nuclear charge, rather than 23 kcal mol^{-1} suggested many years ago by Bartlett[4].

Although PtF_6^-, and even more so AuF_6^-, have very high ionization potentials they are unable to stabilize cations such as KrF^+[19] and ReF_6^+. Those anions lose F^- to the cation with the resulting decomposition of the salt to the component acid and base. Clearly the greater the exothermicity of the fluoride ion enthalpy (all other terms being equal) the greater is the thermal stability of the salt likely to be. Also, the less exothermic the fluoride-ion affinity of the cation (or the smaller the fluoride-ion separation enthalpy of the donor fluoride) the more stable a salt is likely to be.

The fluoride ion separation enthalpies of several hypervalent fluorides are given in Table **2.3**. The similarity of these values is consistent with a simple bonding model which is comparable to that found in interhalogen compounds and the noble gas difluorides.

One model of the bonding in noble gas fluorides and in other non-metal hypervalent compounds does not include **d** orbitals (their participation is traditionally required by the valence bond model). This view of only minor d orbital participation is supported by a number of theoretical studies[20]. For two linear trans fluorine ligands (F) and a central atom (E), the bonding arises from two equally probable canonical forms $\{(F\text{-}E)^{+}F^{-}$ and $F^{-}(E\text{-}F)^{+}\}$ which give a resonance hybrid; in this case one half negative charge is associated with each fluorine, and each E-F bond order is one half that of an electron pair bond. An equivalent description in molecular orbital terms is the delocalized three-center, four-electron bond. In this model one p orbital on the central atom is combined with a p orbital from each of a pair of trans fluorine atoms to form three molecular orbitals. The lowest energy (bonding) molecular orbital is constructed from the in phase overlap of three p orbitals; the highest energy (anti-bonding) orbital is derived from the out of phase combination of these orbitals. A third molecular orbital is approximately non-bonding and involves contributions from each fluorine but no contribution from the central atom. Four electrons, one from each fluorine and two from the central atom, are used to fill the lowest bonding orbital and the non-bonding orbital. This localizes -0.5 charge on each fluorine atom and the E-F bond order is 0.5, which is identical to the predictions of the resonance hybrid model.

This simple bonding model can explain the close similarity in the fluoride ion donor abilities of XeF_2, XeF_4 and XeF_6. The enthalpy involved in fluoride ion abstraction, $\Delta H°(EF_{x(g)} \rightarrow EF_{x-1}^{+}(g) + F^{-}(g))$ can be obtained from the sum of the energies of three processes, (i) the loss of electron delocalization in the formation of an $(F\text{-}E)^{+}F^{-}$ ion pair, (ii) the contraction in bond length of $(E\text{-}F)^{+}$ and the enhancement of that bond energy, and (iii) the separation of $(F\text{-}E)^{+}$ from F^{-} to infinity. The first process is a measure of the energy advantage of the average canonical form (or the three-center, four electron bond): $[F^{-1/2}\text{-}E^{+}\text{-}F^{-1/2}]$ $\{(F\text{-}E)^{+}\text{-}F^{-}$ and $F^{-}(E\text{-}F)^{+}\}$ over $(F\text{-}E)^{+}F^{-}$ or $F^{-}(E\text{-}F)^{+}$. The delocalization energy has been empirically evaluated for the noble gas difluorides[21] to be near 50 kcal mol^{-1}. This must be a consequence of the 50 kcal mol^{-1} energy of the addition of the electron to two F atoms rather than one.

The process, (ii) contributes exothermically to the F^{-} separation process by less than 2 kcal mol^{-1}.[25] The third process is equivalent to the work of separation of ions from $\sim$2.0 Å to infinity, or $\sim$166 kcal mol^{-1}. The sum, 218 kcal mol^{-1}, is remarkably close to the fluoride ion separation energies of these hypervalent fluorides.

Secondary factors can influence the ordering of the enthalpies which are shown in Table 2.3. The positive charge borne by Xe in XeF_4 is higher than that in XeF_2; as expected, the fluoride ion separation energy of XeF_4 is greater than

that of XeF_2. Although the positive charge on the central atom is even higher in XeF_6, this molecule will release fluoride ion more easily than XeF_2. Steric crowding of the fluorine ligands in XeF_6 probably aids the release of fluoride ion, compensating for the greater charge on Xe.

The low value of the ionization enthalpy of ONF is particularly noteworthy in this list of donors. Clearly, from the known interatomic distances and stretching force constants this molecule is close to being the ion pair ON^+F^-. The lone N-F bond (1.52 Å)[22] alone demonstrates a weaker bond than that which occurs in NF_3 (1.36(2) Å)[23]. At most the N-F bond in ONF is a single electron bond. Evidently the NO bonding approaches that of the N_2 molecules, with maximum π boding between those atoms (N-0 (in ONF)[22] = 1.13 Å; N-N (in N_2)[24] = 1.095 Å). It will be noted that close approach of the F ligand to N would bring the π symmetry electrons (formally non-bonding) of the F into an antibonding π role as far as the N-O bond is concerned. The observed arrangement in ONF and its high basicity may therefore be a consequence of this maximizing of NO π bonding and minimizing of F-N antibonding π influences on that bond. In particular the ionization:

$$(ONF_{(g)} \rightarrow ON^+_{(g)} + F^-_{(g)})$$

does not involve the loss of resonance energy such as is typical of the hypervalent species. In this case the electron of the F^- is already largely localized on that atom in the gaseous molecule.

A surprising finding is the close similarity in the fluoride ion separation enthalpies of IF_7 and ReF_7 and those of the noble gas fluorides. The enthalpies of fluoride ion abstraction are consistent with the value predicted from the delocalized bonding model. This implies that the amount of d orbital participation is not great. In IF_7, it may be argued that because the d orbitals are high in energy, the promotion energy required to involve them in bonding, to form something like an sp^2d^3 hybrid, is very great. Because d orbitals are ordinarily available for bond formation in the case of rhenium it has usually been supposed that the bonding in ReF_7 involved seven electron-pair bonds, the valence bond description using an appropriate combination of s, p and d functions of the Re atoms. This observed similarity of IF_7 and ReF_7 suggests similar bonding for both. Perhaps the high ligand field produced by the seven small electronegative F ligands not only contracts the outer d orbitals of iodine to some small participation in the bonding of IF_7 but also contracts those of Re to significantly reduce their importance to the bonding in ReF_7.

2.3 Experimental

2.31 Reaction of IF_7 with BF_3

Iodine heptafluoride (stored over NaF), and boron trifluoride (Ozark Mahoning, Tulsa OK) were used after the high purity had been established by infrared spectroscopy. A small, thick-walled quartz tube, similar to thermometer tubing (1.25 mm i.d., 0.334 ml volume), was employed to allow for higher pressures and a minimal amount of dead space in the reactor. BF_3 and IF_7 were sequentially condensed at -196°C in 4:1 molar ratio (net pressure, 36 atm). Raman spectra were obtained using a Jobin-Yvon HG2S Ramanor Spectrophotometer and a krypton (647.1 nm) ion laser. For lower temperatures, samples were held in a stream of cold nitrogen (jacketed by warm nitrogen to prevent ice formation). At -60°C Raman spectra showed vibrational bands which can be assigned to IF_6^+ (ν_1: 735, ν_2: 711, ν_5: 343 cm^{-1}).

2.32 Reaction of NO with WF_6

1:1 molar ratios of NO and WF_6 were condensed into a quartz capillary. NO and WF_6 alone were not observed to react under these conditions. SO_2ClF was then condensed into the reactor as a solvent, to promote reaction. At -30°C, no new vibrational bands were observed by Raman spectroscopy; unreacted SO_2ClF and WF_6 were visible.

2.33 Reaction of SF_4 with $IF_6^+AsF_6^-$

$IF_6^+AsF_6^-(c)$ was prepared by 1:1 condensation of IF_7 and AsF_5 in a 1/4" o.d. quartz tube at -196°C. SF_4 was then condensed

onto the salt to provide a final stoichiometry of 1:1: :SF_4:$IF_6^+AsF_6^-$. The reactor was allowed to reach room temperature before cooling to -30 °C. This temperature cycle was used in subsequent reactions to promote the reaction. Product composition was obtained from Raman spectroscopy at -30 °C using an Ar^+ exciting line. Addition of more SF_4 to the same sample resulted in increased Raman band intensities of SF_3^+ (ν_1 (strong)= 947, ν_3 (weak) = 928, ν_2(weak) = 534 cm^{-1}) at the cost of those of IF_6^+ (ν_1 (vstrong) = 730, ν_2(weak) = 710, ν_5 (weak) = 342 cm^{-1}):

$$IF_6^+AsF_6^-(c) + SF_{4(g)} \rightarrow IF_{7(g)} + SF_3^+AsF_6^-(c)$$

(see Figure 2.1). This was then countered by the addition of excess IF_7 (3:1::IF_7:$SF_3^+AsF_6^-$); $IF_{7(g)} + SF_3^+AsF_6^-(c) \rightarrow IF_6^+AsF_6^-(c) + SF_{4(g)}$. The reversibility of this reaction indicates that the system in near equilibrium at -30 °C.

2.34 Reaction of SF_4 with $ClF_2^+AsF_6^-$

$ClF_2AsF_{6(c)}$ was prepared by condensing equimolar amounts of ClF_3 and AsF_5 in a 1/4" o.d. quartz reaction tube. SF_4 was then added, following the same procedures as those outlined above for the reaction of SF_4 with $IF_6^+AsF_6^-$. ClF_3 was displaced by the SF_4 but the reverse reaction could not be achieved, demonstrating that the system was not near equilibrium.

Table 2.1 Lattice Enthalpy of $KOsF_6$

Space group: R3 Unit cell‡ : a= 7.487(1), c= 7.487(1) Å
Z= 3

Atom	Atomic Positions	Charge [32] q_j
K (b)	(0.5, 0.5, 0.5)	1.00
F (f)	(0.717(5), 0.789(5), 0.103)	-0.2152
Os (a)	(0,0,0)	0.2912

	a	b	c	d
	U_{elec}	U_{dd}	U_{dq}	U_r
kcal mol^{-1}	140.64	31.95	3.83	40.26

	e	f	
	U_z	U_L(0K)	$\Delta H_L°$(298K)
	0.2	135.96	136.26

(the basic radius r_F = 1.100 Å)

Table 2.1 References

‡ M.A. Hepworth, K.H. Jack and G.J. Westland, **J. Inorganic and Nuclear Chemistry** 2, 79 (1956).

a $U_{elec} = \frac{18\pi R^2}{V} \sum_{hk\ell} |F(hk\ell)|^2 \frac{(\sin\alpha - \alpha\cos\alpha)^2}{\alpha^8} - 3/5R \sum_j q_j^2$

where $F(hk\ell) = \sum_j q_j \exp(2\pi i\, \underline{h}\cdot\underline{r}_j)$, $\alpha = 2\pi R/d_{hk\ell}$, q_j is the charge on atom j [obtained using the electronegativity equalization procedure of Jolly and Perry (**Inorg. Chem.** 13, 2686 (1974))], $\underline{h}\cdot\underline{r} = hx_j + ky_j + \ell z_j$, and x_j, y_j, z_j are the fractional coordinates of atom j. R is one half the shortest interatomic distance in the crystal, $d_{hk\ell}$ is the distance between hkℓ lattice planes and V is the volume of the unit cell. In all calculations enough terms are included in the infinite sum over all hkℓ reciprocal vectors so that the series termination error introduced is less than 0.8 kcal mol^{-1}. The sum over j includes the atoms in one unit cell.

Variations of the charge, q_j, within reasonable limits produced small (1-3%) variations in the electrostatic component of the lattice enthalpy.

b $U_{dd} = -3/2\ \Sigma_{i=j}\ \alpha_i\alpha_j\varepsilon_i\varepsilon_j/(\varepsilon_i + \varepsilon_j)\ r_{ij}^{-6}$

where α and ε are respectively the polarizability and characteristic energy of the ion.

c U_{dq} is given by a summation in r_{ij}^{-8}; it is however, generally 10 to 15% of U_{dd}. In this case it is taken as 0.12 U_{dd}.

d The Born and Mayer equation (**Z.Physik**, 75, 1(1932))was used:

$$U_r = \Sigma_{i\neq j}\ (1 + q_i/n_i + q_j/n_j)\ \exp\{(r_i + r_j - r_{ij})/\rho\}$$

n is the number of electrons in the outer shell of the ion, q is the charge on the ion, r is its "basic radius" and r_{ij} is the distance between i and j. The constants b and ρ have the values of 10^{-12} erg molecule^{-1} and 0.333 Å respectively. The central atom in both the cation and anion were assumed to make no contribution to U_r. Variation of ρ between 0.333 and 0.360 Å produced a variation of less than 2 kcal mol^{-1} in the lattice enthalpy. Likewise, a variation of $U_{dd} + U_{dq}$ by 20% ($\sim$10 kcal mol^{-1}) produced a change in the calculated lattice enthalpy of less than 3 kcal mol^{-1}, because of the compensating changes induced in U_r.

e For relatively large, massive ions such as these in $EF_6^+MF_6^-$ crystals the zero point energy is small: $U_z \approx 0.2$ kcal mol^{-1}.

f $U_L = U_{elec} + U_{dd} + U_{dq} - U_r - U_z$

Table 2.2 Adjustments to Thermochemical Data‡				
	Molecular Volume ($Å^3$)	**Original**† $\Delta H_L°$ kcal mol^{-1}	**Revised*** $\Delta H_L°$	Electron Affinity $MF_{6(g)}$ (revised)
KWF_6	131.5	128	133(2)	111(3) kcal mol^{-1}
$RbWF_6$	132.9	125	133(2)	110(3)
$CsWF_6$	147.9	121	129(2)	110(3)
$KMoF_6$	128.9	129	134(2)	117(3)
$RbMoF_6$	131.0	126	134(2)	118(3)
$CsMoF_6$	145.8	122	130(2)	117(3)

‡ Corrected from original data of reference (12)

† From Kapustinkii's equation, used for the lattice enthalpy determination of reference (12).

* This Work

Table 2.3 Enthalpies of fluoride ion separation from IF_7, ReF_7 and other fluorides

Process	$\Delta H°$(kcal mol^{-1})	Reference
$ReF_{7(g)} \rightarrow ReF_6^+(g) + F^-(g)$	213(5)	(a)
$IF_{7(g)} \rightarrow IF_6^+(g) + F^-(g)$	208(6)	this work
$XeF_{6(g)} \rightarrow XeF_5^+(g) + F^-(g)$	209	(b)
$XeF_{4(g)} \rightarrow XeF_3^+(g) + F^-(g)$	221	(b)
$XeF_{2(g)} \rightarrow XeF^+(g) + F^-(g)$	217	(b)
$SF_{4(g)} \rightarrow SF_3^+(g) + F^-(g)$	211(8)	(c)
$ONF_{(g)} \rightarrow ON^+(g) + F^-(g)$	188(1)	(d)(e)

Table 2.2 References

(a) N.Bartlett, S.Yeh, K.Kourtakis, T.Mallouk, **J. Fluorine Chem.** 26, 97-116 (1984).

(b) J. Berkowitz, W.A. Chupka, P.M. Guyon, J.H. Holloway and R.Spohr, **J. Phys. Chem.** 75, 1461 (1971).

(c) T.E. Mallouk, G.L. Rosenthal, G. Muller, R. Brusasco and N.Bartlett, **Inorg. Chem.** 23, 3167-3173 (1984).

(d) JANAF Thermochemical Table, Dow Chemical Co., Mich. 1971.

(e) H.S. Johnston, H.J. Bertin, **J. Am. Chem. Soc.** 81, 6402 (1959) **J. Mol. Spectroscopy** 3, 683 (1959).

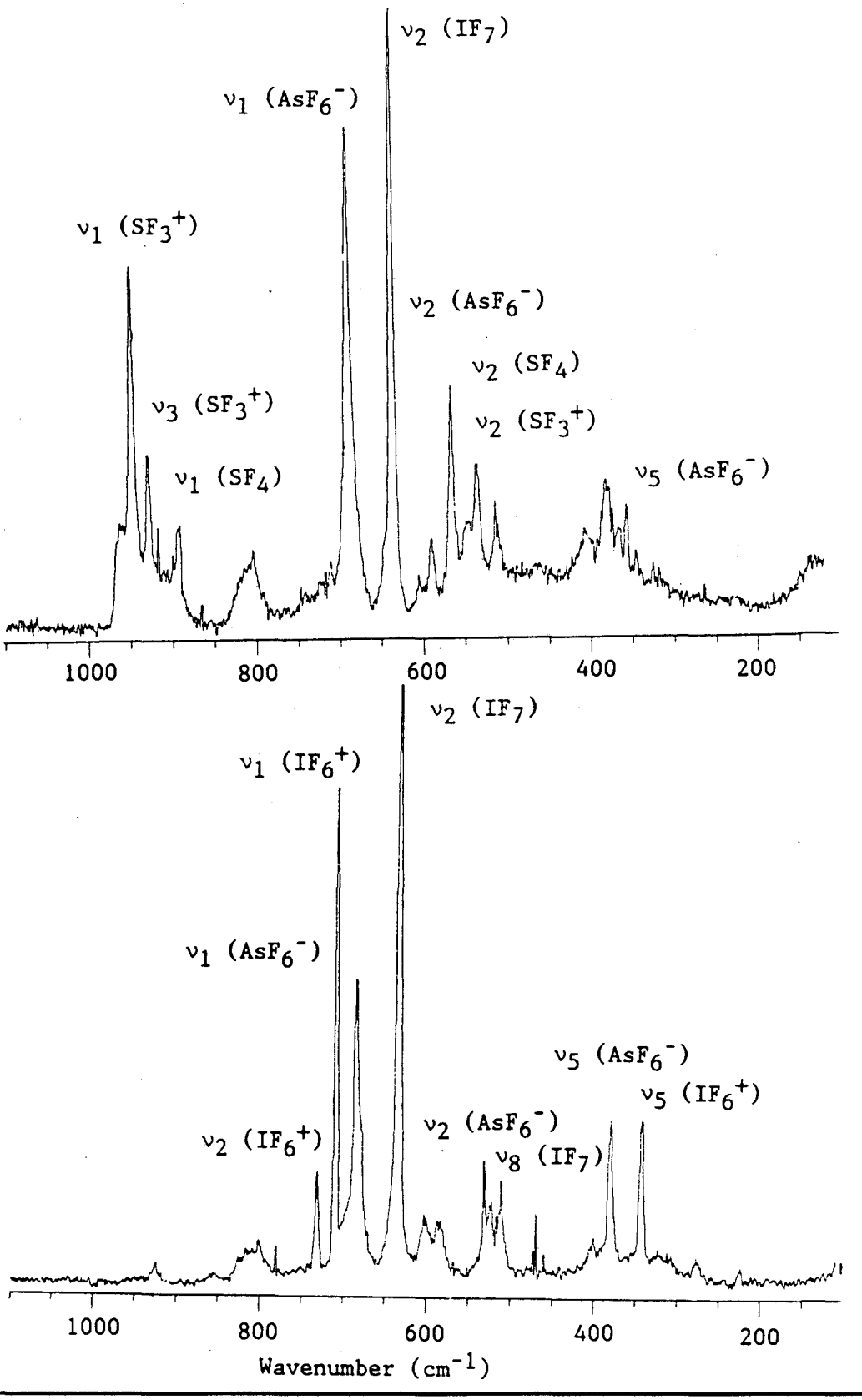

Figure 2.1 Raman Spectra indicating the equilibrium $SF_{4(g)} + IF_6^+AsF_6^-(c) \rightarrow IF_{7(g)} + SF_3^+AsF_6^-(c)$

Chapter 2 References

1. N.Bartlett and D.H. Lohmann, **Proc. Chem. Soc.** 115 (1962).

2. N. Bartlett, **Proc. Chem. Soc.** 218 (1962).

3. N.K. Jha, Ph.D. Thesis, University of British Columbia (1965); S.P. Beaton, Ph.D. Thesis, University of British Columbia (1966); N. Bartlett, S.P. Beaton and N.K. Jha, **Chem. Comm.** 168 (1966).

4. N. Bartlett, **Angew. Chem. Int. Ed.** 7 (6), 433 (1968).

5. T.E. Mallouk, G.L. Rosenthal, G. Müller, R. Brusasco and N. Bartlett, **Inorg. Chem.** 23, 3167 (1984); T. Mallouk, Ph.D. Thesis, U.C. Berkeley (1982).

6. F. Seel and O. Detmer, **Z. Anorg. Chemie** B301, 113 (1959).

7. National Bureau of Standards, Technical Notes 270-3 (1969).

8. E.F. Bertaut, **J. Phys. Radium** 13, 499 (1952).

9. D.H. Templeton, **J. Chem. Phys.** 21, 1629 (1955).

10. This value was precisely calculated based upon a structure derived from powder diffraction data by Bartlett and Beaton; N. Bartlett, S. Yeh, K. Kourtakis and T. Mallouk, **J. Fluorine Chem.** 26, 97-116, (1984).

11. M.A. Hepworth, K.H. Jack and G.J. Westland, **J. Inorganic and Nuclear Chemistry** 2, 79 (1956).

12. M. Burgess, I.H. Haigh, R.D. Peacock and P. Taylor, **J.C.S. Dalton** 1064 (1974).

13. A.F. Kapustinskii, **Zh. Fiz. Khim.** 5, 59 (1934).

14. Cell parameters and hence the formula unit volumes of the alkali hexafluorotungstates and hexafluoromolybdates are accurately known from powder diffraction data (reference 3).

15. E. Miescher, **Can. Journal of Phys.** 54, 2074 (1976).

16. R.N. Compton, P.W. Reinhardt and C.D. Cooper, **Journal of Chem. Phys.** 68, 345 (1979).

17. P.M. George and J.L. Beauchamp, **J. Chem. Phys.** 36, 345 (1979).

18. M.I. Nikitin, L.N. Sodorov, and M.V. Kordoov, **Int. J. Mass Spec. Ion Phys.** 37, 13 (1981).

19. N. Bartlett and F.O. Sladky, "The Chemistry of Krypton, Xenon and Radon", chapter in Comprehensive Inorganic Chemistry, Permagon Press, Oxford and New York, 1972, p. 213.

20. W. Kutzelnigg, **Angew. Chem.** 96, 282 (1984); **Angew. Chem. Int. Ed. Engl.** 23, 272 (1984); A. Reed and F. Weinhold, **J. Am. Chem. Soc.** 108, 358 (1986). Original references on the three-center, four-electron bond include: G.C. Pimmentel, **J. Chem. Phys.** 19, 446 (1951); K.S. Pitzer, **Science** 139, 414 (1963); R.E. Rundle, **Rec. Chem. Progr.** 23, 195 (1962) and J. Musher, **Angew. Chem.** 81, 68 (1969).

21. M. Wechsberg, P.A. Bulliner, F.O. Sladky, R. Mews and N.Bartlett, **Inorg. Chem.** 11, 3063 (1972).

22. R. Schmutzler, **Angew. Ch. Int. Ed.** 7, 440 (1968).

23. "Tables of Interatomic distances," **Chem. Soc. of London** (1959).

24. H.H. Sisler in "Comprehensive Inorganic Chemistry," D.Van Nostrand, Princeton N.J. (1956).

25. The bond length of XeF^+, 1.84 Å [26], is shorter than that of XeF_2, 2.00 Å [27]. The force constant[28] of $XeF^+_{(g)}$ is 3.7 mdyn/Å. The energy change of this contraction should be roughly the product of the force constant of $XeF^+_{(g)}$ and the square of the change in bond distance (0.16 Å). This energy change is essentially negligible.

26. S. Reichman and F. Schreiner, J. Chem. Phys. 51, 2355 (1969).

27. V.M McRae, R.D. Peacock and D.R. Russell, **Chem. Communs.** 26 (1969).

28. F.O. Sladky, P.A. Bulliner and N.Bartlett, **J. Chem. Soc.** 2179 (1969).

Chapter 3

Low Oxidation State Chlorine FLuorides

3.1 Introduction

The transient existence of the molecule Cl_3F had been postulated based on prior work in this laboratory. In their investigations of the interaction of Cl_2 and IrF_6 Graham[1] and Richardson[2] found that the first-formed blue solid of approximately 1:1 stoichiometry decomposed spontaneously through a sequence of products, ending with Ir_4F_{20}.

The initial blue 1:1 solid :

$$Cl_2 + IrF_6 \rightarrow Cl_2^+IrF_6^-$$

is formulated as the dichlorinyl salt on the basis[2] of ESR spectroscopy. At ordinary laboratory temperatures this salt rapidly decomposes and Raman spectroscopy shows the solid product to be $Cl_3^+IrF_6^-$:

$$3Cl_2^+IrF_6^- \rightarrow 2Cl_3^+IrF_6^- + IrF_6$$

with neutral Cl_2 so formed interacting with two adjacent Cl_2^+ cations in the lattice to generate the trichlorine cation, the remaining molecular IrF_6 then escaping.

In each of subsequent decompositions towards Ir_4F_{20} there is a net elimination of Cl_3F. The sequence is probably as follows:

$$2\ Cl_3^+IrF_6^- \rightarrow Cl_3^+Ir_2F_{11}^- + [Cl_3F]$$

$$2\ Cl_3^+Ir_2F_{11}^- \rightarrow Cl_3^+Ir_4F_{21}^- + [Cl_3F]$$

$$Cl_3^+Ir_4F_2^{1-} \rightarrow Ir_4F_{20} + [Cl_3F]$$

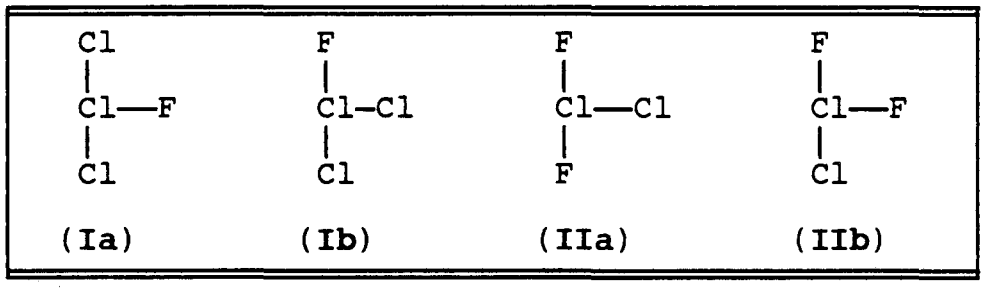

(Ia) **(Ib)** **(IIa)** **(IIb)**

The formation of Cl_3F by fluoride ion addition to Cl_3^+ (**Ia,Ib**) would produce an equatorial fluorine if a "T" type structure, analogous to that of ClF_3, were obtained. According to the bonding schemes advanced by Rundel[3a] and Pimentel[3b] which are described in Chapter 2, axial bonding can be represented in terms of only p orbitals, which form a set of three-center, four-electron bonds; equatorially, a normal electron pair bond is formed. The axial ligands each bear one half negative charge by virtue of the non-bonding molecular orbital of the three-center, four-electron bond. Because of this increased electron density, more electronegative ligands will substitute preferentially at these positions. This has been recently reviewed for a large number of molecules by Burdett[4]. From this perspective, Cl_3F formula (**Ia**) would perhaps be at an energetic disadvantage compared with FCl_2Cl (formula **Ib**).

Following the reasoning above, a molecule Cl_2F_2 (formula **IIa**) in which the fluorines are axial would be more favorable than the Cl_3F species previously discussed. Precise calcula-

tions[5] on a "T" shaped Cl_2F_2 molecule indicates that this geometry is favored over one in which the fluorine occupies the equatorial position (**IIb**). Cl_2F_2 (**IIa**) was also found to be 16 kcal mol^{-1} more stable towards dissociation into 2ClF than Cl_3F (**Ia**) is towards and Cl_2 + ClF.

The reaction of ONCl with $ClF_2^+AsF_6^-$ can involve attack of Cl^- on the bent ClF_2^+ center to produce F_2ClCl (**IIa**). The advantage of this reaction scheme is that the chlorine can be placed directly on an equatorial site. An additional feature is that axial fluorines localize more positive charge on the central atom than there is in Cl_3^+ (in $Cl_3^+IrF_6^-{}_{(s)}$), thereby enhancing the probability of the desired reaction at the central chlorine.

For the proposed reaction,

$$ONCl_{(molecule)} + ClF_2^+AsF_6^-{}_{(s)} \rightarrow NO^+AsF_6^-{}_{(s)} + Cl_2F_{2(g)}$$

the number of moles of gas in reactants and products is the same; therefore, $T\Delta S^\circ \approx 0$ and $\Delta G^\circ = \Delta H^\circ$. Since the lattice energy of $ClF_2^+AsF_6^-{}_{(s)}$ is only slightly less exothermic than that of $NO^+AsF_6^-{}_{(s)}$, because the size of ClF_2^+ is slightly greater than that of NO^+, then $\Delta H^\circ(ONCl_{(g)} \rightarrow NO^+_{(g)} + Cl^-_{(g)})$ must be more than offset by $\Delta H^\circ(ClF_2^+{}_{(g)} + Cl^-_{(g)} \rightarrow Cl_2F_{2(g)})$. This chloride ion affinity should be quite large, since the affinity of $ClF_2^+{}_{(g)}$ for small F^- is more than 220 kcal mol^{-1} exothermic (see in Chapter 2).

Recently, Marsden[5] has performed <u>ab initio</u> calculations to predict the structures of Cl_2F_2, Cl_3F and Cl_4. All deri-

vatives were found to be thermodynamically unstable with respect to dissociation into mixtures of ClF and F_2. These predicted geometries, however, were based on substitutional variations of the "T"-shaped ClF_3 molecule; the angles and bond lengths of these "T"-shaped structures were adjusted to obtain maximum stability. In addition, the theoretical findings do not preclude kinetic stability. Preliminary work[6] in calculating transition state energetics has shown that even for a "T"-shaped ground state geometry, the transition state geometry can impart kinetic stability to the thermodynamically unstable adducts. A kinetic pathway is possible that will permit the formation of an unstable adduct, and which can then trap it in an energy well that can support at least one vibrational level.

3.2 Experimental

3.21 ClF_2AsF_6 was prepared by the reaction of equimolar quantities of ClF_3 (Mattheson Products) and AsF_5 (Ozark Mahoning), the former being stored over NaF to remove HF. The high purity of both gases was assured by infrared spectroscopy prior to their use. No purification of AsF_5 was required. The salt was formed at the bottom of a 1/4" sapphire tube (Saphikon, Inc.) fitted with a Whitey (KS4) low pressure valve. A Raman spectrum could be obtained through the sapphire tube which was passivated with ClF_3 prior to use. No deterioration or surface coatings on the sapphire tubes were

visible as a consequence of any reactions; these reactors proved to be inert to all fluoride compounds for long time periods. In order to obtain enough condensate for the low temperature Raman spectra, a 140 ml stainless steel can was attached to sapphire tube as a reservoir.

3.22 ONCl was freshly prepared for each experiment by the mixing of equimolar amounts of nitric oxide and chlorine at room temperature. Cl_2 (Mattheson Gas, Research Grade (99.965 mole %)) was stored over P_2O_5 to remove any moisture. NO (Mattheson products) was purified by trap to trap distillation from -150°C to -190°C to remove any N_2O_4 impurities. The ONCl prepared in this manner was shown by infrared spectroscopy to be free of undesirable contaminants, prior to each reaction with $ClF_2^+AsF_6^-{}_{(s)}$.

3.23 $Cl_2F^+AsF_6^-{}_{(s)}$ was prepared by the reaction of 2ClF with AsF_5, as reported by Christie[7]. The product was characterized by infrared spectroscopy and X-ray powder photographs.

3.24 Raman spectra were obtained with a Jobin Yvon HG2S spectrophotometer. It was found that Kr^+ irradiation (Spectra Physics 100 mW i.o.p., signal averaged 5-10 times, 1.0 cm^{-1} sec^{-1}, 647.2 nm exciting line) yielded the best spectroscopic results. Typically, signals were accumulated over ten sweeps to yield optimal signal to noise ratios.

The low temperature cell utilized is shown in Figure 3.1. The construction included a copper sample block holder which was in contact with the sapphire tube. Because of the excellent thermal conductivity of sapphire, the temperature gradient along most of the sapphire tube was minimal. A thermocouple was placed at the very base of the tube for temperature measurements.

The copper block was cooled by a stream of nitrogen gas which had been passed through a several windings of copper coil immersed in liquid nitrogen. By appropriate adjustment of the nitrogen flow rate, the temperature could be precisely varied. The entire apparatus was wrapped in several layers of insulating material. The lowest temperature obtained by this method was -130°C.

To prevent ice formation on the sample tube, which would block entry of the laser light for Raman measurements, the inner compartment was evacuated with a small mechanical pump. Warm air was blown across the outside of the enclosure to keep this area ice-free as well, since the amount of ice which would form otherwise is quite considerable at these temperatures.

The windows through which the laser exciting line entered and exited, at right angles, were made of sapphire, which is relatively transparent in the frequency regions of interest.

3.3 Results

3.31 Reaction of ONCl + $ClF_2^+AsF_6$

In order to achieve complete reaction with $ClF_2^+AsF_6^-{}_{(s)}$ while at the same time providing for the trapping of a volatile intermediate which is thermally unstable, the nitrosyl chloride was melted onto the salt by repeated temperature cycling of the sapphire tube from -110°C to -50°C. With each such thermal cycle, the progress of the reaction could be observed in the low temperature Raman spectra. The reaction is slow at these temperatures. At least three vibrational peaks, and, for intense spectra, as many as six modes were attributed to the eliminated Cl_2F_2 from the reaction. The vibrational bands were observed to increase in intensity with cycling. At room temperature, these bands disappear. Infrared spectra of the volatiles produced show an intense ClF vibration band. Since ClF is relatively weak in the infrared, an intense spectrum denotes high ClF concentrations. ClF is therefore a decomposition product of Cl_2F_2. Low temperature Raman spectra of ClF, ONCl, ONF, NO and Cl_2, mixtures of ONCl + Cl_2, $ClO_2^+AsF_6^-$, ClF_3, AsF_5 and AsF_3 were taken under identical conditions in the low temperature cell. From this, the production of each of these potential side products can be ruled out. After several trials, it was found that best results could be obtained by allowing the reaction to proceed in the low temperature spectroscopic cell over a period of several hours with repeated temperature cycles. Debye

Scherrer X-ray photographs of the solid produced indicated the product was $NO^+AsF_{6(s)}$.

3.32 Reaction of ONF + Cl_2FAsF_6

With time, $Cl_2F^+AsF_6^-$ will disproportionate to $ClF_2^+AsF_6^-$ and $Cl_3^+AsF_6^-$. It was evident that in our product some disproportionation had occurred. Upon reaction with ONF, there was no evidence of vibrational bands indicative of Cl_2F_2 formation at -110 °C. Extensive temperature cycling was not necessary because ONF is a liquid at -100°C. Figure 3.7 shows the Raman spectrum of this reaction.

3.33 Mass Spectroscopy

Several attempts were made to detect the unstable Cl_2F_2. Detection of the related molecule ClF_3 was used as a test. Even this task presented some problems. With sufficient passivation of the source (this was accomplished by passing small amounts of ClF_3 through the source for several hours), ClF_3 fragments were visible. Cl_2F_2 proved to be too unstable for these experiments, even when the reactor was prevented from warming up during the source passivation, prior to the addition of its contents to the mass spectrometry chamber.

Another difficulty in these experiments is the temperature of the species at the source and detector. This was probably much greater than the dissociation temperature of Cl_2F_2 (approximately -30°C).

3.34 High Pressure Reaction of ClF

A small narrow bore monel tube, of inner volume 0.6 ml, fitted with a high pressure Autoclave valve was used. ClF was condensed into the tube at -196°C while agitating the reactor so that the liquid/solid filled the opening of the bore. The pressure inside the reactor was about 11,500 psi at 25°C. After reaction for 12 hours, the volatiles were quickly condensed into a 1 liter Monel bulb at -196°C. The container was then held at -78°C and briefly placed under vacuum to remove ClF. Since ClF_3 is solid at this temperature, most likely Cl_2F_2 would be as well. Afterwards, the bulb was immersed in a liquid nitrogen bath and connected to an infrared cell which was then positioned in the infrared spectrophotometer. Infrared spectra of the volatiles were continuously taken as the bulb warmed to room temperature. Neither Cl_2F_2 nor ClF was detected.

3.4 Discussion

From the interaction of $F_2Cl^+MF_6^-$ + ONCl → $NO^+MF_6^-$ + F_2Cl_2, the Raman spectra of which are illustrated in Figures **3.2** and **3.4**, it appears that the Cl_2F_2 product is not a molecule of the type represented by (**IIa**). This is apparent from the comparison of the bands, a, b, c, at 794(1), 752(1) and 673(1) cm^{-1}, with the spectrum of ClF_3 shown in Figure **3.6**. The symmetric stretching vibration characteristic of the

axial species F-Cl-F (in ClF_3) is observed strongly at approximately 517 cm^{-1}. There is no such band for the Cl_2F_2 product. One can conclude, therefore, that the sought after configuration (**IIa**) has not been made. On the other hand the symmetric stretching associated with the equatorial Cl-F of ClF_3 and that of Cl-F monomer itself both occur at 759 cm^{-1}. This clearly represents the stronger bonding associated with the electron-pair bond. The product "Cl_2F_2" does exhibit a broad strong absorption (b) in this same region. Yet there are other bands (a) and (c) which do not occur in Cl-F condensed at the temperatures used in these studies. Since (a), (b) and (c) increase in intensity together as the reaction proceeds they appear to belong to one species. It may be that the "Cl_2F_2" molecule is initially of form (**IIa**) but readily undergoes an intramolecular rearrangement which in essence produces two ClF molecules trapped in the space originally inhabited by (**IIa**). This "trapped dimer" may have the form represented in (**III**):

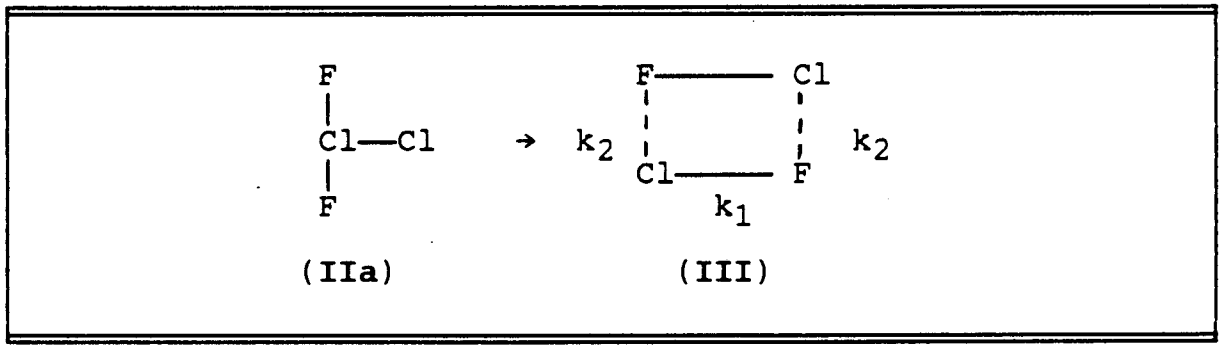

The vibrations of (**III**) involve coupling of the Cl-F stretching both in phase and out of phase. This could be the origin of the bands a and c at 794(1) and 673(1) cm^{-1}. This is shown in **IV** and **V**:

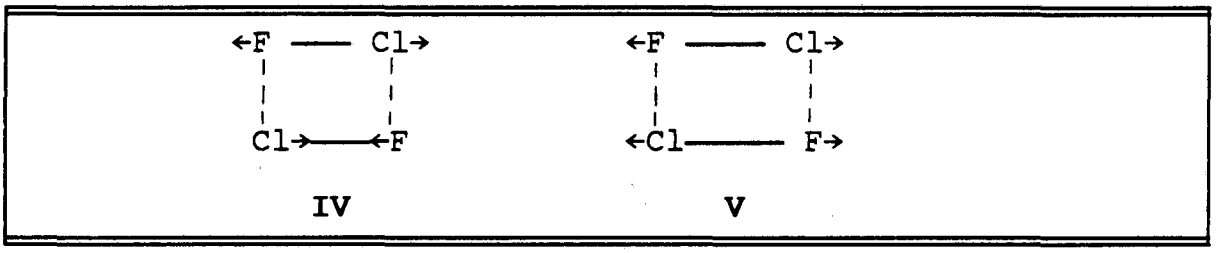

IV **V**

In any case a molecule of form (**IIa**) is not made in experiments such as these.

Our inability to prepare the adduct using alternative reactions shows the importance of kinetic considerations in choosing an appropriate synthetic route. For example, it is not possible to synthesize Cl_2F_2 from the high pressure reaction of ClF, since it is a reversal of the kinetic pathway to thermal decomposition; this would be driving the reaction energetically uphill. The absence of reaction of ONF with $Cl_2F^+AsF_6^-$ salts can be attributed the decreased positive charge at the central chlorine, because the fluorine atom in ClF_2^+ is replaced by a less electronegative chlorine atom. In this case, there are alternative sites introduced for attack by the Cl^- which would not produce Cl_2F_2.

Cl_2F_2 will decompose, as indicated in the Raman spectra, at temperatures higher than -30°C. Assuming that the dimer is

not kinetically trapped in the $ClF^+_AsF_6^-$ salt, this means $\Delta G°_{243}$ ($Cl_2F_2 \rightarrow 2ClF$)$\leq$ 0. If we make the rough approximation that the entropy of Cl_2F_2 is close to that of ClF_3 (67.3 cal mol^{-1} deg^{-1}), then at -30°C, $T\Delta S°$= 9 kcal mol^{-1}. Thus, -($\Delta H°$) for the dissociation is greater than 9 kcal mol^{-1}. Marsden has calculated the enthalpy of the transformation of (**IIa**) to 2ClF to be 17 kcal mol^{-1} using the SCF Hartree-Fock method for the geometry and second-order perturbation theory to include electron correlation. In these calculations, the geometry of Cl_2F_2 is "T"-shaped, with the chlorine ligand filling the equatorial site. However, as mentioned previously, a low energy vibrational mode should be able to convert it to a distorted square geometry. The energy of the square configuration would then be close to that of the "T" geometry, in which case the experimental observations are in reasonable agreement with theoretical predictions.

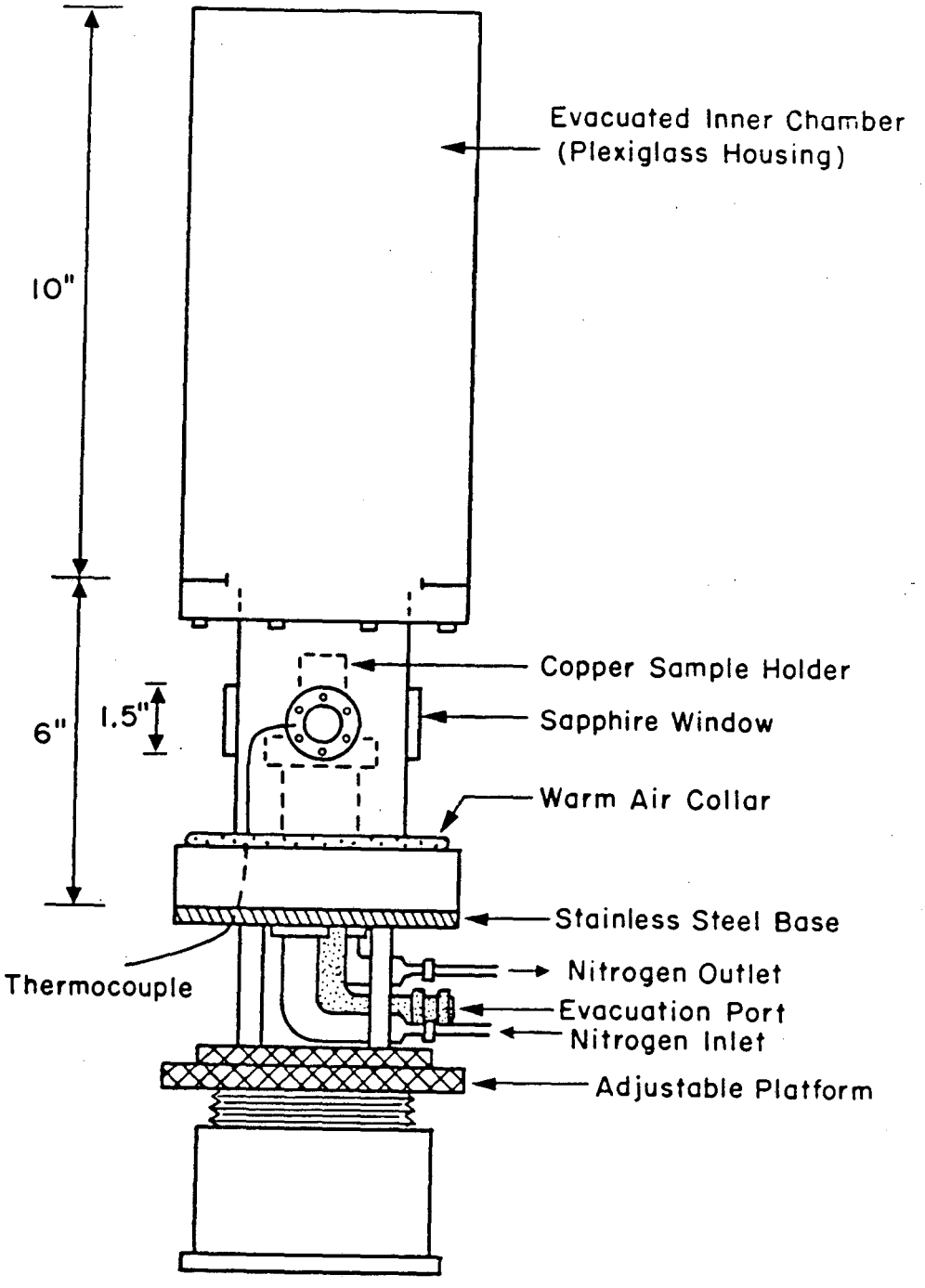

Figure 3.1 Low Temperature Raman Cell

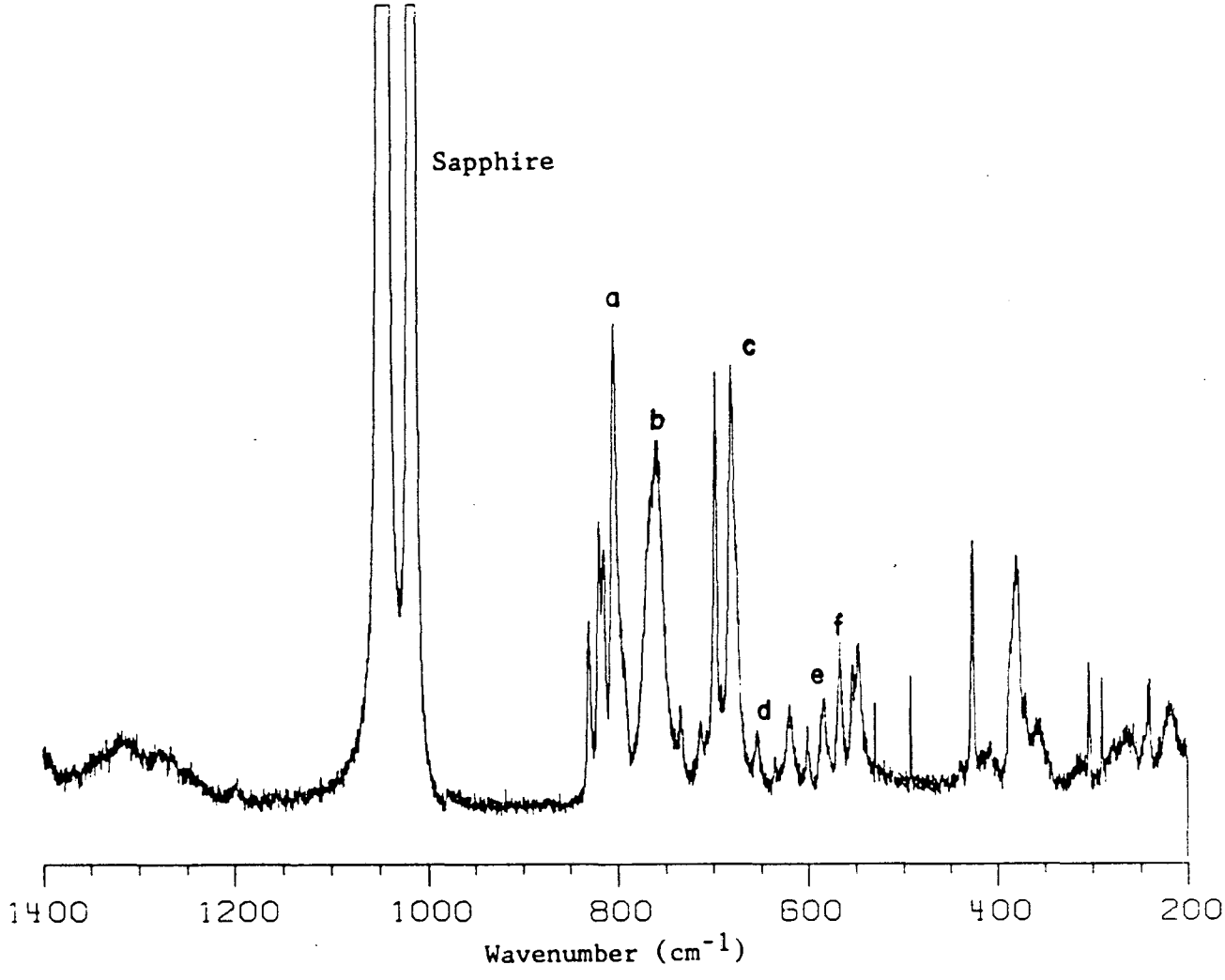

Figure 3.2 Raman Spectrum of the reaction:

$ONCl_{(g)} + ClF_2^+AsF_6^-{}_{(s)} \rightarrow NO^+AsF_6^-{}_{(s)} + Cl_2F_{2(g)}$

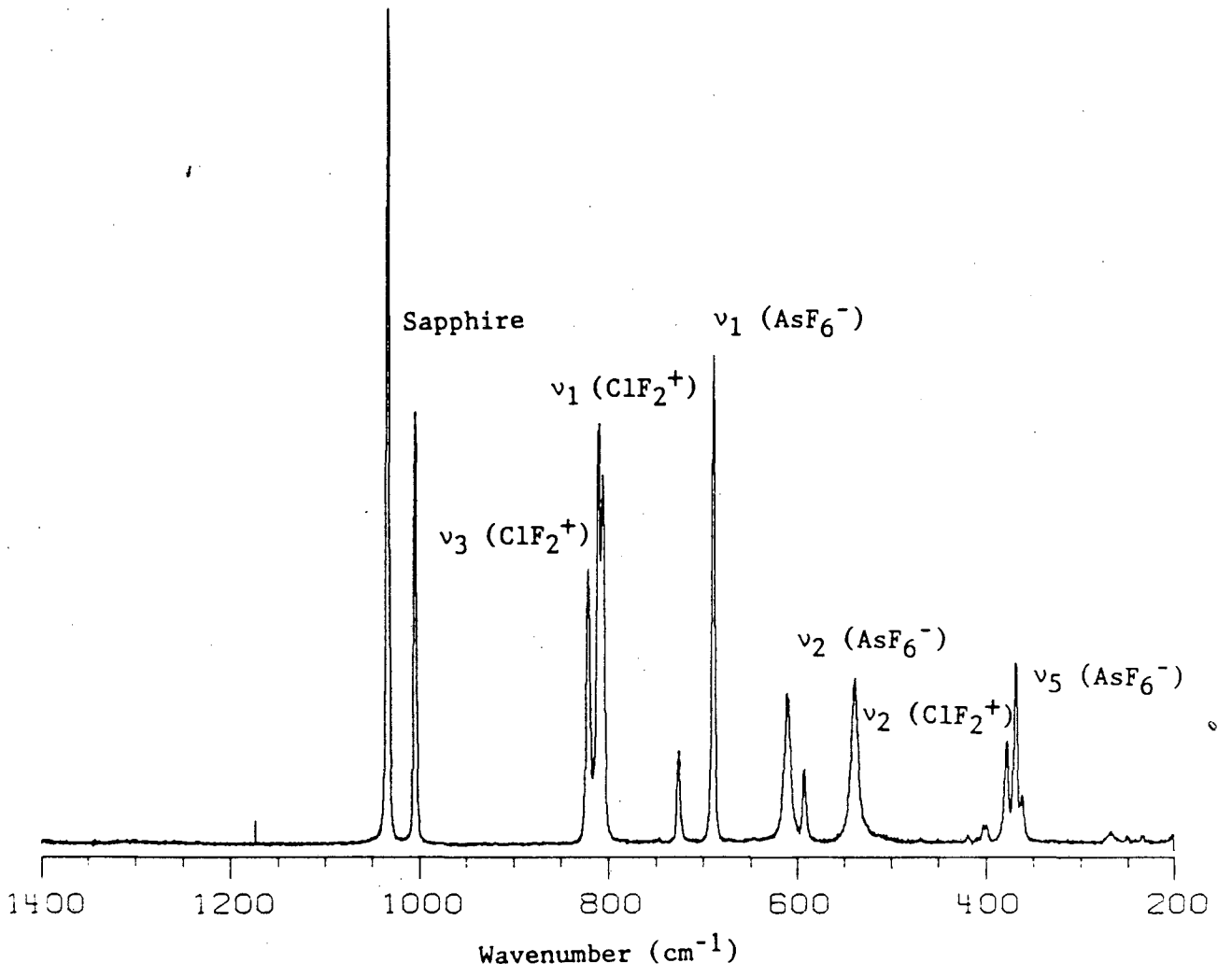

Figure 3.3 Raman Spectrum of $ClF_2^+AsF_6^-(s)$ at -100 °C

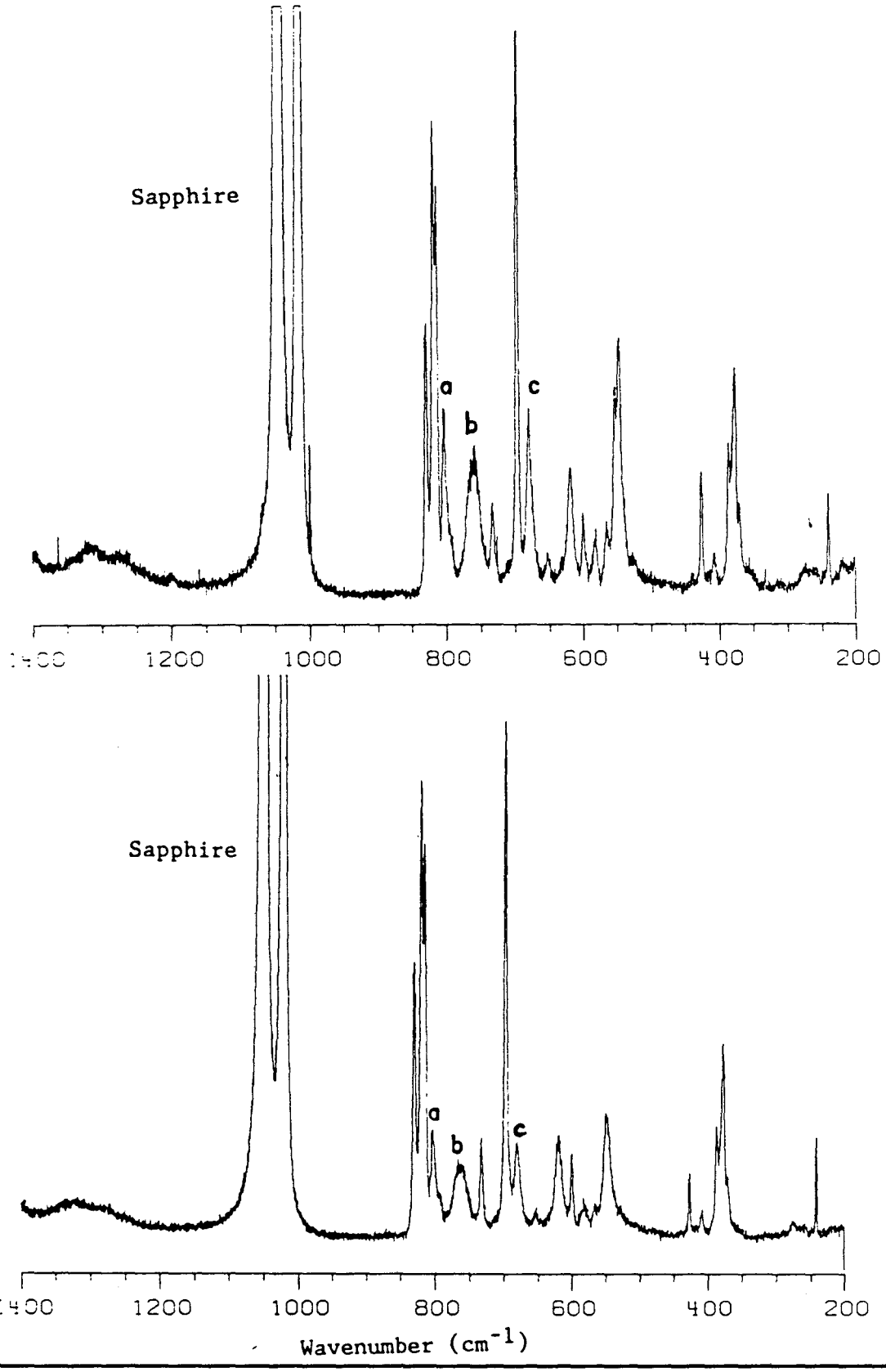

Figure 3.4 Raman Spectra showing the reaction progress [$ONCl_{(g)} + ClF_2^+AsF_6^-{}_{(s)} \rightarrow NO^+AsF_6^-{}_{(s)} + Cl_2F_{2(g)}$]. The growth of $Cl_2F_{2(g)}$ bands is apparent as the reaction proceeds (top to bottom).

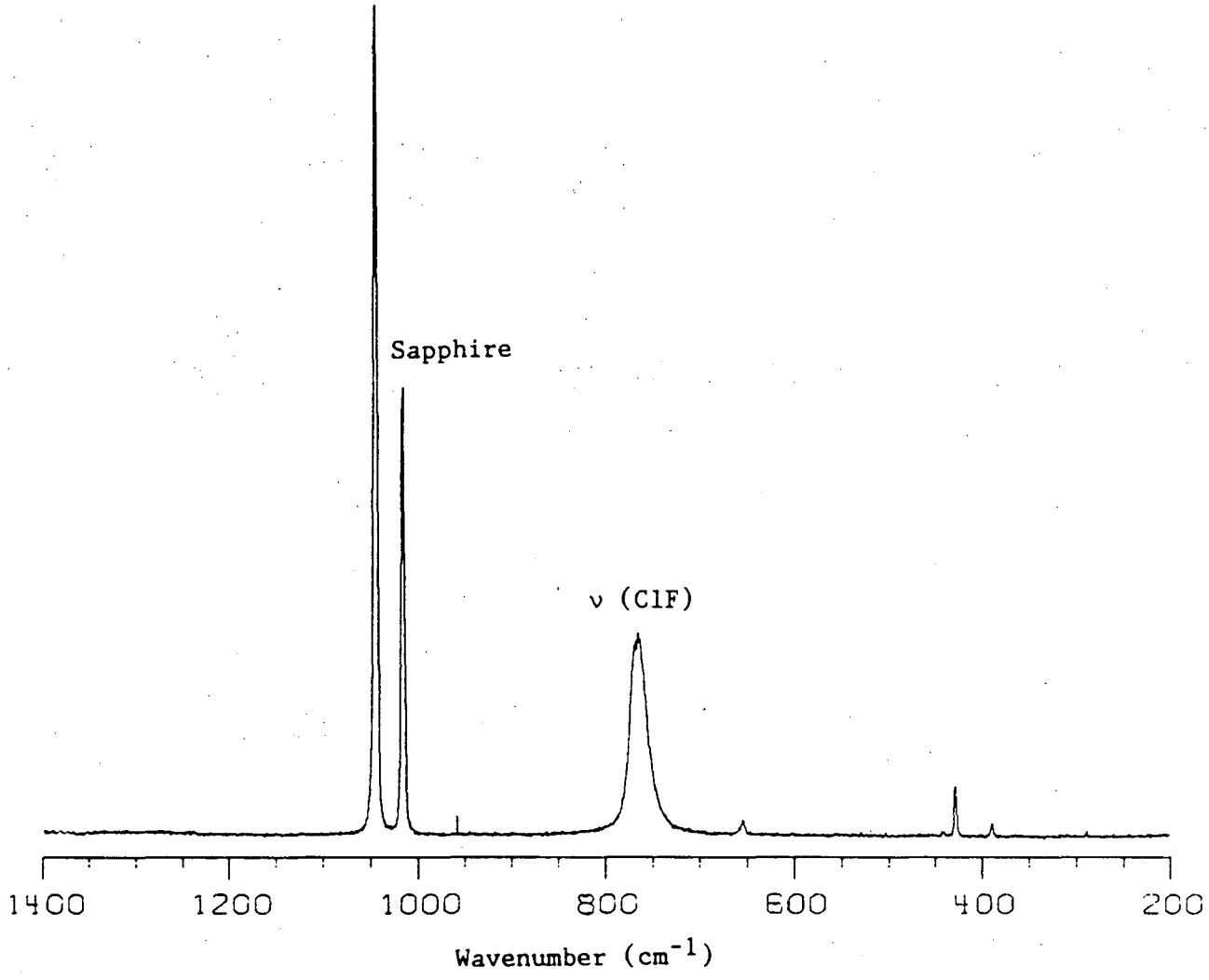

Figure 3.5 Raman Spectrum of ClF at -126°C

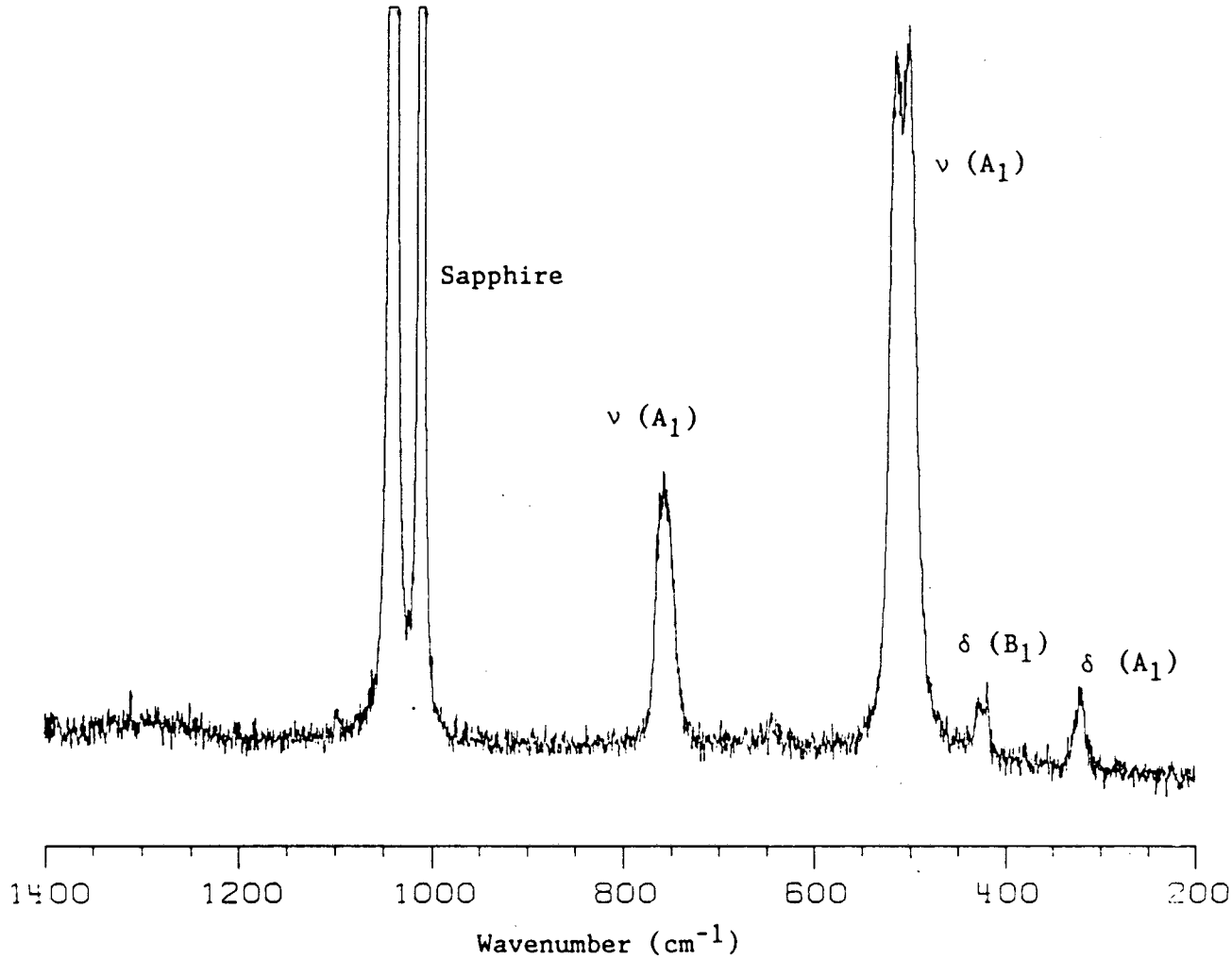

Figure 3.6 Raman Spectrum of ClF_3 at -50 °C

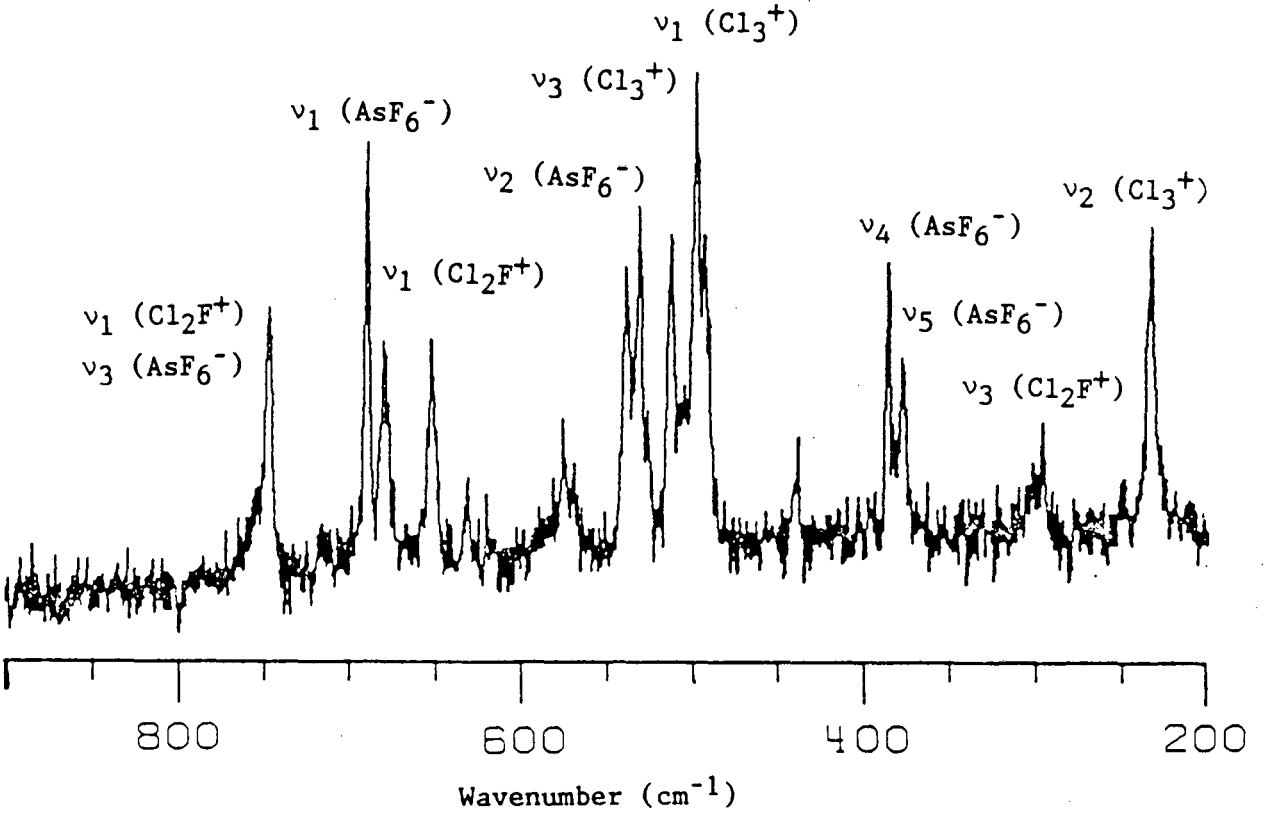

Figure 3.7 Raman Spectrum of the reaction: $ONF_{(g)} + Cl_2F^+AsF_6^-{}_{(s)} \rightarrow NO^+AsF_6^-{}_{(s)} + 2ClF_{(g)}$ at -100°C (the dismutation: $2Cl_2F^+AsF_6^-{}_{(s)} \rightarrow ClF_3^+AsF_6^-{}_{(s)} + Cl_3^+AsF_6^-{}_{(s)}$) is apparent.)

Chapter 3 References

1. L.Graham, Ph.D. Thesis, U.C. Berkeley (1978). Low temperature matrix isolation experiments involving various mixtures of F_2 and Cl_2 have given some circumstantial vibrational evidence for the existence of chlorine fluorides. Cl_3F was not postulated, nor were any of the proposed molecular permutations of chlorine and fluorine established. See: M.R. Clark, W.H. Fletcher, G. Mamantov, E.J. Vasini and D.G. Vickroy, **Inorg. Nucl. Chem. Letters** 8, 611-623 (1972); E.S. Prochaska, L.Andrews, N.R. Smyrl and G. Mamantov, **Inorg. Chem.** 17, 970 (1978).

2. T. Richardson (1984). ESR signals were obtained for the Cl_2^+ radical cation. The color of the solution is deep blue, suggesting a charge transfer band.

3.(a) R.E. Rundle, **J. Amer. Chem. Soc.** 85, 112 (1963); (b) G.C. Pimentel, **J. Chem. Phys.** 19, 446 (1951).

4. J.K. Burdett, N.J. Lawrence, J.J. Turner, **Inorg. Chem.** 23, 2419-2428 (1984).

5. C.J. Marsden, **J. Chem. Soc., Chem. Commun.** 786 (1985).

6. C.J. Marsden, private communication.

7. K.O. Christie and W. Sawodny, **Inorg. Chem.** 8, 212 (1969).

Chapter 4

Thermodynamic Threshold to Graphite Intercalation

4.1 Introduction

Graphite Intercalation Chemistry

Although graphite intercalation compounds have been known and studied since 1841[1], there is still considerable controversy associated with very fundamental concepts.

The carbon atoms in graphite are arranged in sheets. The p orbitals perpendicular to the carbon-atom plane, usually designated p_z, generate the π orbitals which are the highest occupied molecular orbitals of the system. Those π-symmetry orbitals which constitute the lower energy band, usually called the Valence Band (filled in graphite at 0 K) have very small energy overlap with the higher energy band (the Conduction Band). Intercalating oxidants withdraw electrons, thus generating holes in the Valence Band. Reducing species on the other hand populate the Conduction Band, providing electron carriers. Both processes (oxidation and reduction) increase the carrier concentration and hence the conductivity.

The degree of reduction or oxidation of the carbon π system is directly related to the number of carriers; the higher the degree of oxidation or reduction, the higher the number of carriers. The most extensive oxidations of graphite have probably been achieved by fluoroanions, of which the most studied are those salts containing AsF_6^-. There has, however, been much controversy surrounding the precise extent of carbon

oxidation in such systems. For example, it has been claimed that the charge transfer, from measurements of physical properties, is much smaller than suggested by stoichiometries determined by gravimetry and other chemical methods. Milliken[2] and Fischer[3] claim that stages 1 and 2 of $C_{8n}AsF_5$ salts are 40 and 52% oxidized, respectively, compared with the formulation based upon complete conversion according to the equation: $3AsF_5 + 2e^- \rightarrow 2AsF_6^- + AsF_3$ (1). Bartlett and his coworkers[4,5,6] had shown that the intercalation of graphite by AsF_5 has been associated with the formation of AsF_6^- and AsF_3 in accordance with equation (1). The assessment of the ionicities, lower than those which complete conversion according to equation (1) would have produced, were based on studies of reflectivity (screened plasma frequencies) and C(1s) core level X-ray photoemission spectra. From ESR studies of the reaction of C_8K salts with water, Ebert[7] asserts that the composition of the potassium graphites is $C_8^{0.6}K_{0.6}^{+}K_{0.4}^{0}$. Carver[8] has suggested that only 50% of the cesium is ionized in the cesium intercalation compound of chemical composition C_8Cs.

For a variety of reasons there has been a widespread reluctance to accept straightforward ionic formulations such as $C_8^{+}MF_6^{-}$ (eg., M= As, Ir, Os) and $Li^{+}C_6^{-}$. For the oxidation case, values as low as C_{20}^{+} have been proposed[3] as the oxidation limit even though stoichiometries indicative of higher oxidation, e.g. $C_{14}AsF_6$ have been established.

Some of the confusion is probably a consequence of inconsistent preparative techniques and characterization. In the present work, graphite fluoroborate and hexafluorophosphate salts have been investigated. In Chapter 5, the synthesis and characterization of these compounds are described. Emphasis has been placed on assessing the fraction of the guest species present as neutrals as well as the fraction present in anionic form. (Long term removal of neutrals under vacuum has been an important component of that evaluation). A discussion of the effect of the neutrals on the thermochemistry of the materials will be developed in Chapter 6. In this chapter consideration will be given to the evidence for a thermodynamic barrier to oxidation intercalation by fluoro-guest species.

Previous studies in these laboratories[9] had suggested an energetic barrier to graphite intercalation by metal hexafluorides. This originated from the observation that although the third transition series metal hexafluorides are similar in many of their physical properties, only OsF_6, IrF_6 and PtF_6 will intercalate graphite to from $C_8^+MF_6^-$ intercalation salts.

A simple Born-Haber cycle, shown below, illustrates some important factors which contribute to the total enthalpy change for the graphite intercalation by the oxidant MF_6, where M is a transition metal, or by the interaction of a fluorospecies, $A_{(g)}$, with $\frac{1}{2}F_{2(g)}$ to form AF^-:

$$C_x + MF_{6(g)} \rightarrow C_xMF_6$$
or
$$(C_x + A_{(g)} + 1/2F_{(g)} \rightarrow C_xAF)$$

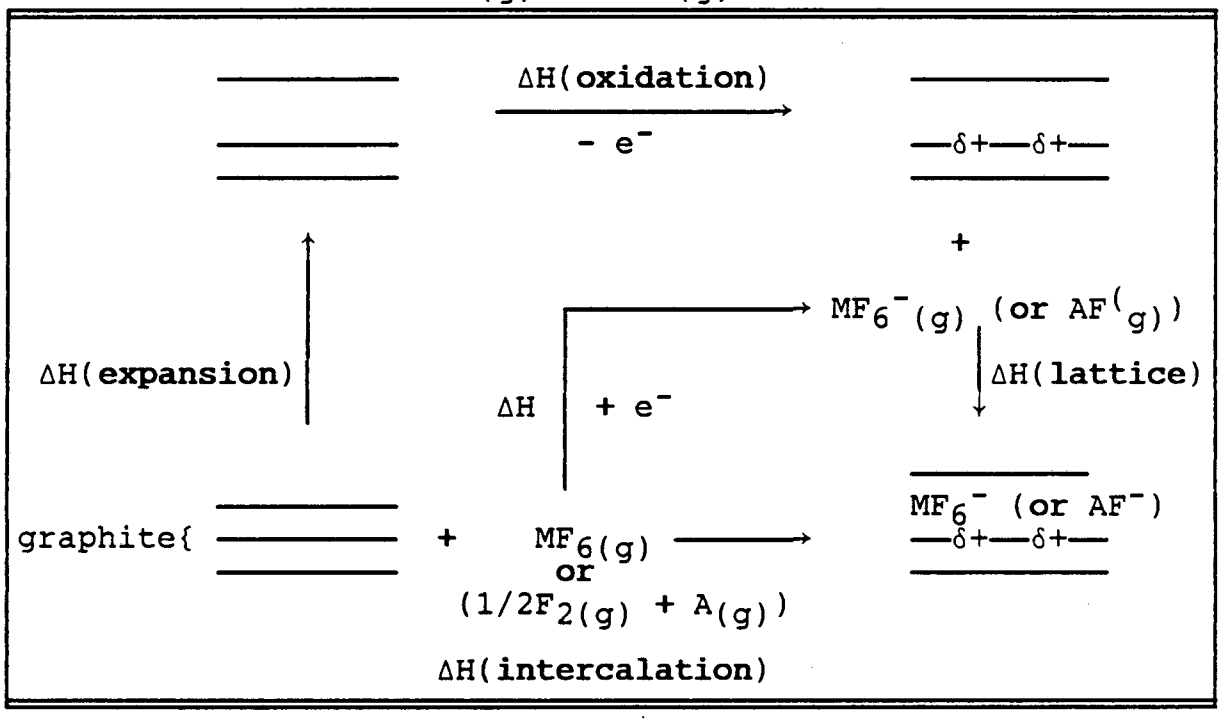

The process of intercalation includes expansion of the carbon layers to permit entry of the intercalant and the withdrawal of electrons from the carbon π band. These two energy requirements are shown as ΔH(**expansion**) and ΔH(**oxidation**). The electron affinity, $\Delta H(MF_{6(g)} + e^- \rightarrow MF_6^-{}_{(g)})$ partly offsets these energy costs. ($\Delta H_f°(F^-_{(g)})$ and the fluoride ion acceptor enthalpy of the neutral fluorospecies (A), $\Delta H°(A_{(g)} + F^-_{(g)} \rightarrow AF^-_{(g)})$, are analogous.) ΔH(**lattice**) is also an exothermic contribution to ΔH(**intercalation**). For the intercalation process to be spontaneous ($\Delta G° < 0$) it is essential that ΔH(**intercalation**) be exothermic since there is

a reduction in entropy associated with the intercalation process.

ΔH(**expansion**) and ΔH(**oxidation**) are almost independent of the identity of the hexafluoro-intercalants, since the effective thickness of the anions and the degree of graphite oxidation are similar for most MF_6^- graphite salts of a given stage. The dimensions of all members in the third transition series MF_6^- are almost the same. Hence, ΔH(**lattice**) is also not very dependent on the identity of M in MF_6. According to this model, the electron oxidizing strength of $MF_{6(g)}$ is the only enthalpy change which will vary with different fluoro-species.

As discussed in Chapter 2, Bartlett[10] had evaluated the electron oxidizing strengths of the third transition series metal hexafluorides from their reactivity with $NO_{(g)}$ and $ONF_{(g)}$. Revised values, presented in Table **4.5**, include the findings of recent experimental observations described in Chapter 2. Since the electron affinity, $\Delta H°(MF_{6(g)} + e^- \rightarrow MF_6^-{}_{(g)}$, (M= W, Re, Os, Ir, Pt), increases smoothly by about 26 kcal mol^{-1} with each increase in atomic number[10], the reactivity with graphite appears to be related to the oxidizing ability of MF_6. Thus, it was proposed that WF_6 and ReF_6 do not intercalate graphite because their electron affinities fall short of an energetic requirement for intercalation. If this is indeed a thermodynamic requirement, its major com-

ponents are the energy cost of carbon sheet separation, $\Delta H(\textbf{expansion})$, and of graphite oxidation, $\Delta H(\textbf{oxidation})$.

The hexafluoroarsenate (V) salts of graphite have been studied by Bartlett and Okino[11]. The nature of the products of the interaction of graphite with AsF_5 had been especially controversial. Okino's studies included those products, as well as those prepared from AsF_5 and fluorine ($AsF_5 + \frac{1}{2}F_2 + e^- \rightarrow AsF_6^-$) and from interaction of graphite with $O_2^+AsF_6^-$ salts ($O_2^+AsF_6^- + xC \rightarrow C_xAsF_6 + O_2$). He demonstrated that the vacuum stable products formed from interaction of AsF_5 with graphite had the composition C_xAsF_6, the minimum value of x after multiple treatment with AsF_5 (oxidation according to equation (1)) being $\sim$16. That material, he showed, was a largely first stage salt in admixture with some second stage material. He also showed that the more powerful oxidizers, such as AsF_5 with fluorine, or $O_2^+AsF_6^-$, gave first stage salts easily. This indicated that the oxidizing power of the AsF_5:

$$3/2\ AsF_5 + e^- \rightarrow AsF_6^- + 1/2\ AsF_3 \quad (1)$$

was inadequate for total first stage oxidation.

It was known previously that graphite was not intercalated by PF_5 alone but that in the presence of fluorine spontaneous intercalation occurred. Rosenthal and Mallouk[12] had evaluated $\Delta H(PF_{5(g)} + 1/2\ F_{2(g)} \rightarrow PF_6^-{}_{(g)}) = -163$ kcal mol^{-1}. Since PF_6^- is similar in size to the transition metal MF_6^- mentioned earlier this observation fits the electron

affinity barrier proposed for the metal hexafluoride salts. The non-intercalation of PF_5 also fits this model since the evaluation of $\Delta H(3/2\ PF_{5(g)} + e^- \rightarrow PF_6^-(g) + PF_{3(g)}) = -86$ kcal mol^{-1}, falls far short of the barrier requirement. This suggested that PF_3 should reduce PF_6^- salts: $PF_6^- + 1/2\ PF_3 \rightarrow 3/2\ PF_5 + e^-$ (2) and Rosenthal was able to demonstrate that at least for second and higher stage C_xPF_6 such reductions did indeed occur.

Difficulties, however, had existed with the salts studied by Rosenthal because of the fluorination of the carbon host resulting from high fluorine concentrations used in the reaction mixture to produce C_xPF_6. In addition, SP1 graphite was traditionally pre-treated with fluorine. (This will be considered in greater detail in Chapter 5, where studies of fluorine concentration in reaction mixtures containing PF_5 are discussed, as well as the preparation and characterization of the fluoroborate salts.) In Rosenthal's experiments, it was found that reduction by PF_3 was never complete; a residue was always present which was ascribed to pockets of carbon fluoride bonding, which may trap PF_6^- anions and PF_5 in the galleries. This work addresses the issues of the existence of a kinetic barrier which prevents full reduction to graphite, and whether a graphite salt which has not been fluorinated will exhibit different behavior. The oxidizing ability of

AsF_5 and PF_5, and the observation of the proposed thermodynamic threshold to intercalation, will also be summarized in light of reaction (1) and the related PF_6^- forming reactions.

4.2 Experimental

4.21 Preparation of Graphite Fluorophosphate and Fluoroborate Salts:

The intercalation compounds $C_{28}PF_6$ and C_xBF_4 were prepared according to the procedure described in detail in Chapter 5. Final stoichiometries were determined by extrapolation of weight loss curves which monitor the escape of neutrals with time. In all preparations, excess neutral was used to minimize graphite fluorination.

4.22 Reaction of Graphite Fluorophosphates and Fluoroborates with PF_3:

Excess PF_3 (PF_3:C_xMF_n::>8:1) was condensed at -196°C on to fluorophosphate and fluoroborate salts in previously described stainless steel reactors. Reaction times were 4-8 days with continuous mechanical agitation. The volatiles lost under vacuum were trapped at -196°C and monitored by infrared spectroscopy and tensimetry. Final stoichiometries were determined by gravimetry for the fluorophosphate system, and by a combination of gravimetry and tensimetry for the fluoroborates.

To the vacuum stable products of these initial reductions were added mixtures of PF_5 and PF_3 in ratios which are listed in Table 4.2 (b). Prior to each reaction, the vacuum line was well passivated with PF_5 followed by PF_3. PF_5 and PF_3 were separately condensed into the reactors at -196°C. Each was in

large molar excess over the intercalation salt (greater than 6 fold excess). The total pressure inside the reactors was about 12 atmospheres. A similar procedure was used in the reaction of the reduction product with BF_3. In these reactions, a large excess of BF_3 (>10:1::BF_3:C_xPF_6) was used.

4.3 Results and Discussion

Results are summarized in Tables **4.1** and **4.2**. Tables **4.4** and **4.5** give the oxidizing strengths of the reactants considered in the discussion.

As noted in the Introduction, Okino had observed that AsF_5 oxidizes graphite only to a limiting composition $C_{15.9}AsF_6$ (Table **4.1**) after six successive treatments of graphite with AsF_5. This compound was a mixture of first and second stages. The fact that O_2AsF_6 will oxidize graphite to a pure first stage salt, of composition $C_{14}AsF_6$, shows that a pure first stage is attainable. Since the intercalation involves the withdrawal of electrons from graphite by O_2^+ (followed by the release of $O_{2(g)}$ and the insertion of AsF_6^-) it seemed that the powerful oxidizing strength of O_2^+ permitted pure first stage preparation ($\Delta G°(O_2AsF_{6(s)} + e^- \rightarrow O_{2(g)} + AsF_6^-{}_{(g)}) = -155$ kcal mol^{-1}, (**k**) in Table **4.4**). The oxidizing strength of AsF_5 is weaker. Since AsF_5 intercalates graphite according to $3AsF_5 + 2\ e^- \rightarrow 2AsF_6^- + AsF_3$, the free energy change, $\Delta G° = -122$ kcal mol^{-1} [**c** in Table **4.4**], shows that it is 33 kcal mol^{-1} poorer than the oxidizing strength of $O_2^+AsF_6^-{}_{(s)}$. Thus, it appeared that there was a thermodynamic barrier to first stage intercalation by AsF_5.

As shown in Table **4.1**, Okino was able to reduce first stage $C_{14}AsF_6$ by treatment with AsF_3 only to a mixture of

first and second stages, $C_{17.8}AsF_6$. This reaction is the reverse of oxidation of graphite by AsF_5:

$$2\ AsF_6^- + AsF_3 \rightarrow 3\ AsF_5 + 2\ e^-$$

The fact that the stoichiometry and staging are very similar for the intercalation of graphite by AsF_5 and the reduction of $C_{14}AsF_6$ by AsF_3 demonstrates thermodynamic reversibility. This shows that a thermodynamic barrier to intercalation exists for the formation of first stage $C_{14}AsF_6$ which is slightly more than $\Delta G°(3/2\ AsF_5 + e^- \rightarrow AsF_6^- + 1/2\ AsF_3) = 122$ kcal mol^{-1}. The barrier to second stage intercalation is below this value[13]. This is in agreement with the energetic barrier of the third transition series hexafluorides described in the Introduction and in Table **4.5.**

In a parallel study, Rosenthal had not observed the reaction of SP1 graphite with PF_5 under conditions similar to those of the AsF_5 study, even though PF_5 and AsF_5 are similar in their physical properties. By analogy to the AsF_5 thermodynamic barrier, this suggested that the oxidizing strength of PF_5 $\Delta G°(3/2\ PF_5 + e^- \rightarrow PF_6^- + 1/2\ PF_3) = 86$ kcal mol^{-1} [**c** in Table **4.4**] is far below for intercalation even to a high stage. However, only partial thermodynamic reversibility was established by the reduction of $C_{28}PF_6$ with PF_3; although X-ray powder diffraction of the product showed it was graphite-like, gravimetry indicated reduction back to graphite had not occurred. $C_{28}PF_6$ used in his study can be prepared by treatment of SP1 graphite with mixtures of PF_5 and F_2, since, using

the reasoning above, the additional oxidizing strength of fluorine makes the half-reaction free energy change, $\Delta G°(PF_5 + 1/2\ F_2 + e^- \rightarrow PF_6^-) = -157$ kcal mol^{-1} [**h** in Table **4.4**] greater than the threshold of first or second stage intercalation to form C_xPF_6.

Rosenthal was also unable to reduce first stage graphite hexafluorophosphate, $C_{12}PF_6$ with PF_3. This is a consequence of the limited access PF_3 has to a crowded first stage. Such a barrier evidently does not exist for AsF_3. The ability of AsF_3 to reduce first stage $C_{14}AsF_6$ probably arises because it forms a bridge bonded $F_3As\text{-}F\text{-}AsF_5^-$ species. PF_3 has no known F^- acceptor properties.

As will be discussed in Chapter 5, difficulties in Rosenthal's study included the fluorination of the carbon host because of the preparative procedures. It was not certain whether the incomplete reduction of $C_{28}PF_6$ was a consequence of a kinetic barrier or due to the presence of islands of fluorine bound to carbon. In this study, the fluorination of carbon has been avoided in order to establish whether a true physical barrier existed which prevented complete reduction.

As is indicated in Table **4.1** and **4.2**, PF_3 will not reduce $C_{29}PF_6$ completely to graphite. Gravimetry demonstrates that the product is at most $C_{42}PF_6$, a stoichiometry which corresponds to a third stage salt although the diffraction data show that an ordered product is not formed.

Graphite fluoroborate is reduced by PF_3. By analogy with the reaction of graphite with AsF_5 considered in the introduction, the half reaction should be:

$$BF_4^- + 1/2\ PF_3 \rightarrow BF_3 + 1/2\ PF_5 + e^- \qquad \Delta G° = 75\ kcal\ mol^{-1}$$

X-ray diffraction of the C_xPF_6 and C_xBFn reduction products reveals a poorly crystalline graphite. This suggests that in the reduction the arrangement of the anions is random throughout most of the material. These results are in agreement with Rosenthal's finding that $C_{29}PF_6$ can only be incompletely reduced to a material which X-ray diffraction shows is graphite-like.

In addition, the conductivity of the fluoroborate and fluorophosphate salts is a sensitive indicator of direct fluorination of carbon, as discussed in Chapter 5. Since the conductivity of these salts is high ($\sigma \approx 1000\ \Omega^{-1}cm^{-1}$), the possibility of secondary reactions, such as the removal of fluorine bound to carbon, is minimized. It can also be concluded that the incomplete reduction is not a consequence of unreacted fluorine bound to carbon in the salt.

The removal of neutrals from the salt after reduction is markedly faster than in cases such as the $BF_4(BF_3)$ salt (Chapter 5) and the C_xAsF_5 materials. This indicates that PF_5 and PF_3 evacuated following reduction were not diffusing slowly through residual ionic guests, but rather represented the total evacuation of fully reduced species. In addition,

further interaction with PF_3 did not occur at room temperature.

With the possibility that the addition of excess PF_5 could promote access of PF_3 into pseudo first-stage regions through the formation of $P_2F_{11}^-$, that reagent was mixed with PF_3. This was no more effective than PF_3 alone, however. Further reaction of the reduction product with PF_5 and PF_3 results in a material which will again rapidly attain vacuum stability (< 50 hours). In contrast, preparation of C_xPF_6 by the reaction of F_2 and excess PF_5 with graphite results in a material in which loss of PF_5 is slow (>500 hours).

Further evidence for a kinetic barrier which prevents anion movement into the salt is found in the reaction of the reduction product ($C_{29}PF_6$ + PF_3) with BF_3. The volatiles produced contain some PF_5, but the intensity of the PF_5 infrared bands shows the reaction has not gone to completion. In contrast, the reaction of second stage $C_{29}PF_6$ with BF_3, which is discussed in detail in Chapter 5 and 6, is favored thermodynamically and is complete. Hence, the reaction with BF_3 shows there is a barrier to neutral penetration. This barrier is somewhat less for BF_3 than for PF_3, because the former molecule is flat and thin (D_{3h} symmetry), whereas the latter is pyramidal and therefore more bulky. The flat shape of BF_3 means that less energy is required for its entry into the galleries.

If PF_3 is thermodynamically unable to reduce $C_{29}PF_6$ completely, then PF_5 might be expected to intercalate graphite to some disordered high stage salt. Intercalation of graphite by PF_5 alone, however, is never observed experimentally, neither for SP1 graphites (particle size 100-200 μ) nor for a Ball Milled Pyrolitic Graphite (particle size 10 μ). Clearly this failure of PF_5 to intercalate, or of PF_3 to reduce C_xPF_6 completely, means that there is a physical barrier to PF_5 or to PF_3 entry.

Conclusion:

The rapid removal of volatiles after reduction of C_xPF_6 with PF_3 clearly shows the neutrals are not slowly percolating through charged species. The remaining guests must be in closed pockets - even PF_5 (to make $P_2F_{11}^-$) did not provide access for PF_3. This is supported by the absence of any evidence of staging in the reduced product. These observations, together with the fact that PF_5 fails to intercalate graphite, show that if the physical barriers were removed the PF_3 would probably completely reduce C_xPF_6 to graphite.

Table 4.1 Synthesis and Reactions of $C_x^+EF_6^-$ Salts

Reactants	Initial reaction(25°C) stoichiometry conditions	Stage	I_c(2nd/1st)† (Å)	Vacuum Stable Stoichiometry
C + AsF_5	C:AsF_5≈4.6:1 reaction: 24 hours evacuation: 214 hours	2nd/1st (mainly second)	10.90/7.64	$C_{20.28}AsF_{6.01}$‡a
C + AsF_5	C:AsF_5≈7.8:1, 6 cycles Net: C:AsF_5≈1.3:1 Net reaction:240 hrs. Net evac.: 207 hours	1st/2nd (mainly first)	10.90/7.84	$C_{15.94}AsF_{5.98}$‡a
C+O_2AsF_6	C:O_2AsF_6≈11.6:1 reaction:384 hours evacuation:72 hours	1st	7.57	$C_{14.01}AsF_{6.01}$‡a
$C_{14}AsF_6$ + AsF_3	AsF_3:$C_{14}AsF_6$≈1.5:1 reaction:96 hours evacuation:192 hours	1st/2nd (mainly first)	10.92/7.65	$C_{17.8}AsF_6$‡a
$C_{33}PF_6$ + PF_3	PF_3:$C_{33}PF_6$≈1:5 reaction:24 hours evacuation:24 hours	graphite like		$C_{65.8}PF_6$‡b
$C_{29}PF_6$ + PF_3	PF_3:$C_{29}PF_6$≈9:1;3 cycles Net reaction:648 hours Net evacuation:216 hrs.	high stage disordered		$C_{42}PF_6$
$C_{30}BF_4(BF_3)_{0.35}$ + PF_3	PF_3:C_{31}≈22:1 reaction:144 hours evacuation:48 hours	high stage disordered (see Table 4.3)		$C_{41}BF_4(BF_3)_{0.35}$

‡ Stoichiometries obtained from chemical analysis performed at Galbraith Laboratories, Inc.

a F.Okino, Ph.D. Thesis U.C. Berkeley, 1984.

b G.Rosenthal, Ph.D. Thesis U.C. Berkeley, 1984.

† Ic represents the c axis repeating unit length, which for a first stage salt represents the perpendicular distance separating the carbon sheets enclosing one layer of guest species. Ic for a second stage is usually close to the sum of Ic for first stage, plus the sheet to sheet separation, which is 3.35 Å.

Table 4.2 (**a**) Reduction of C_xPF_6 and C_xBF_4 by PF_3

Stage	Stoichiometry Initial Salt	Reduction Product	X-ray pattern	Comments
2	$C_{28.6}PF_6$	$C_{37.1}PF_6$	graphite-like pattern with	1
2	$C_{28.0}PF_6$	$C_{41.6}PF_6$	00ℓ reflections broad; see	1
2	$C_{27.1}PF_6$ ($C_{29.9}PF_6(PF_5)_{0.12}$)	$C_{37.2}PF_6$	Table **4.3**	1
4	$C_{30.1}BF_4(BF_3)_{0.35}$	$C_{41.0}BF_4(BF_3)_{0.35}$		2

(**b**)	Further Reactions of the Reduction Products of (**a**)
Stage	Reaction
high	$C_{37.1}PF_6$ + PF_5:PF_3 (1.6:1)
high	$C_{41.6}PF_6$ + PF_5:PF_3 (0.75:1)
high	$C_{37.2}PF_6$ + PF_5:BF_3 (0.74:1)

Reaction product showed no change in weight or X-ray powder pattern from (**a**) product

a Further reduction with PF_3 was not observed.
Volatiles from further reaction with excess BF_3 contain PF_5.
Loss of PF_5 following reduction and displacement with BF_3 is rapid.

b Product stoichiometry assumes that BF_4^- and BF_3 were lost in the same ratio as that present in the starting material, i.e. 1:0.35.

Table 4.3

X-Ray Diffraction of Product from the Reduction of $C_{30.1}BF_4(BF_3)_{0.35}$			X-Ray Pattern of SP1 Graphite		
No.	Intensity	$1/d^2$ (obs.)	Intensity	$1/d^2$	Assignment
1	strong broad	.07802 .08443 .08633	vs	.0891	002
2	weak broad	.0990 .1065			
3	med sharp	.22085	m	.2210	100
4	med broad	.23911 .2439	m	.2433	101
			w	.3101	102
5	mw	.3610	mw	.3564	004
6	vw	.4180	mw	.4215	103
			w	.5774	104
7	med sharp	.6602	m	.6631	110
8	med broad	.7482	m	.7522	112
			w	.7779	105
9	w	.7996	w	.8019	006
			w	.8840	200
10	vw	.9067	w	.9063	201
			w	.9731	202
11	vvw	1.0168			

Table 4.3(b) X-ray Powder diffraction
Second Stage Graphite Fluorophosphate

Second Stage $C_{29.9}PF_6(PF_5)_{0.12}$ a= 2.46, c=10.90 Å

No.	Intensity	$1/d^2$ (obs.)	$1/d^2$ (calc.)	Assignment
1	weak	.0084	.0084	001
2	strong broad	.0729 .0750 (center) .0764	.0756	003
3	weak broad	.1353 (center) .1403	.1343	004
4	med sharp	.2209	.2201	100
5	med sharp	.2267	.2285	101
6	med broad	.2514	.2537	102
7	med sharp	.6601	.6602	110
8	weak broad	.7357	.7358	113
9	vweak	.8819	.8802	200

Table 4.3 (c)

X-Ray Diffraction of Product from the Reduction of $C_{29.9}PF_6(PF_5)_{0.12}$			X-Ray Pattern of SP1 Graphite		
No.	Intensity	$1/d^2$ (obs.)	Intensity	$1/d^2$	Assignment
1	strong broad	.0767 .0790 .0813			
2	med broad	.0882	vs	.0891	002
3	trace	.1039			
4	med sharp	.2203	m	.2210	100
5	med broad	.2400 .2433	m	.2433	101
			w	.3101	102
6	vweak broad	.3564	mw	.3564	004
7	vweak broad	.4175	mw	.4215	103
			w	.5774	104
8	med sharp	.6593	m	.6631	110
9	med broad	.7346	m	.7522	112
			w	.7779	105
			w	.8019	006
			w	.8840	200
10	trace	.8988	w	.9063	201
			w	.9731	202
11	vvw	1.0107			

Table 4.4 Energies of EF_6^- Forming Reactions			
Process	(kcal mol^{-1}) $\Delta H°$	$\Delta G°$	Ref
(a) $AsF_{5(g)} + F^-_{(g)} \rightarrow AsF_6^-{}_{(g)}$	-111(5)		1
(b) $1/2\ AsF_{5(g)} + e^- \rightarrow F^-_{(g)} + 1/2\ AsF_{3(g)}$	-11		2
(c) = (a)+(b) $3/2\ AsF_{5(g)} + e^- \rightarrow 1/2\ AsF_{3(g)} + AsF_6^-{}_{(g)}$	-122	-118	3
(d) $PF_{5(g)} + F^-_{(g)} \rightarrow PF_6^-{}_{(g)}$	-101		4
(e) $1/2\ PF_{5(g)} + e^- \rightarrow F^-_{(g)} + 1/2\ PF_{3(g)}$	15		2
(f) = (d)+(e) $3/2\ PF_{5(g)} + e^- \rightarrow PF_6^-{}_{(g)} + 1/2\ PF_{3(g)}$	-86	-85	5
(g) $1/2\ F_{2(g)} + e^- \rightarrow F^-_{(g)}$	-62		6
(h) = (d)+(g) $PF_{5(g)} + 1/2\ F_{2(g)} + e^- \rightarrow PF_6^-{}_{(g)}$	-163	-157	7
(i) $O_2^+{}_{(g)} + e^- \rightarrow O_{2(g)}$	-278		8
(j) $O_2AsF_{6(s)} \rightarrow O_2^+{}_{(g)} + AsF_{6(g)}^-$	144		9
(k) = (i)+(j) $O_2AsF_{6(s)} + e^- \rightarrow O_{2(g)} + AsF_{6(g)}^-$	-134	-155	10

References

(1) $IF_6^+AsF_6^-{}_{(s)}$ has negligible vapor pressure (<5 torr) at 25°C and 50°C. Thus, $\Delta G°_{323}(IF_{7(g)} + AsF_{5(g)} \rightarrow IF_6^+AsF_6^-{}_{(s)}) \leq -7.3$ kcal mol^{-1}; $T\Delta S° = -20$ kcal mol^{-1}‡. Thus, $\Delta H° \leq -27$ kcal mol^{-1}; $\Delta H°_{lattice} = -124$ kcal mol^{-1} and $\Delta H°(IF_{7(g)} \rightarrow IF_6^+{}_{(g)} + F^-_{(g)}) = 208(6)$ kcal mol^{-1},[Bartlett et al., **J.Fluorine Chem.** 26, 97-116 (1984)], from which we obtain $\Delta H°(a) \geq 111$ kcal mol^{-1}. By similar reasoning, from dissociation pressure data of $SF_3^+AsF_6^-{}_{(s)}$, $\Delta H°(a) = -108$ kcal mol^{-1}. We take 111(5) kcal mol^{-1} as a reasonable value for $\Delta H°(a)$.

‡ $S°(IF_{7(g)}) = 88$ cal mol^{-1} deg^{-1}),[N.B.S. Technical Notes 270-3 (1969)];
$S°(AsF_{5(g)}) = 78$ cal mol^{-1} deg^{-1} [O'Hare, P.A.G.; Hubbard, W.N. **J. Phys. Chem.** 69, 4358 (1965)]; $S°(IF_6^+AsF_6^-{}_{(s)}) = 94$ cal mol^{-1} deg^{-1} [T.Mallouk, Ph.D. Thesis, U.C. Berkeley 1982].

(2) A.A. Woolf, **J.Fluorine Chem.** 15, 533 (1980).

(3) $S°(AsF_3)$= 69 cal mol^{-1} deg^{-1}; N.B.S. Technical Notes 270-3 (1968).

(4) G.Rosenthal, Ph.D. Thesis, U.C. Berkeley (1984).

(5) $S°(PF_{5(g)})$= 72 cal mol^{-1} deg^{-1}; $S°(PF_{3(g)})$= 65 cal mol^{-1} deg^{-1}; "JANAF Tables"; Dow Chemical Co.: Midland, MI (1969).

(6) "JANAF Tables"; Dow Chemical Co.: Midland, M.I. (1977).

(7) $S°(e^-)$= 5 cal mol^{-1} deg^{-1}["JANAF Tables"; Dow Chemical Co.: Midland, MI 1977]; $S°(PF_6^-{}_{(g)})$= 76 cal mol^{-1} deg^{-1}, estimated from similar trends in $BF_{3(g)}$ and $BF_4^-{}_{(g)}$ (64 and 61 cal mol^{-1} deg^{-1}).

(8) Levin, R.D.; Lias, Sharon G. "Ionization Potential and Appearance Potential Measurements" 1971 to 1981, NSRDS-NBS 71, U.S. Dept. of Commerce, October 1982, Superintendent of Documents, U.S. Govt. Printing Office, Washington D.C. 20402.

(9) Lattice enthalpy obtained from a linear correlation between $\Delta H°_{lattice}$ and the inverse cube root of the ionic volume [T.Mallouk, Ph.D. Thesis, U.C. Berkeley (1982)].

(10) $S°(O_2AsF_6)$= 57 cal mol^{-1} deg^{-1} [T.Mallouk, Ph.D. Thesis]; $S°(O_{2(g)})$= 49 cal mol^{-1} deg^{-1}, and $S°(PF_6^-{}_{(g)})$= 76 cal mol^{-1} deg^{-1} see reference 6).

Table 4.5 Electron Oxidizing Capability of Metal Hexafluorides			
Process	‡ΔG°(kcal mol^{-1})	Limiting† Composition	ref
$WF_{6(g)} + e^- \rightarrow WF_6^-(g)$	-81(3)	No Reaction	**a**
$ReF_{6(g)} + e^- \rightarrow ReF_6^-(g)$	-107	No Reaction*	**b**
$OsF_{6(g)} + e^- \rightarrow OsF_6^-(g)$	-134	C_8OsF_6	**c**
$IrF_{6(g)} + e^- \rightarrow IrF_6^-(g)$	-157(4)	C_8IrF_6	**d**
$PtF_{6(g)} + e^- \rightarrow PtF_6^-(g)$	-184	$C_{12}PtF_6$	**e**

‡ Because these half reactions involve the same number of moles of gas in reactants and products, $\Delta S°_{298} \approx 0$ and $\Delta G°_{298} = \Delta H°_{298}$.

† Bartlett, N.; McCarron, E.M.; McQuillan, B.W. and Thompson, T.G. **Synthetic Metals** 1, 221 (1980).

(**a**) See Chapter 2.

(**b**) *Graphite reacts only slightly with $ReF_{6(g)}$ to give a product whose X-ray diffraction pattern does not indicate extensive intercalation. Like PF_5, ReF_6 possesses an electron affinity below the energetic requirement for low stage intercalation.

$NO_{(g)}$ and $ReF_{6(g)}$ [Beaton, Ph.D. thesis, U.C. Berkeley (1963)] combine to give $NO^+ReF_6^-(s)$, which has a vapor pressure of <<2 torr at 298 K. This implies $\Delta G°(NO_{(g)} + ReF_{6(g)} \rightarrow NO^+ReF_6^-(s)) \leq -8$ kcal mol^{-1}. Because $T\Delta S° \approx -23$ kcal mol^{-1} (ref. a), and since $\Delta H°(NO_{(g)} \rightarrow NO^+_{(g)} + e^-) = 213(1)$ kcal mol^{-1} and $\Delta H°_{lattice}(NO^+ReF_6^-(s)) = -133$ kcal mol^{-1} [ref. **9**], Table **4.4**] we obtain $-\Delta H°(ReF_{6(g)} + e^- \rightarrow ReF_6^-(g)) \geq 111$ kcal mol^{-1}. From linear extrapolation assuming a smooth increase with atomic number a value of 107 kcal mol^{-1} is obtained, which is in the compass of our estimate.

(**c**) Unlike $IrF_{6(g)}$, $OsF_{6(g)}$ reacts only slowly with $ONF_{(g)}$ at room temperature according to: $ONF_{(g)} + OsF_{6(g)} \rightarrow NO^+OsF_6^-(s) + 1/2\ F_{2(g)}$ [Beaton,

Ph.D. thesis, U.C. Berkeley (1963)]. $\Delta G° \approx 0$; $S°(ONF_{(g)}) = 59$ cal mol^{-1} deg^{-1}, $S°(OsF_{6(g)}) = 82$ cal $mol^{-1}deg^{-1}$, $S°(F_{2(g)}) = 48$ cal $mol^{-1}deg^{-1}$, and $S°(NO^+OsF_6^-{}_{(s)}) = 56$ cal $mol^{-1}deg^{-1}$ [ref. **9**, Table **6.3**]. $T\Delta S° \approx 18$ kcal mol^{-1}; thus, $\Delta H° = -18$ kcal mol^{-1} for the reaction indicated. Since $\Delta H°(ONF_{(g)} \rightarrow NO^+_{(g)} + F^-_{(g)}) = 188(1)$ [H.S. Johnston and H.J. Bertin, **J. Am. Chem. Soc.** 81, 6402 (1959) and **J. Mol. Spec.** 3, 683 (1959)], and because $\Delta H°(F^-_{(g)} \rightarrow 1/2\ F_{2(g)} + e^-) = -62$ kcal mol^{-1}, $\Delta H°(ONF_{(g)} \rightarrow NO^+_{(g)} + 1/2\ F_{2(g)}) = 250$ kcal mol^{-1}. Using $\Delta H°_{lattice} = -134$ kcal mol^{-1} [ref. 9, Table **6.3**] then $\Delta H°(OsF_{6(g)} + e^- \rightarrow OsF_6^-{}_{(g)}) = -134$ kcal mol^{-1}.

(**d**) N. Bartlett, S. Yeh, K. Kourtakis and T. Mallouk, **J. Fluor. Chem** 26, 97-116 (1984).

(**e**) $O_2^+PtF_6^-{}_{(s)}$ possesses a vapor pressure of 2-5 torr at 373 K (it sublimes under vacuum between 90° and 130°C) [N. Bartlett and D.H. Lohmann, **J. Chem. Soc.** 5253 (1962)]. Thus, $\Delta G°_{373}(O_2PtF_{6(s)} \rightarrow O_{2(g)} + PtF_{6(g)}) \approx 9$-$10$ kcal mol^{-1}; $S°(O_2PtF_{6(s)}) = 57$ cal $mol^{-1}deg^{-1}$ [ref. 9, Table **6.3**], $S°(O_{2(g)}) = 49$ cal $mol^{-1}deg^{-1}$, $S°(PtF_{6(g)}) = 82$ cal mol^{-1} deg^{-1}, so $\Delta H° = -37$ kcal mol^{-1}. Since $\Delta H°_{lattice} = -134$ kcal mol^{-1}, and $\Delta H°(O_{2(g)} \rightarrow O_2^+{}_{(g)} + e^-) = 278$ kcal mol^{-1}, we obtain $\Delta H°(PtF_{6(g)} + e^- \rightarrow PtF_6^-{}_{(g)}) = -181$ kcal mol^{-1}. This is in good agreement with the value of 184 kcal mol^{-1} obtained by Nikitin et al. from gas phase ion-molecule equilibria [**J. Mass Spec. Ion Phys.** 37, 13 (1981)].

Chapter 4 References

1. P. Schaufhautl, **J. Prakt. Chem.** 21, 155 (1841).

2. J.W. Milliken and J.E. Fischer, **J. Chem. Phys.** 78(9) (1983).

3. J.E. Fischer, **J. Chem. Phys.** 78(9) (1983).

4. N. Bartlett, R. Biagioni, B.W. McQuillan, A.S. Robertson, A.C. Thompson **J.C.S. Chem. Commun.** 200 (1978).

5. N. Bartlett, B. McQuillan, A.S Robertson **Mat. Res. Bull.** 17, 301 (1978).

6. N. Bartlett, R.N. Biagioni, E. McCarron, B. McQuillan and F. Tanzella, **Molecular Metals** 293 (1979).

7. L.B. Ebert, **Bull. Am. Phys. Soc.** 23, 185 (1978).

8. G.P. Carver, **Phys. Rev. Sect. B.** 1, 2284 (1970).

9. N. Bartlett and B.W. McQuillan, in S.M. Whittingham and A. Jacobsen (eds.), **Intercalation Chemistry**, Academic Press, Inc., New York, London, 1982. pp. 19-53.

10. N. Bartlett **Angewandte Chemie, Int. Ed.** 7, 433-439 (1968).

11. F. Okino and N. Bartlett, to be published.

12. G. Rosenthal, Ph.D. Thesis, U.C. Berkeley (1984).

13. The dependence of the attainable stage on the power of the oxidizing agent has been illustrated in electrochemical oxidation. First stage salts in admixture with second usually require an oxidizing potential higher than the second/third stage combination. In the case of the graphite hydrofluoride salts the free energy difference between the 1/2 potential and

the 2/3 potential is on the order of 12 kcal mole-1. This is evident in the galvanostatic charge curve of graphite to produce graphite bifluorides in 1M NaF/HF electrolyte solution [M. Kawaguchi, M. Lerner, N. Bartlett, to be published]. Sharp transitions are observed in this curve which correspond to the onset of a new stage; plateau regions indicate charging which converts one stage to another, and is a mixture of stages. A low current density of 100 $\mu A/cm^2$ constrains the system to be near equilibrium throughout charging. Since AsF_5 always generates a mixture of first and second stage nestled C_xAsF_6 salts, it can be concluded that the oxidizing potential of AsF_5 is exactly that which matches the potential of that two stage system.

Chapter 5

Conversion of Graphite Fluorophosphates to Graphite Fluoroborates

5.1 Introduction

As has already been pointed out in Chapter 4 in situations where the effective thickness and charge of the guest species are the same in graphite intercalation compounds, $\Delta H(\textbf{expansion})$ and $\Delta H(\textbf{oxidation})$ are roughly independent of the identity of the guest. This is true for most of the MF_6^- intercalants. Since the thickness of a tetrahedrally close-packed F^- ligand cluster is approximately the same (along a three-fold axis) as that of an octahedral one, it is not surprising to find that graphite fluoroborates and fluorosulfates[1] (the O^- and F^- ligands are similar in volume and Van der Waals radii) have similar interlayer spacings to those of the hexafluorometallates. The question of the relative stabilities of the graphite fluoroborates ($C_x^+BF_4^-$) and their equally charged hexafluorophosphate relative ($C_x^+PF_6^-$) of the same stage, therefore appears at first sight to be a relatively easy one to address. In reactions in which one salt is converted into the other (either PF_5 displacement from PF_6^- by BF_3 or by BF_3 displacement from BF_4^- by PF_5) without change in stage,

$$C_xBF_4 + PF_5 \rightarrow C_xPF_6 + BF_3$$

$$C_xPF_6 + BF_3 \rightarrow C_xBF_4 + PF_5$$

there would not be any change in the total charge. As a consequence of the BF_4^- and PF_6^- having similar effective guest thickness the difference in lattice energy for the two cases would appear to be very small and hence would have little influence in the determination of which fluoroacid would displace the other.

$$C_x + MF_{6(g)} \rightarrow C_xMF_6$$
$$\text{or}$$
$$(C_x + A_{(g)} + 1/2F_{(g)} \rightarrow C_xAF)$$

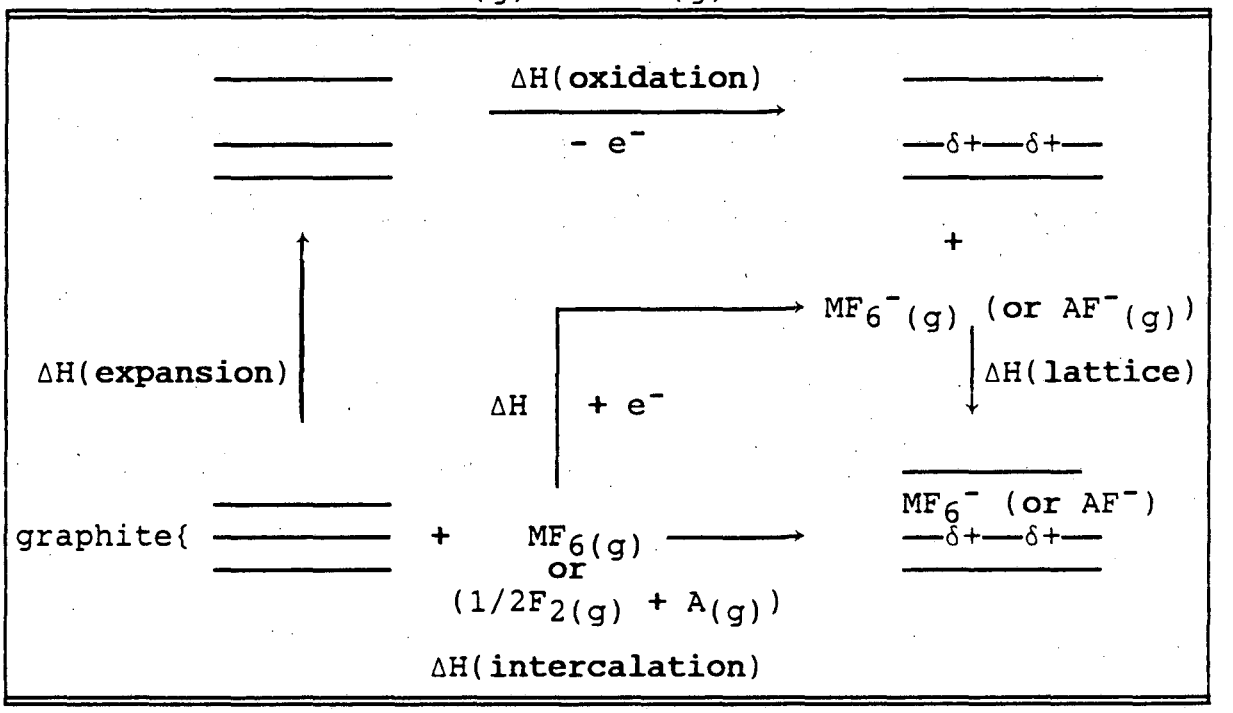

In the Born-Haber cycle reproduced above, a reasonable assumption for the fluoro-intercalants is that the fluoride ion acceptor enthalpy, $\Delta H(A_{(g)} + F^-_{(g)} \rightarrow AF^-_{(g)}$, (or electron affinity, if the reactant is a hexafluoro neutral) is the only one which is substantially different for the different intercalants. A general anion displacement in a perfluoro anion

graphite salt can then be regarded as a donation of fluoride ion from one fluorospecies to the other: $C_x^+AF^- + B_{(g)} \rightarrow C_x^+BF^- + A_{(g)}$). By this reasoning, the neutral fluorospecies with the stronger fluoride ion acceptor strength ought to displace the weaker.

The fluoride ion affinity of $PF_{5(g)}$ and $BF_{3(g)}$ had been reliably determined previously by others in this laboratory.[2,3] $-[(\Delta H(PF_{5(g)} + F^-_{(g)} \rightarrow PF_6^-{}_{(g)}) - (\Delta H(BF_{3(g)} + F^-_{(g)} \rightarrow BF_4^-{}_{(g)})] = 8$ kcal mol^{-1}. Hence, the expected reaction would be the displacement of $BF_{3(g)}$ from $C_xBF_{4(s)}$ by $PF_{5(g)}$. Observations of Rosenthal[2] however had showed that the reverse displacement in fact occurred.

One goal of this study was to establish fully the correctness of Rosenthal's observations and, from a more complete characterization of the graphite salts produced by the displacement of PF_5 by BF_3, to endeavor to understand that unexpected finding.

In 1980 McCarron, Gannier and Bartlett[4] had prepared first stage graphite salts from graphite PF_5 and F_2 but their product was not proved to be simply $C_x^+PF_6^-$. Similar synthesis of a fluoroborate graphite salt (from BF_3/F_2 and graphite) was made by McQuillan[5] but again the material was not shown to be of a simple salt formulation $C_y^+BF_4^-$. The fluoroborate and fluorophosphate salts of graphite were also prepared by Ebert, Selig and their coworkers[6] by reaction of graphite ClF and either PF_5 or BF_3. Additional reports by

Billaud et al.[7] involved reactions of the oxidizing salts $NO_2^+PF_6^-$ and $NO_2^+BF_4^-$ with graphite in nitromethane. These last reactions occur with the liberation of NO_2 and intercalation of PF_6^- and BF_4^- but the preparation invariably involved the insertion of nitromethane. More recently, Rosenthal[2] had more fully characterized the salts formed in reactions of graphite with the mixtures of F_2 with PF_5 and F_2/BF_3 employed earlier. Although Rosenthal demonstrated that neutrals (PF_5 or BF_3) were commonly incorporated together with PF_6^- or BF_4^- within the graphite galleries, the conditions necessary for the preparation of $C_x^+BF_4^-$ or $C_y^+PF_6^-$ salts (free of neutrals) were not well defined. Nor was it clear that these synthetic routes, using as they did elemental fluorine, did not contaminate the salt products with extensive fluorination of the graphite network (C-F bond formation). Milliken and Fischer[8] had attributed the decrease in conductivity of first stage AsF_5 compounds to defect scattering from C-F bond sites, and Okino[9] had observed conductivity decreases upon direct fluorination of first stage arsenic pentafluoride salts which he was able to show involved greater uptake of fluorine than that needed for anion formation.

Accordingly, it was decided that the measurement of electrical resistivity in those fluoroborates and fluorophosphates prepared using elemental fluorine, provided a means of detecting C-F bond formation and all such preparations were therefore monitored in that way.

In this study the effect of changing the ratio of fluorine to PF_5 or BF_3 in the synthesis of graphite intercalation salts C_xPF_6 or C_xBF_4 was followed by gravimetry, tensimetry, conductivity measurements and X-ray powder diffraction. The last was vital to the determination of the phases (stages) present and their dimensions.

To check on the validity of the fluoride-ion enthalpy values for BF_3 and PF_5, and the impact of the lattice enthalpy on the relative stability of tetrafluoroborates and hexafluorophosphates, displacement of BF_3 from BF_4^- and PF_6^- salts of small and large cation, were also undertaken.

5.2 Experimental

5.21 Resistivity Measurements on Graphite Salts

Previous conductivity measurements of graphite intercalation salts used the contactless technique described elsewhere.[10] This technique requires highly conductive HOPG chips. Often, these chips had been previously fluorinated in order to eliminate surface hydroxyl groups. This procedure may involve some graphite fluorination with consequent reduction in conductivity, and such fluorinations have been avoided in these studies. In addition, in the past, graphite salts have usually not been subjected to long term dynamic vacuum to ensure almost complete removal of volatile. It is very probable that the large chips of HOPG studied in the past, which had been subjected to dynamic vacuum for periods of only several hours, contained high concentrations of neutral guest species since vacuum stability of fluorophosphate and fluoroborates prepared from SP1 graphite (particle size 70-100 μ) was only achieved after 500-1000 hours in a dynamic vacuum. If the escape of the neutrals is diffusion limited in SP1 salts, then surely the effect is operative for HOPG salts, and the evacuation time necessary for vacuum stability can be expected to be proportionally longer. Product homogeneity is also less certain with HOPG chips. Conductivity data derived from HOPG chips have therefore uncertain value unless the absence of neutral guest species can be guaranteed and the homogeneity established.

The method used in this study involved four probe conductivity measurements on pressed polycrystalline pellets. An infrared die was loaded with 100-200 mg of the salt inside the dry box and was enclosed in a plastic bag. The bag was removed and placed in a hydraulic press, where pressure was applied thrice at 1000 psi for 2 minutes at room temperature through the plastic bag. All pellets were prepared using the same die and identical hydraulic press conditions.

Conductivity measurements were obtained by utilizing a four-probe device consisting of two 1" x 1" plexiglass squares. Four 0.15 mm Pt/10% Rh wires were affixed to the surface of the square. The pressed pellet was cut into a small rectangular piece whose dimensions were accurately determined and then placed across the wires. Light pressure was applied by the opposing plexiglass square. Current was allowed to flow across the outer leads, and voltage was measured across the inner contacts. The current polarity was reversed and the current-voltage linearity was checked to establish the ohmicity of the contacts. Results obtained by this method were reproducible to 10-15% accuracy. The small discrepancies can be attributed to the variation in the exact point of electrical contact between the platinum wire and the pellet. This error could be minimized by using narrowly cut pellets. In this way, conductivity measurements were obtained for materials which are well characterized and homogeneous.

5.22 Reactions of Simple Tetrafluoroborate and Hexafluoro phosphates:

KPF_6 (IPR, Gainsville FA) and $NaBF_4$ (Alfa, Danvers MA) were used as obtained. $Bu_4N^+PF_6^-(s)$ was prepared from 1:1 mixtures, in aqueous solution, of Bu_4NBr (Eastman, Rochester NY) and $NaPF_6$, followed by recrystallization from CH_2Cl_2.

All reactions were carried out in a 1/4 " sapphire tube fitted, via Teflon gasketed compression fittings, with a Whitey valve. The volume was small enough to allow pressures of ≈ 3 atmospheres to develop with the gaseous reagent used. BF_3 or PF_5 was condensed onto each of the salts at -196°C and the mixture was then allowed to approach room temperature. Two or three such temperature cycles were used to promote the reaction. The volatiles were then vented to the infrared cell and an infrared spectrum was recorded.

5.22.1 BF_3 + KPF_6: PF_5 was produced when BF_3 was reacted in the molar ratio BF_3:KPF_6::1:1. Almost all of the BF_3 was consumed. With additional BF_3 no further displacement of PF_5 was observed, thus indicating a quantitative displacement of the PF_5 in the first interaction. Finally, the absence of any reaction of the fluoroborate product with excess PF_5 demonstrated that the process was irreversible. Hence,

$$BF_3 + KPF_6 \rightarrow KBF_4 + PF_5$$

5.22.2 BF_3 + $Bu_4N^+PF_6^-$: BF_3 was reacted with $Bu_4N^+PF_6^-$ in a molar ratio BF_3:$Bu_4N^+PF_6^-$::2:1. PF_5 was detected in the infrared spectra of the volatiles. The reaction stoichio-

metry, as determined from the intensity of the infrared bands, was roughly one mole of PF_5 eliminated for every mole of BF_3 consumed. Further reaction with BF_3 produced only small evolution of PF_5. The reaction was reversed by the addition of PF_5 in the molar ratio PF_5:Bu_4N^+::2:1. These displacements demonstrate that the salts and their counter fluoroacids are close to equilibrium:

$$BF_3 + Bu_4N^+PF_6^- \rightarrow Bu_4N^+BF_4^- + PF_5$$

5.22.3 PF_5 + $NaBF_4$: No reaction was observed when PF_5 was added to $NaBF_4$, the reaction stoichiometry being PF_5:$NaBF_4$::2:1. Thus,

$$PF_5 + NaBF_4 \not\rightarrow NaPF_6 + BF_3$$

5.23 Graphite Hexafluorophosphate

5.23.1 Reaction of equimolar PF5 and F_2

Small, ≈2 ml, stainless steel reactor tubes were joined via a 3/8" to 1/4" Swagelock union to a stainless steel Whitey valve. To retain the fine powders within the reactor (especially during initial evacuation), two to four Teflon filter - papers were sandwiched between two stainless steel (100 mesh) screens. This sandwich was placed at the top of the swagelock assembly. The reactors were passivated with ClF_3 vapor and loaded under a dry Ar atmosphere with graphite (SP1, Union Carbide) which had been previously heated to a red heat under dynamic vacuum for approximately 1-2 hours. Previous workers

in these laboratories had fluorinated SP1 and HOPG graphite, prior to intercalation, as a standard procedure to clean its surface and edges. This procedure was never used in this study because of the effect that fluorine has in reducing the electrical conductivity of these materials. PF_5 was purified by trap to trap distillation, at dry ice-acetone temperature, to remove any OPF_3 impurity. Fluorine was stored over NaF to remove HF. The purity of both reactants was established by infrared spectroscopy. The vacuum line and reactors were passivated with ClF_3 prior to all reactions.

The reaction conditions are shown in Table 5.3. Reaction times were on the order of 100 hours. The volatiles remaining after reaction were examined by infrared spectroscopy at liquid N2 and at room temperature.

Volatiles were trapped under dynamic evacuation by a 1/4" diameter copper U tube held at -196°C. The volume of the copper tubing and vacuum line was determined tensimetrically by the expansion of helium from it into a known additional volume.

All weights (± 0.1 mg) were made outside the dry box. The stainless steel reactor, detached from the Swagelock-Whitey valve assembly, was capped with a plastic cover in the argon atmosphere and taken outside of the dry box to be weighed. Vibrations rendered weighings made within the dry box less precise.

5.23.2 Reactions of F_2 with excess PF_5

Stainless steel reactor vessels (5 ml volume) were fitted with a filter assembly, as previously described, to a Swage-lock assembly and Whitey valves. PF_5 and F_2 were used following trap to trap distillation and storage over NaF. SP1 graphite which had been heated to red heat under dynamic vacuum for 1-2 hours was used. The reactor and vacuum line was passivated with ClF_3 vapor prior to all reactions.

Both tensimetry and gravimetry were used to monitor these reactions. Reaction conditions are summarized in Table 5.1. Typically evacuation times exceeded 500 hours. Plots of the weight lost after different time intervals fitted smooth single exponential curves, each with a parameter added for the offset to extrapolate to time zero (see Figures 5.2).

5.24 Preparations of Graphite Tetrafluoroborate

5.24.1 Direct reaction of BF_3 and F_2:

Stainless steel reactors and filter assemblies similar to those described above were used. The reactors and vacuum line were passivated with ClF_3 prior to use. Preheated SP1 graphite was used. F_2 and BF_3 were used after establishing their high purity by infrared spectroscopy. F_2 was stored over NaF prior to use (to remove HF).

5.24.2 Synthesis by displacement of PF_5 from Graphite Hexafluorophosphate with BF_3

Graphite fluoroborates prepared by reaction of second or higher stage hexafluorophosphate with BF_3 formed the central concern of this study. The reactions were followed by gravimetry, tensimetry, and infrared spectroscopy as described previously. In addition, X-ray powder diffraction patterns of the solids were recorded routinely. The reaction conditions and stoichiometries are tabulated in Tables 5.2 and 6.1. Evacuation times are indicated.

5.24.3 Attempted reaction of graphite with NO_2BF_4

Attempts were made to prepare the fluoroborate salt directly, without solvent. NO_2BF_4 was prepared by interaction of NO_2F and BF_3. This salt was formed in a 1/4" sapphire tube by condensing a 1:1 mixture of the two gases. NO_2F was prepared by treating $NaNO_2(s)$ with F_2 in a Monel can equipped with a Teflon gasket. Impurities (F_2, N_2O_4) were removed by fractional distillation, and the product was characterized by infrared spectroscopy. An excess of NO_2BF_4 was placed with SP1 graphite in a sapphire tube. The reaction mixture was treated with ultrasonic agitation at room temperature for 17 days with no visible reaction. The reactor was also heated mildly with no effect. Apparently, a solvent is necessary to induce reaction, and as solvent incorporation is an inevitable consequence of this technique, this is not an acceptable

synthetic route for pure graphite intercalation salts. In contrast O_2AsF_6 does intercalate graphite without a solvent; this is probably due to the slight vapor pressure of the salt, so that the actual process may involve the interaction of the graphite with $AsF_{5(g)}$ and $F_{2(g)}$ (the last derived from O_2F):

$$O_2AsF_{6(s)} \rightarrow O_2F_{(g)} + AsF_{5(g)}.$$

5.24.4 Electrochemical reduction of graphite fluoroborates

The electrochemical reduction of fluoroborate salts was carried out in an attempt to determine the degree of oxidation of the graphite π system in these salts.

An EG&G Model 271 Potentiostat/Galvanostat was employed. The electrode was fabricated by hydraulically pressing the graphite fluoroborate onto a platinum mesh which was attached to a platinum wire, after enclosing the materials in a plastic bag in the dry box. A copper counter electrode was used. The three electrodes were immersed in anhydrous HF, which had been stored over SbF_5 to remove any moisture. ≈1 M Sodium Fluoride served as the electrolyte. The cell body was a Kel-F cross, fitted with 1/2" Teflon ferrules on three ports and a 1/4" Whitey valve on the fourth. Electrodes were prepared by pressing mixtures of the fluoroborate salts, prepared from the reaction with SP1 graphite, with carbon black and teflon. The intercalation salt alone was not sufficiently cohesive to function as an electrode in the electrochemical cell.

The kinetics of the reaction at the electrode were too slow to achieve complete reduction. When a constant current of +50 μA was applied, the voltage fell to below zero, where coulometry is no longer valid. Likewise, under constant applied potential, the current fell to essentially zero in a matter of hours indicating less than 10% reduction of the salt. Reduction of the edges of the graphite proceeded first, followed by very slow reduction and migration of the bulk intercalant to the surface. Because of the air and moisture sensitivity of the oxidized material, as well as its strongly oxidizing character, alternative cell designs were not readily apparent.

5.24.5 ESCA measurements on graphite fluoroborate salts

In an attempt to obtain quantitative information on the oxidation state of the fluoroborate population in the graphite intercalant, X-ray photoelectron spectra were obtained for the fluoroborate salts prepared by PF_5 displacement for graphite fluorophosphate and for those salts which had been fluorinated.

The photoelectron spectra were collected using a GCA/McPherson ESCA 36 spectrometer. Approximately 100 mg of the air sensitive samples were pressed into small 1 mm x 1 mm plates and secured to an aluminum sample holder by epoxy in the dry box. They were loaded into the high vacuum ESCA apparatus in an inert helium atmosphere.

Boron 1s binding energies were measured. Signals obtained were discernible over the noise of the spectrum, but because of the poor quality of the spectra, no conclusions could be drawn concerning the differences in oxidation state populations between the various samples. A drawback to the technique, aside from its characterization of only the surface and not the bulk of the material, was that the heat generated from electron bombardment may have affected surface composition.

5.3 RESULTS and DISCUSSION

5.31 A Study of PF_5 Displacement by BF_3 and *vice versa*, involving alkali and tetra-alkyl ammonium salts of PF_6^- and BF_4^-

In the typical Born-Haber cycle shown below, the enthalpy change associated with formation of $A^+EF_6^-(s)$ or $A^+EF_4^-(s)$ from $AF_{(s)}$ and $EF_{5(g)}$ or $EF_{3(g)}$ is the sum of three enthalpies: the fluoride ion donor enthalpy, $\Delta H°(AF_{(g)} \rightarrow A^+(g) + F^-(g))$, the fluoride ion acceptor enthalpy, $\Delta H°(EF_{5(g)} + F^-(g) \rightarrow EF_6^-(g))$ or $\Delta H°(EF_{3(g)} + F^-(g) \rightarrow EF_4^-(g))$, and the lattice enthalpy of $A^+EF_4^-(s)$ or $A^+EF_6^-(s)$.

$AF_{(s)} + BF_{3(g)} \rightarrow A^+BF_4^-(s)$	$AF_{(s)} + PF_{5(g)} \rightarrow A^+PF_6^-(s)$
$\downarrow \quad \searrow F^-(g) \downarrow \quad \nearrow$	$\downarrow \quad \searrow F^-(g) \downarrow \quad \nearrow$
$A^+(g) \quad BF_4^-(g)$	$A^+(g) \quad PF_6^-(g)$

For the small cation salts (where differences in anion sizes are maximized) the lattice energy evaluations are reliable and typically, for the alkali salts, BF_4^- lattice enthalpies are 10 kcal mol^{-1} more exothermic than those of the corresponding PF_6^- salts.[11] Because the fluoride ion affinity of PF_5 is only 8 kcal mol^{-1} more exothermic than that of BF_3, and because other terms are the same for the two cycles, it can be concluded that BF_3 should displace PF_5 in such small cation cases. Indeed such a displacement was observed for the

potassium salt. Also, PF_5 was unable to displace BF_3 from the fluoroborate of sodium ($NaBF_4$).

The next case involved use of very large cation salts, the tetrabutylammonium fluoroborate salts. In this instance, one might speculate that because the cation is bulky, the lattice enthalpies would be more similar; any energetic advantages gained by small anions are thereby minimized. Experimentally an approximate equilibrium was observed between fluoroborate and fluorophosphate salts. The sum of the lattice enthalpies and fluoride ion affinities is evidently of the same value for these two salts. This means that the effect of increasing cation size to that of the tetrabutylammonium cation has been to diminish the lattice enthalpy advantage of the fluoroborate over the hexafluorophosphate by approximately 2 kcal mol^{-1}. The fluoroborate lattice enthalpy advantage is now equivalent to the fluoride ion affinity advantage possessed by PF_5.

These observations on the alkali and tetrabutlyammonium salts confirm the general validity of the Born-Haber cycle evaluations and the relative fluoride ion acceptor strengths of the BF_3 and PF_5. Since graphite, in its salts, might be expected to behave as a macro-cation rather than a small cation, it is apparent that the observed displacement of PF_5 from graphite hexafluorophosphate by BF_3 is not simply a one for one displacement. The characterization of the fluoroborate product was clearly of crucial importance. But it was

also important to use well characterized graphite hexafluorophosphate as the starting material.

5.32 The Preparation and Characterization of Graphite Fluorophosphates

Tensimetric and gravimetric results are shown in Table 5.3, for preparations in which the PF_5: F_2 ratio was approximately 2:1. It is evident that as the fluorine concentration, in the admixture of PF_5 with F_2, approaches that ideally required for the oxidizing half reaction: $PF_5 + 1/2\ F_2 \rightarrow PF_6^-$, the possibility of direct interaction of the fluorine with the graphite to make C-F bonds increases. Both reactions **a** and **c** show CF_4 in the infrared spectrum of the volatiles, a clear indication that reaction of graphite with fluorine has occurred. The identity of the evolved volatiles indicated in the table was established using infrared spectroscopy. The volatiles were trapped continuously under dynamic evacuation, and the absence of F_2 was verified by checking residual pressure at -196°C. From this technique good estimates of the final stoichiometries could be made. The presence of residual PF_5 in experiment **b** strongly implies that, in that preparation, some of the fluorine (intended for PF_6^- formation) is being consumed in forming C-F bonds in the solid phase. It is concluded that reactions with graphite in which the neutral fluoroacid is not present in excess of the fluorine required for anion formation is highly undesirable.

Weight loss as a function of time was also evaluated and typical curves are shown in Figures 5.1. Although the weight measurements are very reliable, unlike the weight loss of neutral-rich reaction mixtures described in the next section, these evacuation curves (see Figure 5.2) are not smooth; they have a broken pattern. This may be a consequence of significant amounts of relatively immobile fluorine attached to the carbon layers which intermittently blocks the orderly diffusion-limited exit of neutrals. Another possible effect of the fluorine bonding is the alteration of the plasticity or pliability of the layers, causing slower stage changes. In such C-F-bond containing materials the stage changing may be on a comparable time scale to that of the diffusion time scale of the neutral guests. The departures from smooth curve behavior (see Figure 5.2) could be a consequence of stage (phase) changes occurring fitfully over the time of the evacuation of the volatiles.

Table 5.1 summarizes the results of fluorophosphate preparations in which PF_5, in excess of that required to form PF_6^-, was used in their combination with fluorine to bring about graphite intercalation. The stoichiometries of the vacuum stable products are listed there. The loss of volatiles in these reactions is gradual and the evacuation curve illustrated for typical cases (Figures 5.2) is smooth. The exponential form of the curve suggests that the loss of PF_5 is diffusion limited. It seems likely, in light of the NMR

evidence[6] which suggests that $P_2F_{11}^-$ dimers are present in non-vacuum stable hexafluorophosphate intercalants, that the migration of the neutral PF_5 out of the bulk occurs through dimer formation:

$$'PF_5 + PF_6^- \rightarrow F_5'P\text{-}F\text{-}PF_5 \rightarrow 'PF_6^- + PF_5$$

Thereby neutral is transferred from one site to another.

Tensimetry and X-ray diffraction evidence indicate that the initial product of the reaction is at least a mixture of first stage and second stage (see Chapter 6). The first-stage salt convert to second stage as PF_5 removal proceeds. Since no break is observed in these evacuation curves, the stage changes must be occurring rapidly and continuously from the beginning of PF_5 loss. The system from the outset of the PF_5 loss is then a two stage one (two phase) involving first and second stages. The quantity of PF_5 lost in those circumstances is simply dependent on the quantity of first stage material remaining.

Unless complete vacuum stability is established, neutrals remain and are identified as anions. If that occurs the oxidation appears to be greater, than in fact it is, yet physical measurements will show lower overall charge transfer. Such confusion may lie behind the interpretation of some findings in the graphite AsF_5 system and could account for much of the controversy.

The present studies and those of Okino[9] and Rosenthal[2] have shown that close packed first stage salts containing

neutral molecules do convert to higher stage if properly evacuated. True first stage salts, containing few neutrals, are preparable however if appropriate (usually more powerfully oxidizing) conditions are employed. An instance of that approach is Okino's[12] employment of $C_6F_6^+AsF_6^-$ to prepare first stage (vacuum stable) $C_{10}AsF_6$:

$$10\ C + C_6F_6AsF_6 \rightarrow C_{10}AsF_6 + C_6F_6.$$

Conductivity measurements were made on the graphite solids to monitor the fluorination of carbon in these intercalation compounds, and to determine whether excess neutral protects the carbon layers from its reaction with fluorine. Okino[9] had observed marked impact of fluorine uptake (in excess of that required to form the anion) on the conductivity. In the system $C_{14}AsF_6$ (a first stage nestled salt) the addition of two additional F atoms per formula unit ($C_{14}AsF_6 \cdot 2F$) brought the specific conductivity down by an order of magnitude. The best known system where C-F bonding impact on conductivity has been studied however is that of C_2F which is an insulator.[3] Similar effects have been noted in this work.

The conductivities of the graphite fluorophosphates are tabulated in Table **5.4**. This data demonstrates that hexafluoride compounds which have been slightly fluorinated exhibit a marked drop in conductivity. The highest observed specific conductivities for these pelletized solids were close to 1300 Ω^{-1} cm^{-1}- a five to six fold decrease in conductivity

from that of the unfluorinated carbon relative. Second stage fluoroborate salts which have been prepared with higher fluorine concentrations, than strictly required for anion formation, in the reaction mixture show conductivities in the region of 200-300 $\Omega^{-1}cm^{-1}$. This indicates that in the fluorine rich systems some fluorination of the carbon layers has occurred. In contrast, fluorophosphate salts which were prepared with excess of neutral over fluorine exhibit higher conductivities. A large excess of neutral evidently diminishes the opportunity fluorine has of encountering graphitic carbon; evidently the fluorine reacts preferentially with the neutral fluoroacid. The findings are clear: a preparation using excess neutral achieves the goal of inhibiting fluorination of carbon. Such salts prepared in this study, because of their higher conductivities, must have minimal direct C-F bonding.

These findings suggest mechanisms which may both cause fluorination of the graphite when fluorine is present in high concentration and avoid that process when excess neutral is present.

Since the formation of graphite salt $C_x^+AF^-$ (A is a fluoride-ion acceptor such as BF_3 or PF_5) means that the carbon sheets become positively charged, it is at first sight surprising that the electrophilic fluorine atom would attack the positive carbon. Indeed it is probable that the attack on the positive carbon involves transfer of F^- from an anion.

Since F^- is likely to be more firmly held by two acceptor species A than by one, it is less likely that such a process will occur when the anions are $P_2F_{11}^-$ and $B_2F_7^-$, than if the anions are BF_4^- and PF_6^-. It is even possible, that in regions of high fluorine concentration, species such as PF_7^{2-} and BF_5^{2-} could form transiently. Certainly such doubly charged anions would be potent F^- donors, but the singly charged PF_6^- and BF_4^- may be sufficient for that purpose. This F- transfer will probably occur much more readily in first-stage systems, since, under those circumstances, an anion on each side of a given carbon sheet viz:

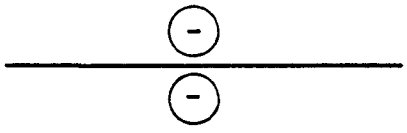

is more likely to localize a higher positive charge at a given carbon atom than is possible for any higher stage material[13]. Certainly the experimental findings show that fluorination of the carbon sheets is more likely to occur in first-stage salts than in those of higher stage.

5.33 Fluoroborate salts prepared by displacement of PF_5

As previously noted, the displacement of PF_5 by BF_3 was first investigated by Rosenthal[2] in these laboratories. There remains, however, some question as to whether the reaction products were correctly described, since the procedure used by Rosenthal failed to address the problems of fluorination of carbon and vacuum stability of the product.

In this work, the complete displacement of PF_5 by BF_3 was checked by subsequent treatment of the reaction product with the superior fluoroacid AsF_5. Arsenic pentafluoride was shown to displace both BF_3 and PF_5 from second stage graphite fluoroborate and fluorophosphate salts. This is achieved because arsenic pentafluoride possesses a fluoride ion affinity[3] of -117 kcal mol^{-1}, which greatly exceeds those of BF_3 and PF_5, for which the fluoride ion affinities[3] are -92 and -100(1) kcal mol^{-1}, respectively. Since the displacement reaction is an exchange of fluoride ion ($AsF_5 + PF_6^- \rightarrow AsF_6^- + PF_5$), the stronger fluoride ion acceptor, AsF_5, will displace the weaker ones, BF_3 and PF_5. The product of the reaction of BF_3 with the hexafluorophosphate salt was further reacted with AsF_5, as described in the experimental section. Infrared spectra of the displaced volatiles were consistent with complete elimination of BF_3 by AsF_5; PF_5 was not observed. X-ray powder photographs show a mixture of first and second stage arsenic hexafluoride salts typical of the product of interaction of AsF_5 with graphite itself.

$$C_{28}PF_6 + (xs)\ zBF_3 \rightarrow C_{28}(BF_3)_x(PF_5)_y + (1-y)PF_5 + (z-x)BF_3$$

$$C_{28}(BF_3)_x(PF_5)_y + AsF_5 \rightarrow C_{28}AsF_6(AsF_5) + xBF_3 \quad (y = 0)$$

It can be safely concluded that boron trifluoride completely displaces phosphorus pentafluoride quantitatively from $C_{28}PF_6$.

Table **5.2 (b)** shows some compounds obtained from the elimination of PF_5 from C_xPF_6 by BF_3. The reaction products contain neutrals together with anions at the extreme limits of

evacuation, as determined by gravimetry. It is noteworthy that through this displacement a second-stage hexafluorophosphate intercalation salt is converted to second stage fluoroborate, and there is evidence (see high pressure BF_3 studies, Chapter 6) that first-stage materials also formed.

From Table 5.2 it is seen that the limiting (vacuum stable) composition for the fluoroborate prepared from C_xPF_6 is approximately $C_xBF_4 \cdot 1/3(BF_3)$. The persistent presence of neutral BF_3 is almost certainly an important factor in the energetics which results in the quantitative displacement of PF_5. As has been discussed earlier, if the displacement were simply one BF_3 for one PF_5 and there was no change in stage (or charge) the displacement could not occur.

The $C_xBF_4 \cdot 1/3(BF_3)$ is always one of close packed F ligands (see Chapter 6) whereas the C_xPF_6 from which it is derived is never so. Thus when one starts with second stage C_xPF_6, the resulting $C_xBF_4 \cdot 1/3(BF_3)$ is third stage or higher (see Tables 5.5 and 6.1). Clearly the presence of the BF_3 provides for a high volume concentration of anions in the $C_xBF_4 \cdot 1/3(BF_3)$ than in C_xPF_6. Therefore the BF_3 is acting as an effective dielectric spacer. Alternatively it could be forming the species:

$$[F_3B - F - BF_3]^-$$

The observed close packing however indicates that each BF_3 may

be shared with two or more BF_4^- in which case the simple dielectric spacer model is more appropriate.

It is clear that this dielectric spacer (or bonding) impact of the BF_3 provides energy advantage which is crucial to the displacement of PF_5 from the graphite fluorophosphate by BF_3.

Table 5.1		Representative Preparations of C_xPF_6			
Ratio PF_5:$\frac{1}{2}(F_2)$		Reaction Time(hrs) (20°C)	Evacuation Time(hrs) (20°C)	Stoich. at termination of neutrals removal	Comment and Stage
a	5.7:1	352 (net) (4 rxns)	259	$C_{31}PF_6$	2
b	3.1:1	179 (net) (2 rxns)	394	$C_{27.9}PF_6$	2
c	5.6:1	624 (net) (4 rxns)	324	$C_{30.7}PF_6$	2
d	3:1	48	499	$C_{32.7}PF_6(PF_5)_{0.12}$‡ ($C_{29.74}PF_6$)	2(3 trace)
e	3:1	48	499	$C_{30.1}PF_6(PF_5)_{0.08}$‡ ($C_{28.23}PF_6$)	2
f	3:1	48	499	$C_{23.3}PF_6(PF_5)_{0.01}$‡ ($C_{23.2}PF_6$)	2
g	5:1	92	950	$C_{26.4}PF_6(PF_5)_{0.04}$‡ ($C_{25.4}PF_6$)	2
h	4.5:1	92	950	$C_{30.4}PF_6(PF_5)_{0.18}$‡ ($C_{26.3}PF_6$)	2(3? trace)
i	4.8:1	92	950	$C_{29.9}PF_6(PF_5)_{0.12}$‡ ($C_{27.1}PF_6$)	2
j	4.3:1	191 (net) (2 rxns)	624	$C_{31.3}PF_6$	
k	5.5:1	191 (net) (2 rxns)	624	$C_{31.7}PF_6$	
l	5.4:1	191 (net) (2 rxns)	624	$C_{33.1}PF_6$	
m	4.0:1	220 (net) (2 rxns)	720	$C_{30.5}PF_6$	
n	3.6:1	220 (net) (2 rxns)	720	$C_{28.6}PF_6$	
o	4.1:1	220 (net) (2 rxns)	720	$C_{28.0}PF_6$	2

See Next Page for Notes to Table 5.1

Notes to Table 5.1

‡ see Table 5.5 for Second and Third Stage X-ray powder patterns for these materials.

† to obtain compositions at infinite evacuation time subtract the PF_5 residue.

Table 5.2 Graphite Fluorophosphate and Fluoroborate Stoichiometries /Vacuum Stability			
	Extrapolated Stoichiometry	PF_5 Displacement† by gravimetry	by tensimetry
a	$C_{32.7}PF_6 \cdot (0.12)PF_5$	$C_{32.7}(BF_3)_{3.0}F$	$C_{32.7}(BF_3)_{3.8}F$
b	$C_{30.1}PF_6 \cdot (0.08)PF_5$	$C_{30.1}(BF_3)_{3.0}F$	$C_{30.1}(BF_3)_{4.1}F$
c	$C_{23.3}PF_6 \cdot (.006)PF_5$	$C_{23.3}(BF_3)_{3.4}F$	$C_{23.3}(BF_3)_{3.2}F$

† The compositions listed under tensimetry are those determined from the BF_3 consumption as measured by the pressure drop in the system of known volume. The compositions listed under gravimetry were obtained by weighing the samples briefly opened to the argon atmosphere of the dry box. The tensimetry composition is a more reliable measure of the composition of the BF_4^-/BF_3 complex under BF_3 pressure.

Table 5.2 (cont.)			
Evacuation Time (hours)	Stoichiometry **a**	**b**	**c**
45	$C_{32.7}(BF_3)_{1.50}F$	$C_{30.1}(BF_3)_{1.48}F$	$C_{23.3}(BF_3)_{1.46}F$
122	$C_{32.7}(BF_3)_{1.44}F$	$C_{30.1}(BF_3)_{1.45}F$	$C_{23.3}(BF_3)_{1.42}F$
139	$C_{32.7}(BF_3)_{1.41}F$	$C_{30.1}(BF_3)_{1.41}F$	$C_{23.3}(BF_3)_{1.39}F$
445	$C_{32.7}(BF_3)_{1.37}F$	$C_{30.1}(BF_3)_{1.36}F$	$C_{23.3}(BF_3)_{1.37}F$
40 days in dry box	$C_{32.7}(BF_3)_{1.32}F$	$C_{30.1}(BF_3)_{1.35}F$	$C_{23.3}(BF_3)_{1.36}F$

Table 5.3 Tensimetry and Gravimetry Employed to Determine Fluorine Incorporation when $PF_5:F_2$ Approaches Unity

	Reaction Conditions	Residual Fluorine	Infrared of Volatiles	Comments
a	F:C = 1:33.6 PF_5:C = 1:29.8	0	CF_4	Some Fluorine uptake to make CF_4
b	F:C = 1:33.3 PF_5:C = 1:33.3	0	PF_5	Residual PF_5 indicates some Fluorine bond formation with graphitic carbon
c	F:C = 1:34.2 PF_5:C = 1:33.6	0	$PF_5:CF_4$ 3:4	Some Fluorine to make CF_4

Evacuation (-196°C)		
	Evacuation Time (hours)	Calibrated Infrared of Volatiles trapped
a	105	$PF_5:CF_4$ = 2:1
b	105	PF_5
c	105	PF_5, trace CF_4

Stoichiometry Based Upon Tensimetry and Gravimetry	
a	$C_{56.8}PF_6 \cdot (0.3)\ PF_5$
b †	$C_{38.3}(PF_6) \cdot (0.12)\ F$
c †	$C_{45.3}(PF_6) \cdot (.02\text{-}.06)\ F$

† Since the compositions stated are those for the vacuum stable limit in which neutral PF_5 can be assumed to be absent, it is appropriate to express the phosphorus species as PF_6^-.

Table 5.4 Conductivity of Polycrystalline Graphite Salts (Pressed Pellets Using Four-Probe Method)

Stoichiometry	Stage (c) (Å)	σ (Ω^{-1} cm^{-1})	σ_N‡	remarks
SP1 Graphite	-	642	642	
Fluoroborates:				
$C_{14.5}BF_4$	2 (≈10.8)	194	313	prepared with excess fluorine
$C_{16.2}BF_4$ ($C_{22}(BF_3)F_{1.8}$)†	2 (10.95)	163	266	
$C_{28}BF_4(BF_3)_{0.6}$	3 (14.5)	1377	1987	
$C_{28}BF_4(BF_3)_{0.6}$ + ≈0.50 F	3/2 (14.62)	410	596/445	
$C_{28}BF_4(BF_3)_{0.4}$* + 0.5 F	2 (10.6)	490	775	
* = idealized	† obtained from tensimetry and gravimetry			
Fluorophosphates:				
$C_{27.8}PF_6$	2 (≈10.9 Å)	876	1425	
$C_{31}PF_6$	2 (≈10.9 Å)	1257	2045	
Fluorophosphate +1/2 F_2	2 (a)	113	184	*
	2 (b)	100	162	

* Compared with the fluoroborate salts, the impact of fluorine in lowering conductivity is much more severe. This (as well as the stage change observed) indicates the presence of neutral BF_3 in fluoroborate salts.

‡ σ_N = Normalized to graphite. $\sigma(2/n)(c/c_{graphite})$, where c = unit cell "c" spacing, $c_{graphite}$ = 6.7 Å, and n = stage.

Table 5.5 X-ray Powder diffraction of Fluoroborate Salts

Fourth Stage $C_{30.1}BF_4(BF_3)_{0.35}$ a= 2.46 Å, c= 17.8

No.	Intensity	$1/d^2$ (obs.)	$1/d^2$ (calc.)	Assignment
1	vstrng	.07802	.0786	005
2	med broad	.1121 .1148 .1162	.1132	006
3	med sharp	.2209	.2204	100
4	weak broad	.2355 .2398 .2455	.2334 .2490	102 103
5	vw	.3121	.3144	00 10
6	mw	.3819	.3804	00 11
7	med sharp	.6610	.6613	110
8	vw	.7401	.7399	115
9	vvw sharp	.8040	.8049	00 16

Third Stage $C_{23.3}BF_4(BF_3)_{0.39}$ a= 2.46, c= 14.6 Å

No.	Intensity	$1/d^2$ (obs.)	$1/d^2$(calc.)	Assignment
1	strng	.0751	.0751	004
2	med	.1213	.1174	005
3	sharp	.2209	.2201	100
4	medium	.2290	.2301	007
5	weak(broad)	.2489	.2506	102+103/2
6	weak	.3059		
7	weak	.3883	.3891	106
8	sharp	.6113	.6603	110
9	weak	.7345	.7354	114
10	vw	.8766	.8804	200

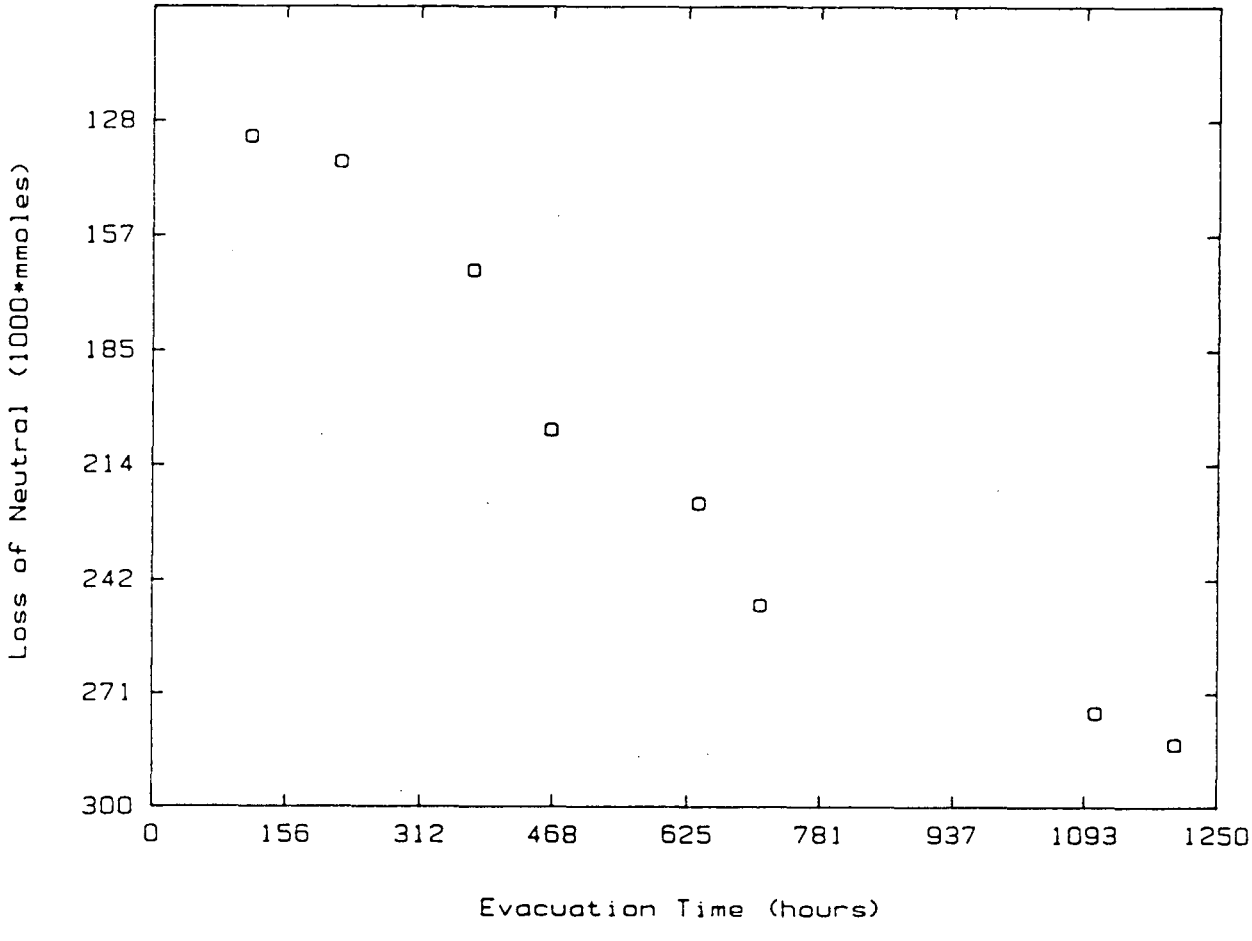

Figure 5.1 Evacuation Curve of Graphite Fluorophosphate where PF_5 : 1/2 F_2 approaches unity.

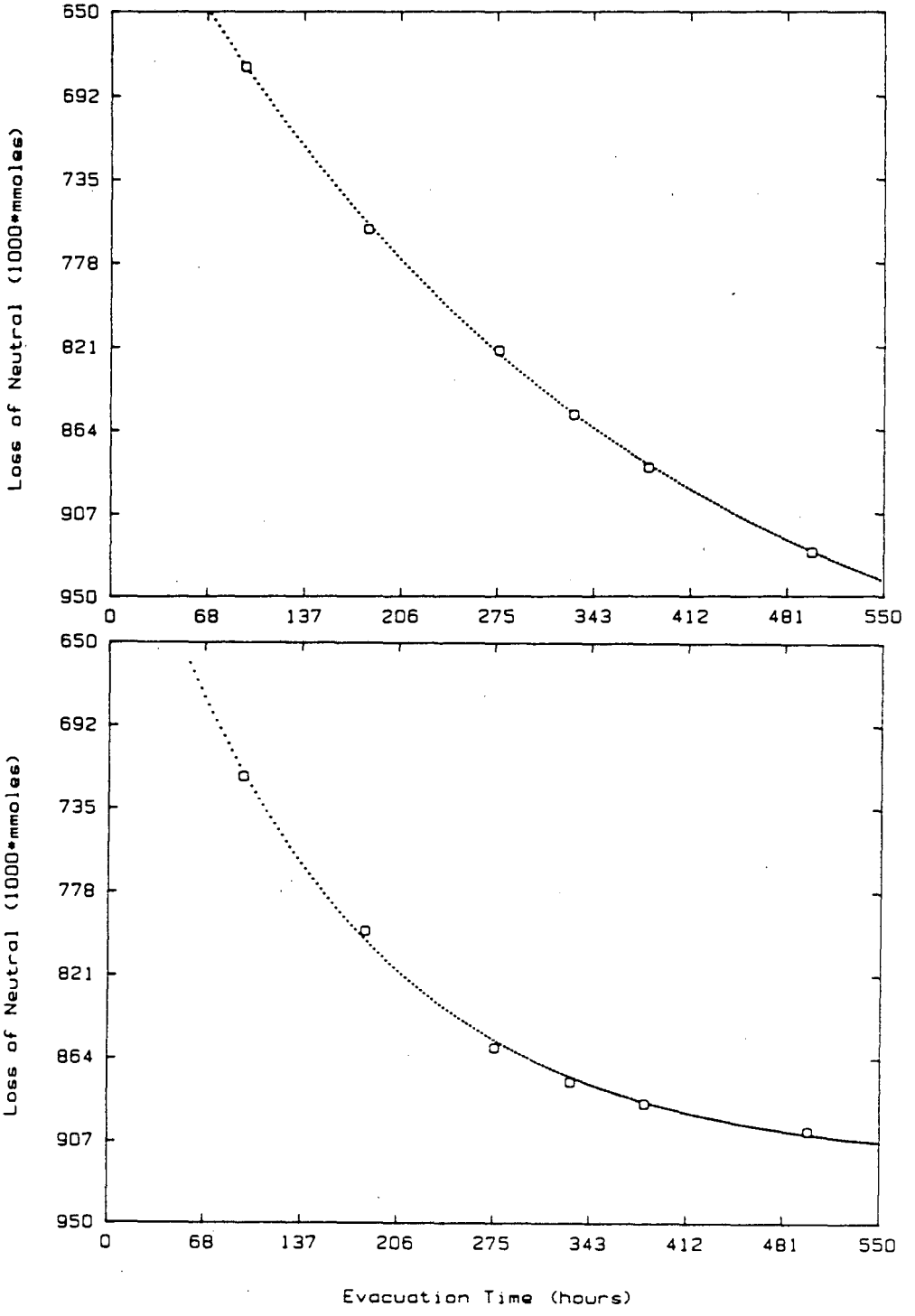

Figure 5.2 Weight loss of PF_5 upon long term evacuation for graphite fluorophosphate salts.
Dotted line is a single exponential fit to the data.
Stoichiometries after 500 hours of evacuation are:
(a) $C_{32.7}PF_6 \cdot (.115)PF_5$ (b) $C_{23.3}PF_6 \cdot (.006)PF_5$

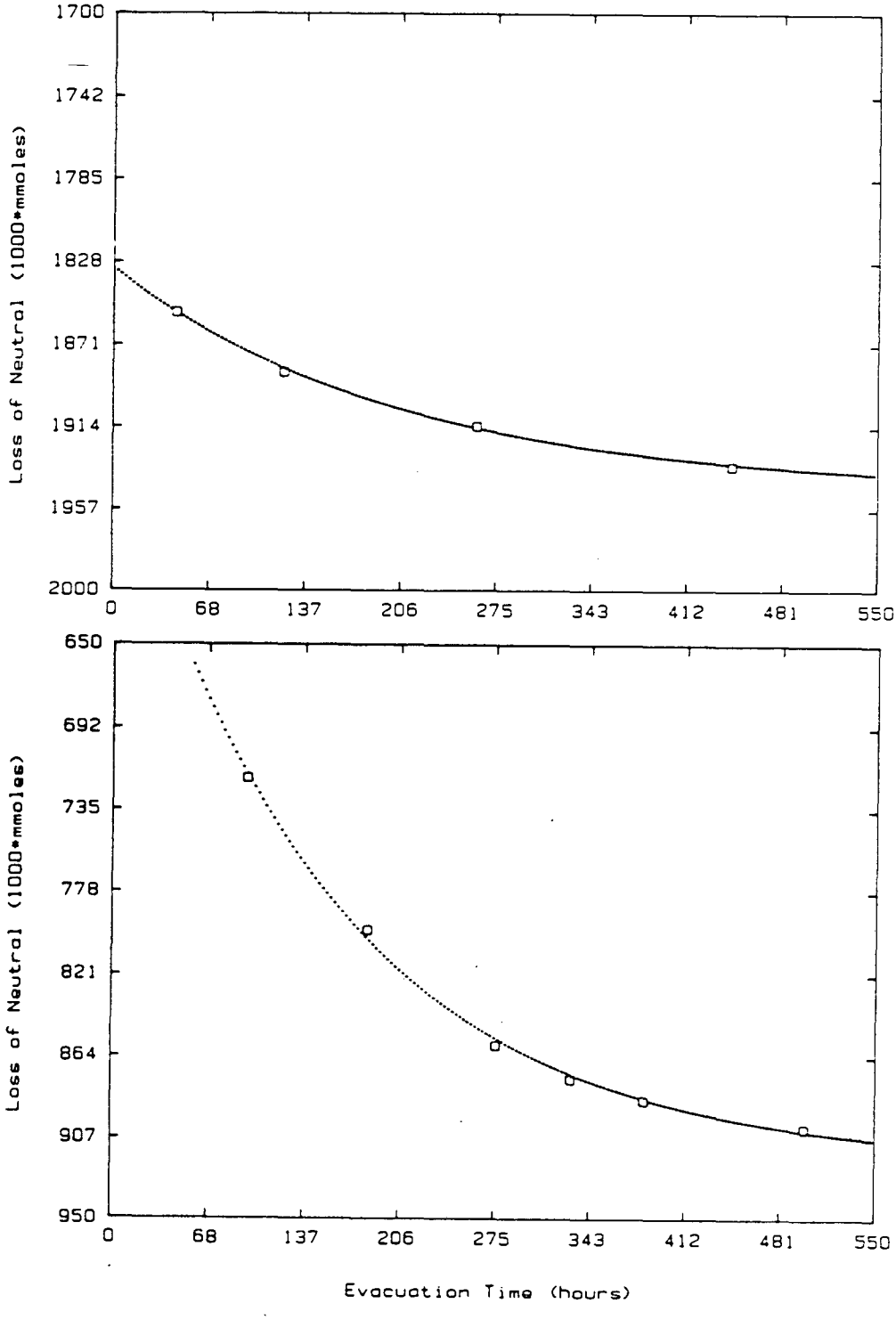

Figure 5.3 Comparison of rate of neutral loss between graphite fluoroborates and fluorophosphates. Stoichiometries after 445 and 500 hours of evacuation are: (a) $C_{23.3}BF_4 \cdot (0.37)BF_3$ (b) $C_{23.3}PF_6 \cdot (0.01)PF_5$

Figure 5.3 Notes

It is evident that, compared to the fluorophosphates, the fluoroborate salts approach vacuum stability more quickly. Apparently, diffusion of boron trifluoride through the bulk, probably through the transient formation of the $B_2F_7^-$ dimer, is more rapid than PF_5 diffusion but still slow compared to the time scale of stage changes. $B_2F_7^-$ species as well as $P_2F_{11}^-$ have been observed for simple ionic salts. The fluoroborate dimers are less stable than the fluoro phosphate dimers, and this could explain the difference in diffusion rates. The weaker fluorine bridge-bonding may manifest in faster diffusion through the salt.

Chapter 5 References

1. N. Bartlett, R.N. Biagioni, B.W. McQuillan, A.S. Robertson and A.C. Thompson, **J. Chem. Soc., Chem. Comm.**, 200-201 (1978); N. Bartlett, R.N. Biagioni, E. McCarron and F. Tanzela, **Molecular Metals** 293-299 (1979); R.N. Biagioni, Ph.D. Thesis, U.C. Berkeley (1980).

2. G. Rosenthal, Ph.D. Thesis, U.C. Berkeley (1984).

3. T.E. Mallouk, G.L. Rosenthal, G. Müller, R. Brusasco and N. Bartlett, **Inorg. Chem.** 23, 3167 (1984); T. Mallouk, Ph.D. Thesis, U.C. Berkeley (1982).

4. E. McCarron and N. Bartlett, unpublished results.

5. B. McQuillan and N. Bartlett, unpublished results.

6. L.B. Ebert, D.R. Mills, J.C. Scanlon and H. Selig, **Mat. Res. Bull.** 16, 831-840 (1981).

7. D. Billaud, A. Chenit, **Mat. Res. Bull.** 18, 1001-1006 (1983); **Synthetic Metals** 2, 177-184 (1980); D. Billaud, A. Pion, F. Vogel and A. Herold, **Mat. Res. Bull.** 15, 1627-1634 (1980).

8. J.W. Milliken and J.E. Fischer, **J. Chem. Phys.** 78, 3 (1983).

9. F. Okino, Ph.D. Thesis, U.C. Berkeley (1984).

10. E. McCarron, Ph.D. Thesis, U.C. Berkeley (1980).

11. This was shown for a variety of simple ionic salts, to within 1 kcal mol^{-1} (reference 3).

12. F. Okino and N. Bartlett, unpublished data.

Chapter 6

Graphite Fluoroborates and the Structural and Energetic Roles of BF_3

6.1 Introduction:

As noted in Chapter 5, the conversion of C_xPF_6 through treatment with excess BF_3 occurs with the addition of $y(BF_3)$ to the form $C_xBF_4 \cdot y(BF_3)$. In this process, if only BF_4^- was formed in a one on one displacement of PF_5, and if the stage remained the same, voids would be left in the salt, because the BF_4^- ion has only 2/3 the volume of PF_6^-. However, BF_3, which is flat and thin, can enter voids between the BF_4^- ions. These two properties, the size of the anion (BF_4^-) and the shape of the neutral (BF_3) permit a high concentration of BF_3 per formula unit volume for the same effective volume as PF_6^-. The nature (composition and structure of graphite/BF_4/BF_3 phases) will be the focus of this chapter.

The fact that BF_3 can fill most of the space not occupied by BF_4^- will be shown through analysis of stoichiometries obtained of salts rich in BF_3 (second stage) and of salts in which some BF_3 (but not all) is released during the conversion to higher stages. Modelling of the X-ray diffraction behavior of second and fourth stage graphite fluoroborates will be used to show that a hard-sphere, close packing model of BF_4^- and BF_3 is in good agreement with the observed X-ray diffraction data.

The simple model of BF_3 as an electrostatic spacer (described in Chapter 5) will be used to explain the experimental observations of the stoichiometry-stage dependence of fluoroborate salts $C_xBF_4 \cdot y(BF_3)$, when the parameter "y" varies. The effect of high BF_3 and PF_5 pressure on the stage of graphite salts will be discussed in terms of this model. In addition, the effect on stage (and close packing) when the anion concentration is increased by fluorine oxidation (BF_3 + 1/2 F_2 + e^- → BF_4^-), and **y** decreased, will also be considered in those same terms.

6.2 Experimental

6.21 Tensimetric, gravimetric and X-ray experiments to determine the composition of graphite fluoroborate salts under BF_3 pressure

A quartz reactor was prepared for in situ X-ray experiments. This permitted gravimetric and tensimetric measurements to be made simultaneously with an X-ray powder diffraction photograph of the solid. A 1/4" o.d. quartz tube joined via a graded seal to a stainless steel tube was attached, with metal ferrules, to a 1/4" Whitey valve. Two small 100 mesh stainless steel metal filters and two pieces of coarse TFE (Zitex, Norton Chemplast) filter paper were placed in the Swagelock union (see Table **6.4**). The quartz tube was drawn down to an approximately 0.7 mm diameter (≤ 0.1 mm wall thickness). The volume of the reactor and vacuum line was determined tensimetrically by the expansion of helium from a known volume. The weight of the reactor assembly was recorded when evacuated and while containing different pressures of BF_3.

Tensimetry revealed the amount of neutral BF_3 absorbed by the salt. A correction for the volume occupied by the salt was applied using its unit cell dimensions, composition and weight.

The amount of BF_3 taken up by the salt while under pressure was also ascertained by measuring the weight change of the reactor. After correcting for the residual weight of

$BF_{3(g)}$ in the reactor, the difference between the weight of the evacuated salt and the weight after reaction and venting to a static vacuum gave the quantity of BF_3 taken up by the solid. The X-ray powder pattern obtained <u>in situ</u> was thereby associated with a stoichiometry obtained by two independent methods: tensimetry and gravimetry. Hence, the stoichiometry and stage of a non-vacuum stable salt was reliably determined.

6.22 High Pressure, <u>in situ</u> X-ray Experiments

Typically, 0.7 mm quartz capillaries were loaded with ≈5 mg of the appropriate salt. The capillaries were attached to a 1/8" to 1/4" Swagelock reduction union with Teflon ferrules and connected to a Whitey valve. The whole assembly and the vacuum line were passivated with ClF_3 vapor prior to use. The assembly was directly pressurized to ∿95 psi; the pressure was monitored with an Acco (Helicoid, inc.) Monel Bourdon gauge. X-ray (Cu Kα, Ni filtered) powder photographs were obtained, with 36-48 hour exposures (without the advantage of rotation of the capillary in the X-ray beam). The reactions are listed in Table **6.6**.

6.23 Fluorination of Fourth Stage Fluoroborates

Procedures similar to those described in Chapter 5 were followed. Large (200-300 mg) samples were employed in order to obtain sufficient weight change for accurate gravimetry. Previously described stainless steel reactors were used.

Stoichiometric amounts of fluorine was added to the sample. The reactor was agitated for slightly less than 1 day. X-ray photography indicated that when stoichiometric amounts of fluorine were incorporated, second stage salts were formed:

$$\underset{\text{third stage}}{C_{23.3}BF_4(BF_3)_{0.39}} + 0.4F \rightarrow \underset{\text{second stage}}{C23.3(BF4)1.39}$$

$$\underset{\text{third stage}}{C_{28}BF_4(BF_3)_{0.6}} + 0.5\ F \rightarrow \underset{\text{second stage}}{C28(BF4)\sim 1.6}$$

In related experiments, <u>in situ</u> X-ray photographs were obtained in a fluorine atmosphere as described in the section above (for PF_5 and BF_3 atmospheres). Much lower fluorine pressure (< 1 atmosphere) was applied. These <u>in situ</u> photographs showed second stage formation, from fourth stage $C_xBF_4 \cdot y(BF_3)$ starting material, in all cases.

6.3 Results and Discussion

6.31 Structural Models for the Graphite Fluoroborates $C_xBF_4 \cdot y(BF_3)$

The method used to prepare graphite fluoroborate was described in detail in Chapter 5. In these preparations, BF_3 was condensed on to $C_{29}PF_6$ in larger excess than that required for a 1:1 displacement of PF_5 by BF_3. The composition obtained after several hours of evacuation was roughly C_xBF_4 $1/3BF_3$, as shown in Table 5.2 (**b**). As demonstrated in Table **6.1**, the intercalant volume for these fluoroborates, and those of low stage which are BF_3 rich, appear to closely match the volume available in the gallery. The volume available between the carbon layers was calculated from the unit cell volume, determined from powder X-ray diffractions, less the volume of the carbon atoms. The volume of the carbon atoms was evaluated from the unit cell parameters of graphite. The intercalant volume (for instance, $BF_4 \cdot 1/3\ BF_3$), was determined by assuming that F ligands are the only contributors to the total volume. As shown in Table **6.1**, two extremes of fluoride ion volumes were used, 17.2 and 17.8 $Å^3$, respectively. These fluoride ion volumes were obtained from well known crystallographic data on binary fluorides and alkali complex fluorometallantes. In all cases, following Zachariasen[1], the coordinating atom is assumed to occupy negligible space-simply occupying octahedral and tetrahedral holes.

Hence, the intercalant volume was determined by multiplying these volumes by the number of fluorine ligands. The ratio of the intercalant volume and the available gallery volume is also listed in Table **6.1**. This ratio is a measure of the relative space filling efficiency of the intercalant.

Table **6.1** clearly demonstrates that in fourth stage fluoroborate salts the intercalant approaches high space filling efficiencies. This is also true for second and third stage BF_3 rich salts, such as $C_{29}(BF_3)_{2.65}F$ and $C_{32.7}(BF_3)_{2.2}F$, which will be discussed shortly. In contrast, fluorine ligands of PF_6^-, such as in the salt $C_{30}PF_6$, fill much less of the available space.

These observations suggest a structural model for fourth stage $C_{30.1}BF_4(BF_3)_{0.35}$ and $C_{32.7}BF_4(BF_3)_{0.37}$, second stage $C_{28.8}BF_4(BF_3)_{1.7}$ and third stage $C_{32.7}BF_4(BF_3)_{1.2}$ (shown in Table **6.1**). In this model, illustrated in Figure **6.1**, the intercalant is envisioned as a simple closed packed double layer of fluorine ligands between the carbon sheets, since the close packed arrangement is the most efficient at filling space.

The effective volume per F ligand of 17 $Å^3$ is the volume per F ligand in a close packed array and therefore includes the volume of the close packing voids. The 100 % space filling observed in the $C_xBF_4 \cdot y(BF_3)$ adducts therefore is consistent with the close packing of the F ligands between the carbon sheets.

If BF_4^- is regarded as a tetrahedral anion composed of hard sphere ligands, then these ligands can form a close packed double layer. For such a double layer, for each fluorine ligand there is one tetrahedral hole (for close packing which involves many layers, the number of tetrahedral holes is twice the number of ligands). Since there are four fluorine ligands for each tetrahedral anion, 1/4 of the tetrahedral holes are occupied. For a stoichiometry such as $C_{28.8}BF_4(BF_3)_{0.35}$, every fourth tetrahedron is replaced by BF_3. Every fourth boron atom must then (on average) occupy a trigonal position (in the face of the tetrahedron) in the close packed double layer. In second stage $C_{28.8}BF_4(BF_3)_{1.7}$, for every 3 tetrahedral there are 5 trigonal borons.

The BF_3 rich second stage salts, such as $C_{28.8}BF_4(BF_3)_{1.7}$ provided a convenient means for testing this hypothesis, because of the reasonable quality of the X-ray diffraction data available. The indexing of the X-ray powder diffraction pattern of this salt in shown in Table **6.2**. It is noteworthy that whenever there was excess neutral in these intercalation salts, the X-ray diffraction patterns appeared sharper and more highly defined than their counterparts from which much neutral BF_3 had been removed. This effect is probably due to the close packed F array in the occupied galleries of the former and the more haphazard placement of anions in the latter. The haphazard placement of anions probably cause small variations in layer spacing, thus broadening 00ℓ dif-

fraction lines to give the diffraction character typical of poor crystallinity. With neutrals present the galleries become completely filled and the carbon sheet - carbon sheet spacing, as a consequence, more uniform.

In a calculated simulation of the second stage salt $C_{29}BF_4(BF_3)_{1.7}$ and fourth stage $C_{30}BF_4(BF_3)_{0.35}$, the borons were placed in idealized trigonal and tetrahedral interstices. The fluorine ligands were placed in a closed packed double layer. The carbon atoms were also placed at idealized positions; the distance between contiguous carbon layers was the same as that in graphite, 3.35 Å. The atomic coordinates are listed in Table **6.3**.

In the calculation, both layers of the fluorine double layer were moved simultaneously towards and away from the center line of the gallery (see Figure **6.1**). Hence, a single parameter, "**delta**" was varied, the distance of the fluorine layers from the gallery center divided by **c**, the crystallographic "c" spacing. Since the value of the **c** parameter is not the same for a second as for a fourth stage salt, the units of **delta** are different for the two salts. For each fractional increment in **delta**, a set of 00ℓ diffraction intensities was calculated. These results are displayed in Figures **6.2** and **6.4**. The extreme left of these plots shows **delta** at "0"; both fluorine layers are at the gallery center. The extreme right hand side shows the fluorine layers at their

maximum separation. At this point each layer will overlap with a carbon layer.

Appropriate scattering factors, geometric and thermal parameters were included in the calculations and are tabulated in Table **6.3**. Values for the thermal parameters chosen were similar to those used for arsenic fluoride intercalant modelling.[2] Variation of the thermal parameters for C, B, and F did not produce significant changes in the 00ℓ relative intensities. However, some thermal motion of the borons was required to obtain reasonable intensity ratios.

A comparison to the experimental 00ℓ intensity ordering was made. Microdensitometer tracings can give quantitative intensities of the X-ray diffraction lines in the Debye Scherrer patterns of second and fourth stage salts; these are shown in Figures **6.3** and **6.5**. The X-ray indexings of these diffraction patterns are shown in Tables **6.2** and **5.6**. Upper traces shown in the figures are those obtained using higher gain and show more detail. Dotted lines show diffuse scattering from the quartz X-ray capillaries (0.3 mm o.d.). The amount of diffuse scattering was slightly different for the two samples probably because of differences in exposure time and slight attack on the quartz by the second stage BF_3-rich salt.

In the second stage salt, I[observed] (001) : (003) : (004) is approximately 1 : 3 : 0.9. (005), (006) and (002) are all weak lines and are only faintly visible. Because the

measurement of sharp (001) and (003) intensities is more accurate than that of the diffuse (004) line, the ratio of these intensities was used to determine the fluorine layer separation. Figure **6.2** displays the intensity dependence of fluorine layer distance from the center of the gallery (in units of delta). When the fluorine layers are 1.11 Å away from the center line of the gallery (delta = 1.11 Å/10.85 Å = 0.102), the theoretical intensities approximate those observed. I[calculated] (001): (002):(003):(004):(005):(006)= 1 : 0.4 : 3 : 1.2 : 0.07 : 0.12. An exact determination of the observed intensities was not possible for (002), (005) and (006) because of their low intensities and the poor quality of the Debye Scherrer photographs. Visually, (006) and (002) are more intense than (005), which is in agreement with calculated intensities.

The calculated value for the separation between fluorine layers, 2.22 Å, is appropriate for a nearly close-packed double layer of fluorines. At these fluorine layer heights, some overlap or penetration of the fluorine ligands into the carbon layers is required. The amount of this penetration is 0.39 Å. This is determined as follows: The ideal covalent radius of fluorine is 1.35 Å and the carbon layer thickness (from that of graphite) is 3.35 Å/2= 1.675 Å. The sum, 3.025 Å, represents the case where the fluorine touches the carbon ρ layer but does not overlap with it. The calculated results show the separation between each fluorine layer is

2.22 Å. Since the **c** spacing of the second stage salt is 10.85 Å, the distance between the center of one carbon layer to another, in an occupied gallery of a second stage salt, or the **Ic** value, is 10.85-3.35= 7.50 Å (the distance between carbon layers which are contiguous is 3.35 Å). Hence, in the calculation the distance from the fluorine layer center to the carbon layer center is (7.50 - 2.22)/2= 2.64 Å. This value is 0.39 Å shorter than the 3.025 Å value which assumed no overlap of the fluorine ligands with the carbon π cloud. 0.039 Å, therefore, represents the distance the fluorine ligand penetrates the π cloud of the carbon layer or nestled in the C_6 rings. Studies by Okino[2] show a similar effect in first stage $C_{14}AsF_6$, which possesses a **c** spacing of 7.6 Å and in which the fluorine atoms on AsF_6^- nestle in the C_6 rings by 0.2 Å (for a fluorine with a covalent radius of 1.35 Å).

In the case of the fourth stage salt, I[obs](005):(006)= 4.1 : 1. The other observed 00ℓ reflections are much weaker. (0011) is faintly visible and is stronger than (0010). The predicted 00l orderings are shown in Figures **6.4**. A fluorine layer distance at delta = 0.046 (0.82 Å away from the center line of the gallery) yields relative intensities which are in reasonable agreement with those observed; I[calculated] (001):(002):(003):(004): (005) : (006)= 0.4 : 0.06 : 0 : 0.09 : 3.9 : 1. In the case of very weak diffraction lines, low-angle diffuse scattering from quartz makes (001), (002) and (003) slightly less visible than (0011). The delta value is

again in agreement with the close packing model proposed. The predicted fluorine layer separation is 1.64 Å, which is slightly less than the amplitude of the F ligand tetrahedron in BF_4^- which is ≈1.83 Å. The calculated fluorine to carbon distance is 3.07 Å, and is slightly greater than the sum of the fluorine covalent radius and one half the carbon layer separation of graphite (3.03 Å).

In each case, data modelling indicates that the fluorine layers are roughly 2 Å apart, which is appropriate for tetrahedral BF_4^- and BF_3. Almost certainly, this rules out a case where the fluorines are evenly distributed throughout the gallery in a random and non-periodic manner in the "c" direction. The presence of dimeric $B_2F_7^-$ is possible since this anion can be represented as two tetrahedra sharing an F ligand common to two BF_4 units. Certainly the B atoms could be placed in tetrahedral holes in the double layer of F ligands to provide for such units. Superlattice reflections were not observed, indicative of a lack of ordering in the "a" direction; however, the scattering power of 30 carbons is much greater than that of 3 borons atoms so that ordering could occur and be undetectable with such low quality X-ray diffraction data.

The size of the domain will also affect the relative intensities of the (00ℓ) reflections. This effect was examined by allowing a gradual change in the height of the carbon layers at the end of the domain. A large unit cell

containing 194 carbon atoms was modelled. The carbon atoms were placed in a "c" axis profile in which 2/3 were planar and 1/3 were linearly varied from full height to the center of the gallery. Other anions were placed in their regular positions. As before, the fluorine layer distance was varied above and below the center line of the gallery. In the second stage salt model, the calculated intensity of (001) was comparable to that of (003) over a wide range of delta. This eliminates the possibility of this type of unit cell arrangement. Either the domains are larger than 300 carbon atoms, or this model is too simple to mimic the domain structure reasonably; in either case, the impact on the observed (00ℓ) ordering is too great to allow this model to be valid. The effect of small variations of "c" spacing on these (00ℓ) lines, as well as variations in the C-C bond length, were found to be relatively minor.

6.32.1 Layer stacking in fluoroborate salts

The second and higher stage fluoroborate salts possess observed I(110):I(100) intensities which are approximately 3:1. In SP1 graphite, these intensities are approximately equal. For the unnestled first stage AsF_6^- salts of graphite[2], I(100)> I(110). The presence of (100) lines in second stage salts discounts the possibility of a randomly staggered arrangement of carbon layers, as in first stage, nestled AsF_6^- salts[2]. The diminishment of (100) for second stage salts,

however, suggests an arrangement in which some of the carbon layers are staggered whereas others are in non-registry.

6.32.2 Tensimetric, gravimetric and X-ray experiments to determine the composition of fluoroborate salt under BF_3 pressure

For a given x in $C_xBF_4 \cdot y(BF_3)$, the stoichiometries in Table **6.3** of x ≈30 show: second stage $C_{28.8}BF_4(BF_3)_{1.7}$, third stage $C_{28}BF_4(BF_3)_{0.6}$ and fourth stage $C_{30.1}BF_4(BF_3)_{0.35}$. This indicates that the fourth stage is deficient by 1.35 BF_3 compared to the second stage, when x ≈30.

A determination of the composition of a salt obtained from the reverse reaction, incorporation of BF_3 into fourth stage $C_xBF_4 \cdot 1/3(BF_3)$, was desireable to investigate reversibility. It was indeed possible to reverse fourth stage fluoroborate salt to second stage by the application of BF_3 pressure. However, while loading the X-ray capillary in the inert atmosphere dry box, the composition can change, because the escape of BF_3 is continuous. For this reason, the composition of a fourth stage fluoroborate salt subjected to BF_3 pressure was determined <u>in situ</u>, so that this composition is truly associated with a particular X-ray diffraction pattern.

Table **6.4** shows the third stage stoichiometry obtained, and Table **6.5** its X-ray pattern. By gravimetry, this stoichiometry is $C_{32.7}(BF_3)_{2.0}F$ and by tensimetry, $C_{32.7}(BF_3)_{2.2}F$.

X-ray diffraction under BF_3 pressure shows a third stage salt with a larger unit cell than that obtained from loading salts in the Argon atmosphere dry box. The enlargement of the unit cell is a consequence of the greater BF_3 content under BF_3 pressure, as shown in the next section on high pressure capillary reaction. When the effect of gallery expansion (unit cell enlargement under pressure) is corrected, the stoichiometry-stage dependence of the reverse reaction (the incorporation of BF_3), agrees with that obtained from the forward reaction (the loss of BF_3). This is also seen from the space filling efficiencies (> 90 %) of the intercalant.

This demonstrates that the process:

$$C_xBF_4 \ (y + 1/3)BF_3 \ \rightarrow \ C_xBF_4 \cdot 1/3 \ (BF_3) + y \ BF_3$$

where $y \approx 1.2\text{-}1.3$

is near equilibrium for similar gallery heights of the intercalation salts on both sides of the equilibrium.

6.33 The Role of BF_3 in Lattice Energetics

Since in layered materials of the type under study, the anions are not screened from one another by cations (except from gallery to gallery) it is clear that neutral molecules interspersed between the anions can appreciably increase the lattice energy. Because of the flat geometry of BF_3 it is easily intercalated into the small voids left by replacement of PF_6^- by the smaller ($\approx$ 2/3 volume) BF_4^-. Indeed the thinness of the molecule BF_3 must also provide for much easier migration into the graphite galleries than for molecules such as PF_5. In addition the positive (B-atom) center of BF_3 is "exposed" to atoms which approach along the threefold axis. Such open exposure of the positive center does not occur in PF_5. It is not surprising then, to find that BF_3 has much greater impact as a dielectric spacer molecule than PF_5.

Similarly, because of the smaller dimensions of BF_4^- and BF_3 relative to PF_6^-, higher stages are obtained than for the same anion concentration of a PF_6^- graphite salt. This is shown by the fourth stage stoichiometries listed in Table **6.1** and **5.2**. The closer anion proximity in higher stages should produce larger anionic repulsion. BF_3 incorporated into the voids diminishes these repulsions and stabilizes the stage.

Moreover, the oxidation of $BF_4^- \cdot \mathbf{y}(BF_3)$, in a graphite intercalation salt, with $\mathbf{y}(1/2)F_2$ demonstrates the importance of BF_4^--BF_4^- anionic repulsion and of the dielectric spacers

(BF_3) which diminish these repulsions. As mentioned in the experimental section, the second stage salts are obtained from fluorine oxidation of third stage graphite fluoroborates: $C_{23.3}BF_4(BF_3)_{0.36}$ + 0.4F and $C_{28}BF_4(BF_3)_{0.6}$ + ≈ 0.5 F. When enough fluorine is added to convert **y** BF_3 to **y** BF_4^- in high stage $C_xBF_4 \cdot y(BF_3)$ the close packed arrangement of BF_4^- and **y** BF_3 will be converted to close packed anions with (1+**y**) BF_4^- per formula unit. The increased anion concentration and the absence of neutral BF_3 renders this stage unstable. The result is a conversion to a lower stage; this is usually a change of two stages. The anions in $C_{28}(BF_4)_{1+y}$ in the lower stage will no longer fill the gallery space efficiently, since the volume available to it has increased, usually by a factor of two. This is as predicted qualitatively from the reasoning above.

In addition, as previously noted, a second stage fluoroborate salt will release approximately 1.3 BF_3 molecules as it changes from second to fourth stage of similar interlayer spacings. This conversion appears to be reversible, in which case the second to fourth conversion is near equilibrium. This permits an estimation of the enthalpy change associated with the incorporation of 1.3 BF_3 and is described below.

The energetic factors important in stage transformations are delicately balanced. The energy gained in ordering the anions and neutrals to higher stages must compensate for the entropy term in the removal of BF_3. Energetic factors which

contribute to stages changes have been reviewed by Saffran.[3] Factors which favor high stage may be the increased coulombic attraction between the more localized charge on the carbon atoms and the neighboring anions, and the energy gained from the van der Waal's attraction of the greater number of contiguous carbon layers present at higher stages. Bartlett and Okino[2] have shown from studies on graphite intercalated by arsenic pentafluorides that the arrangement of anions in one layer of a first stage salt does not affect the placement of anions in neighboring layers. This somewhat surprising lack of interlayer interaction is an indication of the diminished importance of repulsions between anions in neighboring galleries. It is also probable that the delocalization in the π bands is sufficient to prevent a significant accumulation of charge at different carbon atom sites. The arsenic pentafluoride study shows that interlayer terms may be less important than intralayer anion-anion repulsive energies.

The energy costs, in the addition of 1.3 BF_3 to fourth stage fluoroborate, are the entropy loss in condensing 1.3 BF_3 ($T\Delta S°_{298}$= 26 kcal mol^{-1})[4] and the energy of carbon layer expansion (approximately 5 kcal mol^{-1})[5]. The other energetic costs mentioned above may also come into play. Hence, for the process to be near equilibrium, the shielding effect of 1.3 BF_3 upon the anion-anion repulsion must increase ΔH(**lattice**) of the second stage salt by at least 31 kcal mol^{-1}.

6.34 High pressure in situ X-ray experiments with fluoroborate and fluorophosphate salts

In a comparison of the stability of two salts of a given stage which contain anions of different volumes, such as $C_{29}PF_6$ and $C_{29}BF_4 \cdot y(BF_3)$, the presence of an electrostatic spacer in the latter salt has been discussed. The model of decreased interanionic repulsions in the latter salt, by virtue of **y** BF_3, can also account for observations of reactions of fluoroborate and fluorophosphate salts under high pressure of BF_3 or PF_5.

X-ray diffraction data in Table **6.6** shows that the formation of graphite fluoroborate, $C_xBF_4 \cdot y(BF_3)$ from the displacement of PF_5 from second stage C_xPF_6 with BF_3, results in an initial product which is a mixture of first and second stage salts (this X-ray diffraction was not <u>in situ</u>, which may explain the mixture of stages). In contrast, a fourth stage fluoroborate salt ($C_{33}BF_4 \cdot y(BF_3)$) (formed from a similar displacement of PF_5 under high pressure of BF_3 followed by long term evacuation), is not transformed to a first stage material by BF_3. In this case, the high stage fluoroborate cannot be converted back into the first stage salt which must be formed in the initial displacement. This result is shown in Table **6.7.**

High pressure PF_5 acting on fourth stage fluoroborates will produce a mixture of stages, but again not a first stage salt. By way of contrast, a second stage graphite hexa-

fluorophosphate shown in Table **6.7** ($C_{28}PF_6$) with similar anion concentration can be converted into a second and first stage mixture by treatment with PF_5 in a high pressure experiment.[6]

The results show that high pressure phosphorus pentafluoride and boron trifluoride can each alter the stage of an intercalation salt. The difference in their effect on the stage of $C_{29}BF_4 \cdot yBF_3$ (fourth stage) and $C_{29}PF_6$ (second stage) can be explained by the diminished inter-anionic repulsion of the first compound. Since the energy required to separate carbon layers in the conversion of fourth stage to first stage salt is only slightly more (roughly 3 kcal mol^{-1}) than that of the second stage to first stage conversion, the entropy loss in the process of condensing gaseous molecules into the salt is the major energy cost in these stage conversions. The energy needed to change a high stage compound to low stage is countered by the diminution of the repulsive interactions between the anions which is brought about by neutral screeners of the anionic repulsions. In this case, the repulsive energy of the fluoroborate salts ($C_{29}BF_4 \cdot y(BF_3)$), because of the original presence of BF_3, is not great enough to pay for the energy costs of stage change all the way to first stage. When BF_3 is not present, and when the anion concentration is larger such as in second stage $C_{14}BF_4$ (a salt which will not release BF_3 because all BF_3 had been fluorinated in the initial preparation) a first stage is obtained when a high pressure of BF_3 is applied, as shown by X-ray diffraction in Table **6.8**.

6.35 Anion Repulsion and the 14n Rule for Nestled (smaller "c" spacing) Fluoroanion Intercalation Compounds.

The effect of anion size and neutrals on the stage and its composition is displayed in Table **6.9.** These systems were selected because the concentration of neutrals is accurately known. For the bifluoride salts, coulometry and gravimetry agree giving the listed stoichiometries with only a small margin of error. The upper and lower ranges for each stage are indicated. The hexafluoroarsenate salts were studied to monitor AsF_5 as well as AsF_3 loss (because of the conversion $3AsF_5 + 2e^- \rightarrow 2AsF_6^- + AsF_3$); these stoichiometries are accurate. Compounds in this investigation were carefully characterized in this respect.

The stoichiometries for the PF_6^- and AsF_6^- salts fit the "14n" rule for nestled structures as first established by Okino[2]. That is, in the measured stoichiometry of higher stage salts, the carbon atoms are present in a proportion of approximately 14n to each anion, where n is equal to the stage of the compound. This represents the highest stoichiometry possible with F ligands of MF_6 each nestled in a C_6 ring of the graphite (see F.Okino thesis, ref.(2)). The carbon stoichiometry in smaller anion systems is greater and, for anions larger and more complex than MF_6^-, it is less.

As noted earlier, interlayer interactions do not seem to be important. For a given center to center distance, a larger

anion may be more repulsive than a smaller one because of the steeply rising repulsive potential (Figure **6.6**). The mutual repulsions of the fluoroborate anions must, for the same anion concentration, be less than for the fluorophosphate anion.

Smaller anions can be accommodated to a slightly higher degree before the stage transformation is required; therefore, in such cases the observed stoichiometries can be less than 14 carbons for each anion. The stoichiometries of the fluoroborates, because of the small size of BF_4^-, are similar to those of the bifluorides. When some boron trifluoride is present, however, the concentration can increase to as much as C_8^+. It seems that only when good dielectric screeners are present, the 14n rule can be broken since close-packing can be observed for high stage salts. Close-packing of intercalants of first stage compounds which do not have neutral intercalants is also possible[7] if sufficient energy is provided by the oxidizing intercalant.

Table 6.1 Space Filling Efficiencies in Fluoroborate and Fluorophosphate Salts

Stage	Stoichiometry	Volume (A^3) Formula Unit (less carbon atom volume)	Total Ligand Volume (F^- volume) 17.8 / 17.2 $Å^3$	% Gallery Space Filling 17.8/17.2
2	$C_{30}PF_6$	167	107/103	64/62
2	"$C_{23.2}BF_4$"	175	71/69	40/39
2	$C_{28.8}BF_4(BF_3)_{1.7}$	156	162/157	104/101
3	$C_{32.7}BF_4(BF_3)_{1.2}$	134	135/131	101/98
3	$C_{23.3}BF_4(BF_3)_{0.39}$	92	92/89	100/97
3	$C_{28}BF_4(BF_3)_{0.6}$	115	103/100	90/87
4	$C_{32.7}BF_4(BF_3)_{0.37}$	91	91/88	100/96
4	$C_{30.1}BF_4(BF_3)_{0.35}$	87	90/87	103/100
2/3	$C_{26.3}BF_4(BF_3)_{0.25}$	139 (2nd) 101 (3rd)		
2/3	$C_{25.4}BF_4(BF_3)_{0.28}$	144 (2nd) 104 (3rd)		

Notes to Table 6.1

See text for a description of the calculation of percent space filling. An example is $C_{30.1}BF_4(BF_3)_{0.35}$, a stage 4 salt with a= 2.46 and c= 17.83 Å. $V_{unit\ cell}= (a^2c)\sin(120)= 93$ Å^3. The unit cell contains 8 carbon atoms, since a fourth stage salt has four carbon layers per unit cell, each layer containing two carbon atoms. The volume of the formula unit $C_{30.1}BF_4(BF_3)_{0.35}$ is then (30.1/8)93= 350 Å^3. The volume of the carbon atoms is then subtracted from the total formula unit volume. For the unit cell of graphite, which contains four carbon atoms, a= 2.456 c=6.7 Å and $V_{cell}= (a^2c)\sin(120)= 35.0$ Å^3; $V_{carbon}= 8.75$ Å^3.
In $C_{30.1}BF_4(BF_3)_{0.35}$, we subtract the carbon atom volume, (30.1)(8.75)= 263 Å^3, from the formula unit volume (350 Å^3) to give 87 Å^3. This is the volume of the formula unit tabulated in the first column.

As described in the text, the F ligand volume is either 17.2 or 17.8 Å^3. Thus, for $BF_4(BF_3)_{0.35}$, 5.08 F occupy a volume of 87 or 90 Å^3. These are the values tabulated in the second column.

The ratio of the F ligand volume to available gallery volume is a measure of space filling efficiency. This is tabulated in the last column as a space filling efficiency percentage. For $C_{30.1}BF_4(BF_3)_{0.35}$, these are (for 17.2 and 17.8 Å^3 F volumes, respectively) 87/87= 100 and 90/87= 103 %.

Table 6.2 X-Ray Diffraction of Second Stage Graphite Fluoroborate

Second Stage $C_{28.8}BF_4(BF_3)_{1.7}$ a= 2.46, c= 10.85 Å

No.	Intensity	$1/d^2$ (obs.)	$1/d^2$(calc.)	Assignment
1	med	.00835	.0084	001
2	weak shadow	.03355	.0336	002
3	weak shadow	.06214	---	Kβ
4	str broad	.07594	.0755	003
5	med	.13643	.1343	004
6	vw shadow	.21417	.2100	005
7	weak	.22204	.2210	100
8	weak	.22882	.2293	101
9	weak broad	.25449	.2545	102
10	weak	.30617	.3024	006
11	weak broad	*.41753	.4116*/.4310	007(105)
12	med	.66153	.6629	110
13	weak	.67103	.6713	111
14	weak	.69617	.6964	112
15	broad	.73961	.7384	113
16	vweak	.79679	.7972	114
17	vweak	.88636	.8838	200
18	vweak	.96906	.9650	116
19	vweak	1.0799	1.0745	117

Table 6.3 Summary of X-ray Diffraction Simulations

Fourth stage : Theoretical $C_{30}BF_4(BF_3)_{0.333}$
Experimental $C_{30}BF_4(BF_3)_{0.35}$

Parameters:

c = 17.83 Å
Z = 6 molecules/unit cell
Number of atoms = 218

Coordinates:

	z	Number of Atoms
(i) Carbon	0	45
	.4363	45
	.6242	45
	.8121	45
(ii) Fluorine	.2182 ± δ	30
(iii) Boron	.2007	1 trigonal
	.2356	1 trigonal
	.2335	3 tetrahedral
	.2029	3 tetrahedral

Second stage : Theoretical $C_{29}BF_4(BF_3)_{1.67}$
Experimental $C_{28.8}BF_4(BF_3)_{1.7}$

Parameters:

c = 10.85 Å
Z = 6 molecules/unit cell
Number of atoms = 244
200 data points

Coordinates:

	z	Number of Atoms
(i) Carbon	0	87
	.6912	87
(ii) Fluorine	.3456 ± δ	54
(iii) Boron	.3169	5 trigonal
	.3743	5 trigonal
	.3205	3 tetrahedral
	.3708	3 tetrahedral

Table 6.3 (Cont.) Summary of X-ray Diffraction Simulation

Thermal Parameters:

$Å^2$	U_{11}	U_{22}	U_{12}	U_{33}
C	0.02	0.02	0.02	0.01
B	0.2	0.2	0.1	0.1
F	0.3	0.3	0.2	0.2

$$T(\text{anisotropic}) = \exp[-2\pi^2(U_{11}h^2a^{*2} + U_{22}k^2b^{*2} + U_{33}l^2c^{*2} + 2U_{12}hka^*b^* + 2U_{13}\,hla^*c^* + 2U_{23}klb^*c^*]$$

Lorentz Polarization:

$LP = (1 + \cos^2 2\theta)/((\sin^2\theta)\cos\theta)$

Scattering Factors:

Reference: International Tables for X-Ray Crystallography, Vol.IV, Kynoch Press, 100 (1974).

Table 6.4 In Situ Gravimetry/Tensimetry/X-Ray

Apparatus:

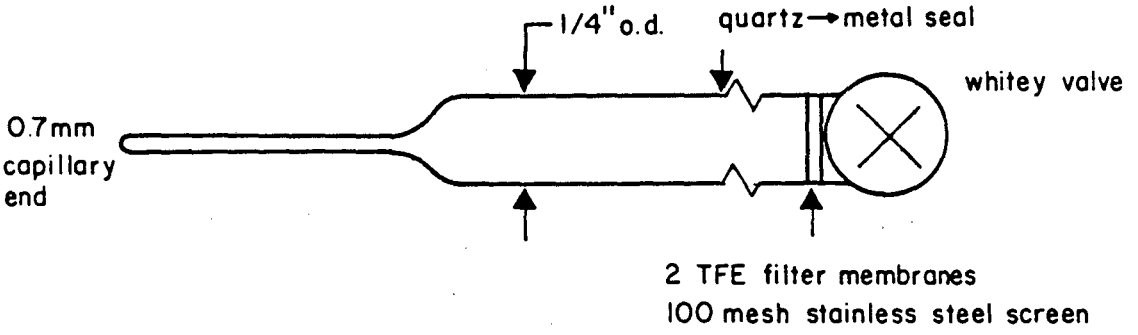

$C_{32.7}(BF_3)_{1.37}F$ (Fourth Stage)

↓ + BF_3

V_{cell} = 134.1 Å^3

expanded

tensimetry: $C_{32.7}(BF_3)_{2.2}F$ (third stage) 100% space filling

gravimetry: $C_{32.7}(BF_3)_{2.0}F$ (third stage) 90% space filling

Table 6.5 X-Ray Diffraction Data For **In Situ**/Gravimetry Tensimetry/X-Ray (from Table 6.1)

Third Stage — tensimetry: $C_{32.7}(BF_3)_{2.2}F$; gravimetry: $C_{32.7}(BF_3)_{2.0}F$

a= 2.46, c= 14.8 Å

No.	Intensity	$1/d^2$ (obs.)	$1/d^2$(calc.)	Assignment
1	strong sharp	.0734	.0735	004
2	weak med-broad	.1168	.1149	005
3	weak sharp	.2193	.2211	100
4	weak	.3785	.3722	009 (questionable)
5	medium sharp	.6631	.6632	110

Table 6.6 Second Stage Fluorophosphate + BF_3

No.	Int.	$1/d^2$ (obs.)	Second Stage $1/d^2$ (calc.) a= 2.45 c=11.31 Å	Second Stage Assignment	First Stage $1/d^2$ (calc.) a= 2.45 c= 7.62 Å	First Stage Assignment
1	vw	.0088	.0078	001		
2	msharp	.0171			.0169	001
3	msharp	.0416				*
4	strong broad	.0680 .0708 .0735	.0702	003	.0676	002
5	vw	.1241	.1248	004		
6	vw broad	.1363				
7	medium weak	.1545			.1548	003
8	weak sharp	.1689				*
9	weak sharp	.2095				*
10	medium	.2232	.2211	100	.2209	100
11	weak broad	.2555	.2523	102		
12	medium sharp	.6619	.6633	110	.6628	110
13	sharp weak	.6779			.6799	111
14	weak broad	.7328	.7335	113	.7316	112

* likely SiF_6^{2-} salt from capillary attack

Table 6.7 In Situ High Pressure Reactions	
	Reaction
a	SP1 graphite + BF_3 $\xrightarrow{85\ psi}$ No Reaction
b	Pyrolitic Coke + BF_3 $\xrightarrow{100\ psi}$ No Reaction (Pyrolitic coke is similar to carbon black - small particle size (< 80 μ))
c	$C_{14}BF_4$ (2nd stage) + BF_3 $\xrightarrow{100\ psi}$ 2nd (c=11.1 Å) 1st (c= 7.9 Å) stage mixtures
d	$C_{14}BF_4$ (2nd stage) + PF_5 $\xrightarrow{78\ psi}$ 2nd (c= 11.2 Å) 1st (c= 8.2 Å) stage mixtures
e	C_xPF_6 (4th stage) + BF_3 $\xrightarrow{85\ psi}$ 3rd and 2nd stage mixtures $\xrightarrow{3\ hour\ evacuation}$ 3rd stage (I_c = 7.8 - 7.95 Å)
f	$C_{28}PF_6$ (2nd stage) + PF_5 $\longrightarrow$ (X-ray not in situ) 2nd and 1st stage mixtures

Around I_c = 7.9 Å, the energy required for further expansion is less than that required to change stage. This is perhaps facilitated by neighboring carbon separation effects.

Notes to Table 6.7

A general structural feature, in the high pressure reactions is the appearance of an expanded higher stage (I_C= 8.0 Å) and a contracted lower stage (I_C= 7.6-7.8 Å). The higher stage, prior to changing to lower stage, becomes saturated with neutrals and to accommodate them expands by approximately 0.4 Å.

Further expansion is energetically unfavorable because the lattice energy begins to decrease quickly as the attraction energy decreases with increased separation of the positively charged carbon sheets and the negatively charged guests. On the other hand, the spacers have had their maximum favorable impact. Further addition of neutral will have little or no beneficial influence on the anion repulsion energy (which of course is unfavorable to the lattice energy).

In addition, under high pressures of boron trifluoride, no gallery expansion is seen in graphite. Pyrolitic coke, a graphite with smaller particle size, was also employed because the small particle size allows for faster diffusion. In this graphite, X-ray hkℓ reflections are broader and weaker than in SP1 (100-200 μ) and the crystallinity and particle size is much smaller (<20μ) that of carbon black. No change in the X-ray pattern was observed under 100 psi BF_3 pressure. This indicates that the crystallite size is not the factor which is kinetically inhibiting the carbon layer expansion, and that some repulsion between the positively charged carbon layers is

necessary for intercalation. The presence of anion formation as well as neutrals is required to initiate the process.

Table 6.8 In Situ X-ray Diffraction

(Second Stage) $C_{14}BF_4$ + 100 psi BF_3

No.	Int.	$1/d^2$ (obs.)	Second Stage $1/d^2$ (calc.) a= 2.46 c=11.1 Å	Assignment	First Stage $1/d^2$ (calc.) a= 2.46 c= 7.9 Å	Assignment
1	weak	.00887	.0080	001		
2	med	.01605			.0162	001
3	strong	.06470			.0650	002
4	med strong	.07057	.0724	003		
5	med weak	.13011	.1288	004		
6	med	.14634			.1462	003
7	med	.22244	.2210	100	-	100
8	broad weak	.25302	.2532	102	[.2592	004]
9	sharp weak	.39423	.3943	007		
10	sharp weak	.40620			[.4050	005]
11	med strong	.66243	.6629	110	-	110
12	broad weak	.72426				
13	weak	.88376	.8840	200	-	200

Table 6.9 Anion Size Influence on the Staging/Composition Formula

Stage	Stoichiometry	Equivalent first stage	Ref.
Second	$C_{19}HF_2$	$C_{9.5}HF_2$	a
	$C_{26}HF_2$	$C_{13}HF_2$	
Third	$C_{42}HF_2$	$C_{14}HF_2$	a
	$C_{55}HF_2$	$C_{18}HF_2$	
Fourth	$C_{70}HF_2$	$C_{18}HF_2$	a
First	$C_{14}AsF_6$ (average)	$C_{14}AsF_6$	b
	$[C_{12}AsF_6$ - $C_{15}AsF_6]$		
Second	$C_{29}PF_6$ (average)	$C_{14.5}PF_6$	this work
	$[C_{22.7}PF_6$ --------	$C_{11.4}PF_6]$	
	$[C_{30}PF_6$ --------	$C_{15}PF_6]$	
Fourth	$C_{32.7}BF_4 \cdot (0.4)BF_3$	$C_{8.1}BF_4 \cdot (0.1)BF_3$	this work
Third	$C_{23.3}BF_4 \cdot (0.4)BF_3$	$C_{7.8}BF_4 \cdot (0.13)BF_3$	this work
	$C_{28}BF_4 \cdot (0.6)BF_3$	$C_{9.3}BF_4 \cdot (0.2)BF_3$	this work
Second	$C_{25.3}(BF_3)_{1.39}F_{1.4}$	$C_{11.7}BF_4$	this work
Second + third mixture	$C_{26.4}BF_4 \cdot (0.3)BF_3$	$>C_{13}$	this work
	$C_{26.3}BF_4 \cdot (0.25)BF_3$	$>C_{13}$	this work

Table **6.8** References

a M. Kawaguchi, M. Lerner, and N. Bartlett, to be published. Based upon electrochemical charging in 1 M NaF/HF.

b F. Okino and N. Bartlett, to be published

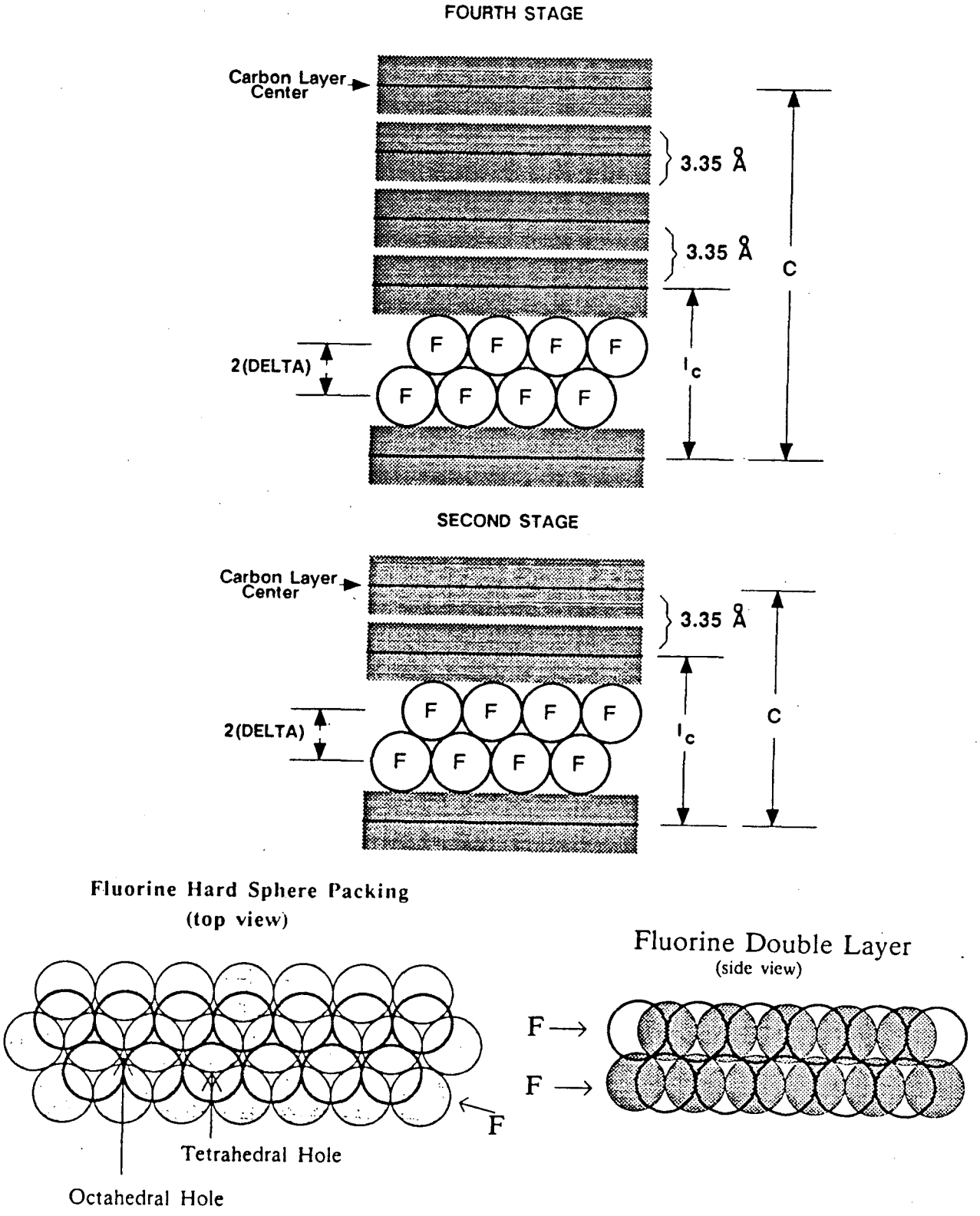

Figure 6.1
Schematic of the Model used for X-ray Intensity Simulations

Notes to Figure 6.1

Each carbon layer is represented by a solid line. The shading shows the thickness of each layer, which is 3.35 Å, because the carbon layers are 3.35 Å apart in graphite. It is reasonable to assume the same holds for contiguous carbon layers in graphite salts.

The gallery is the space between the carbon layers where the intercalant lies (in this case, BF_4^- + **y** BF_3). Only the fluorine atoms of the intercalant are shown since a hard sphere model is used. The boron atoms were placed at idealized positions, and their position was not varied. The distance between the fluorine layers was varied, and the effect of this variation on the 00ℓ intensities was calculated, as described in the text. "2(Delta)" is a measure of the separation between the hard sphere fluorine layers.

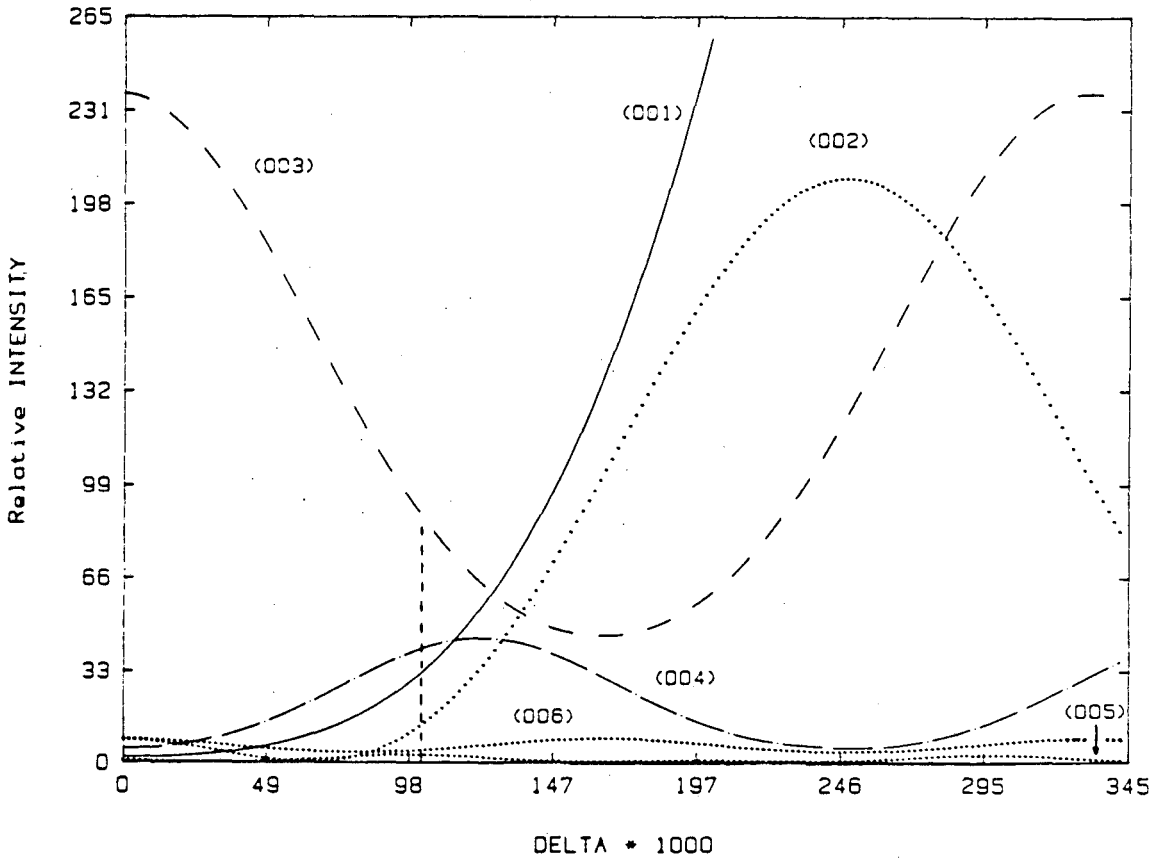

Figure 6.2 Calculated 001 Intensities as a function of Fluorine Layer separation : $C_{29}BF_4(BF_3)_{1.67}$

Figure 6.2 Notes

(00ℓ) intensities were calculated as a function of fluorine layer separation. Delta is the distance from the gallery center ($I_c/2$) to the center of either fluorine layer. Delta = 0 corresponds to no separation between the fluorine layers. The fluorines, in this case, are exactly midway between the two carbon sheets in the gallery (at $I_c/2$). At 2(Delta)= 220, the fluorine atoms are near maximum separation. At this point, 2(Delta)= I_c.

Each (00ℓ) line is plotted as a function of Delta, a single parameter. The vertical dotted-dash line corresponds to a reasonable fit with the observed intensities from the microdensitometer trace of the Debye-Scherrer diffraction pattern (see Figure **6.3**). At this separation, Delta= .102; the separation between fluorine layers is (2)(.102)10.85 = 2.21 Å.

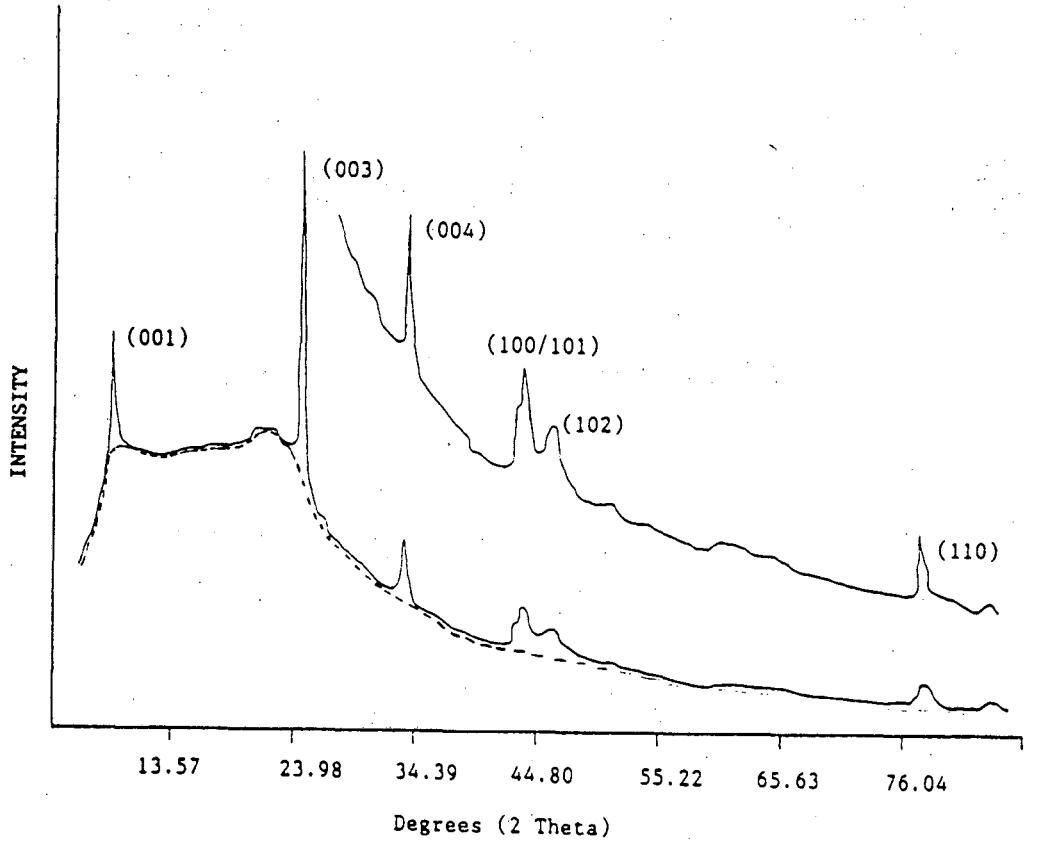

Figure 6.3 Microdensitometer Tracing of Debye-Scherrer Photograph : $C_{29}BF_4(BF_3)_{1.67}$

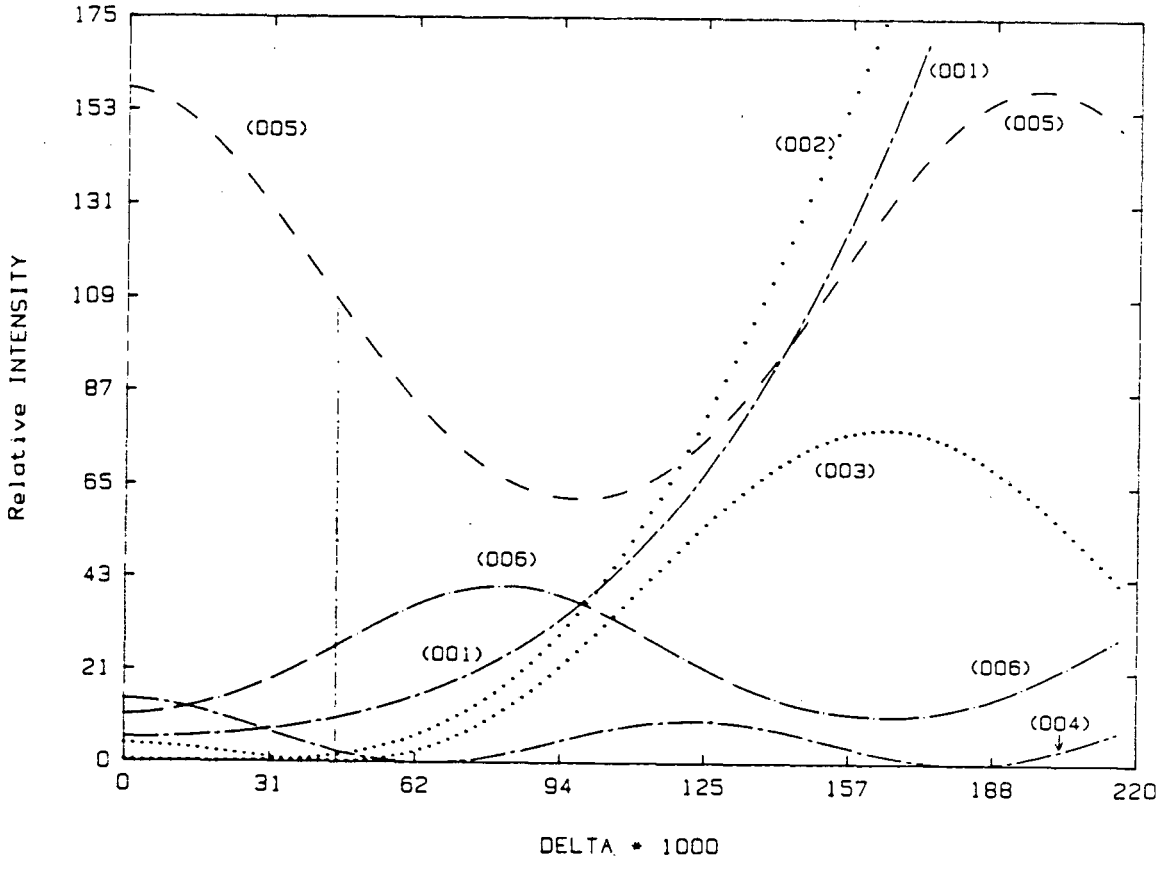

Figure 6.4 Calculated 00ℓ Intensities as a Function of Fluorine Layer separation : $C_{30}BF_4(BF_3)_{0.333}$. See next 2 pages for notes to this figure.

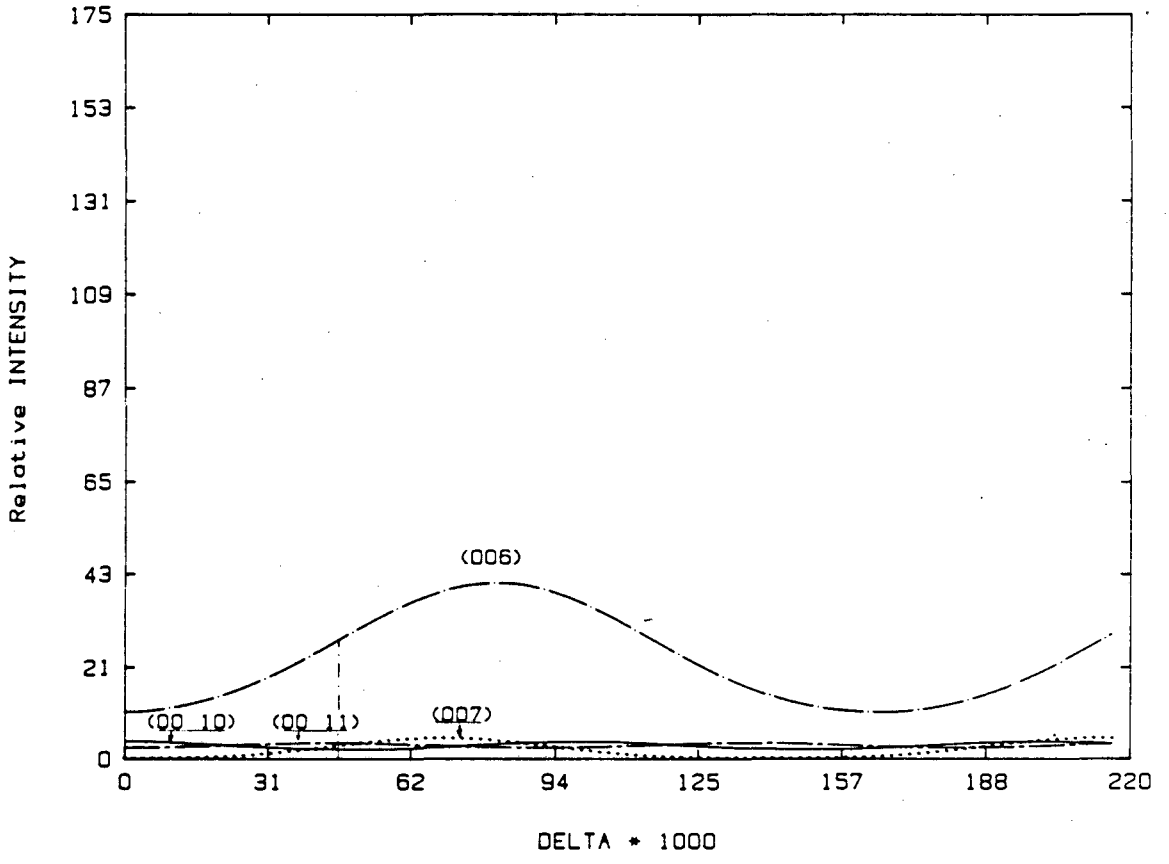

Figure 6.4 (Continued) Calculated 00ℓ Intensities as a Function of Fluorine Layer separation : $C_{30}BF_4(BF_3)_{0.333}$

Notes to Figure **6.4**

See Figure **6.2** for a description of this diagram. A fluorine layer separation of Delta= .046, shown by the dotted-dash vertical line, gives an ordering of the 00ℓ intensities which agrees with that observed (see Figure **6.6**). For this fourth stage salt, since c= 17.83 Å, the separation between the fluorine layers is (.046)(2)(17.83)= 1.64 Å.

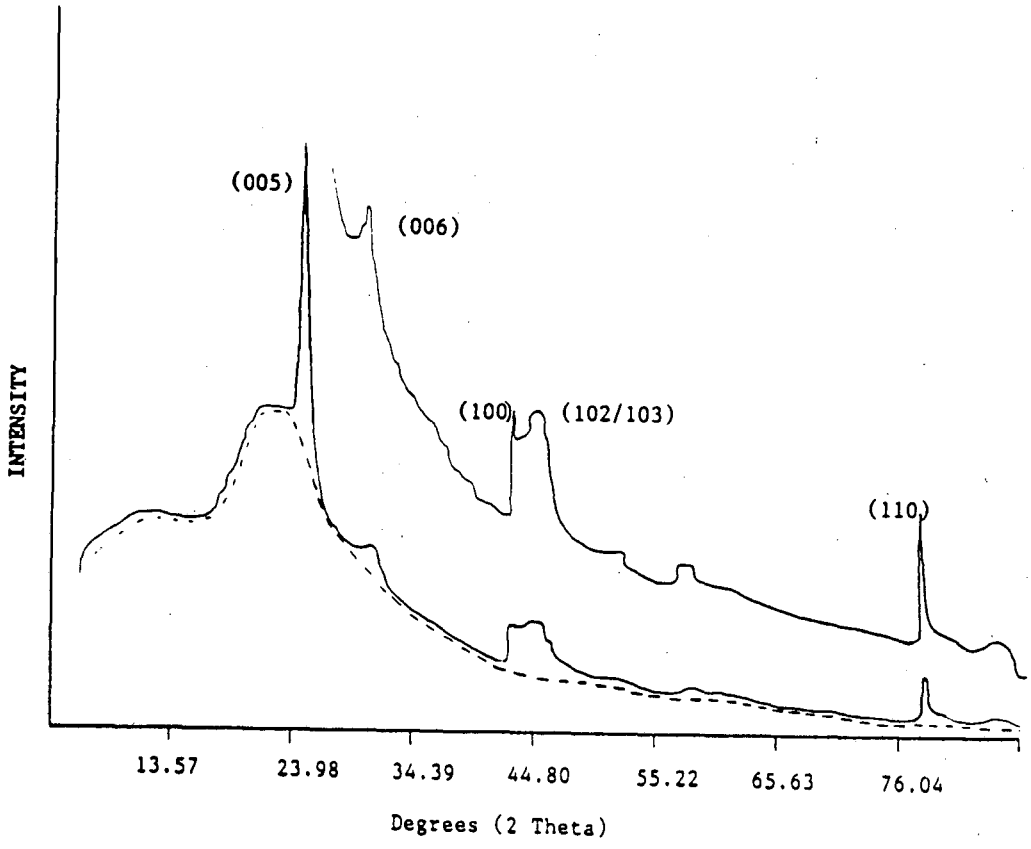

Figure 6.5 Microdensitometer Tracing of Debye-Scherrer Photograph : $C_{30}BF_4(BF_3)_{0.333}$

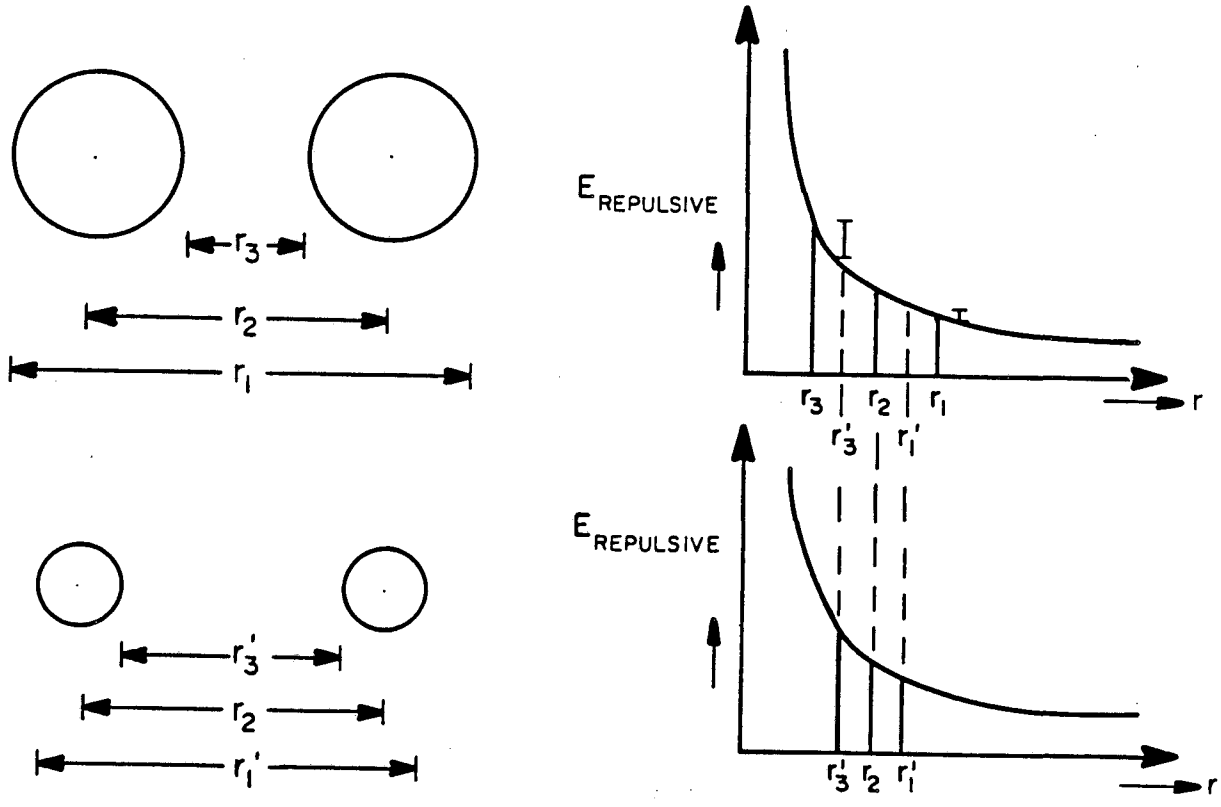

Figure 6.6 Diagram Illustrating the Effect of Anion Size on E (repulsive). Electron density on the near side of the larger ions (r_3) will be more repulsive than the diminution of repulsion on the far size (r_1). The result is a higher net repulsive energy than for the smaller anion.

Chapter 6 References

1. W.H. Zachariasen, **J. Am. Chem. Soc.** 70, 2147 (1948).

2. F. Okino, Ph.D. Thesis, U.C. Berkeley (1984).

3. S. Safran, **Synthetic Metals** 2, 1-15 (1980).

4. N.B.S. Technical Notes 270-3 (1969).

5. L.A. Girifalio and R.A. Lad, **J. Chem. Phys.** 25, 693 (1956).

6. This was originally shown by G.Rosenthal (Ph.D. Thesis, U.C. Berkeley (1984)) and was corroborated in this work.

7. This has been observed for first stage C_8IrF_6. Magnetic susceptibility data shows only IrF_6^- and no IrF_5; E. McCarron, Ph.D. Thesis, U.C. Berkeley, 1980.; N. Bartlett, R.N. Biagioni, E. McCarron, B. McQuillan and F. Tanzella, **Molecular Metals** 293 (1979).

Acknowledgements

I would like to thank my research advisor, Professor Neil Bartlett, for sharing his creative and enthusiastic approach to science, and for his patient guidance, especially in the preparation of this thesis.

Thanks also to Dr. Tom Richardson, for his help in the "Cl_2F_2" project and his instructive presence in the laboratory, and to Drs. Tom Mallouk, Guy Rosenthal and Fujio Okino for their advice during my first two years at Berkeley.

I am very grateful to Maria Madigan for proof-reading and commenting on this manuscript, and to Mike Lerner, for carrying through many of the bureaucratic details of the preparation of this thesis in my absence. Finally, I thank the rest of the Bartlett group, Steve Mayorga, John Kouvetakis, Dr. Richard Kaner and Margarett Atkinson for friendship and for providing a pleasant environment in which to work.

LAWRENCE BERKELEY LABORATORY
TECHNICAL INFORMATION DEPARTMENT
UNIVERSITY OF CALIFORNIA
BERKELEY, CALIFORNIA 94720